Pacific Northwest
NATIONAL LABORATORY

PNNL-39689
ZP1-RPT-003, Rev. 0

Carbon Tetrachloride Degradation Results for 200-ZP-1 Operable Unit

August 2026

Christopher Bagwell
Guohui Wang
Danielle Saunders
Katherine Heal
Alex Kugler
Josh Torgeson
Shelby Brooks
Nancy Escobedo
Judy Robinson

U.S. DEPARTMENT of ENERGY

Prepared for the U.S. Department of Energy
under Contract DE-AC05-76RL01830

DISCLAIMER

PACIFIC NORTHWEST NATIONAL LABORATORY
operated by
BATTELLE
for the
UNITED STATES DEPARTMENT OF ENERGY
under Contract DE-AC05-76RL01830

Printed in the United States of America

Available to DOE and DOE contractors from
the Office of Scientific and Technical Information,
P.O. Box 62, Oak Ridge, TN 37831-0062
www.osti.gov
ph: (865) 576-8401
fax: (865) 576-5728
email: reports@osti.gov

Available to the public from the National Technical Information Service
5301 Shawnee Rd., Alexandria, VA 22312
ph: (800) 553-NTIS (6847)
or (703) 605-6000
email: info@ntis.gov
Online ordering: http://www.ntis.gov

PNNL-39689
ZP1-RPT-003, Rev. 0

Carbon Tetrachloride Degradation Results for 200-ZP-1 Operable Unit

August 2026

Christopher Bagwell
Guohui Wang
Danielle Saunders
Katherine Heal
Alex Kugler
Josh Torgeson
Shelby Brooks
Nancy Escobedo
Judy Robinson

Prepared for
the U.S. Department of Energy
under Contract DE-AC05-76RL01830

Pacific Northwest National Laboratory
Richland, Washington 99354

Executive Summary

Carbon tetrachloride (CT) contamination in the 200-ZP-1 Operable Unit (OU) at the Hanford Site originated from large-volume discharges to the subsurface during plutonium production operations between 1955 and 1973. Contamination migrated through more than 70 meters of unsaturated sediment to reach the underlying unconfined aquifer, where it persists as a large and complex groundwater plume. The 200-ZP-1 OU Record of Decision (ROD) requires that groundwater CT concentrations be reduced to 3.4 µg/L within 125 years. Current groundwater modeling projections estimate that the existing pump-and-treat, even when combined with monitored natural attenuation (specifically hydrolysis), will not achieve this target within the designated timeframe. A fundamental contributor to this shortfall is the extremely slow rate of CT hydrolysis under Hanford aquifer conditions, which has been estimated to have a half-life of 630 years. If faster-acting biotic and abiotic degradation processes are operating within the aquifer, their contribution to CT mass reduction could have a meaningful impact. However, site-specific measurements of these processes and their rates have not previously been performed.

This report documents the results of a two-phase laboratory investigation designed to characterize and quantify the capacity of site-specific 200-ZP-1 OU sediments and groundwater to support natural attenuation of CT through biotic and abiotic pathways. In this context, degradation capacity is defined as the intrinsic potential of the subsurface matrix to transform CT under optimized, controlled conditions. System capacity is evaluated in two ways: (1) as rate-limited capacity, which establishes the maximum kinetic velocity of CT transformation and is measured using half-lives and first order rate constants; and (2) as mass limited capacity, which defines the total contaminant mass the batch experimental system can degrade before reactants are exhausted, representing the maximum amount of contaminant the microbial community and reactive mineral phases can transform under the experimental conditions.

Because bench-scale batch studies eliminate field-scale constraints (e.g., hydrologic heterogeneity, groundwater flow dynamics, mass transfer limitations), these quantitative results represent an upper-bound potential of the aquifer matrix rather than a confident prediction of *in situ* rates. Phase I was a scoping study conducted in fiscal year (FY) 2024 using sediment cores from both the high-concentration source zone and the low-concentration plume perimeter to establish qualitative evidence of attenuation. Phase II, conducted in FY25, incorporated improved core preservation protocols, standardized experimental procedures, and a more sensitive gas chromatography – electron capture detector analytical method to build on the initial findings of Phase I and produce quantitative site-specific degradation rate estimates detailed herein.

Geochemical Environment and Constraints

The bulk 200-ZP-1 OU aquifer groundwater is highly aerobic and nutrient-limited, presenting conditions that are broadly unfavorable for sustained CT natural attenuation. Nitrate concentrations ranging from 49.8 to 256 mg/L across the examined wells confirm that the bulk redox sequence has not progressed to the anaerobic stages necessary for robust reductive dechlorination. The absence of nitrite and the consistent non-detection of dissolved organic carbon in most groundwater samples further indicate that both the thermodynamic and kinetic prerequisites for microbial CT transformation are not evident in the bulk aquifer under current conditions. High background nitrate acts as a thermodynamically preferred electron acceptor ($\Delta G^{\circ\prime} \approx$ -115 kJ/mol $\bar{e}$), biologically outcompeting CT for reducing equivalents from microbial metabolism and reactive mineral surfaces. Because nitrate reduction poises the ambient redox potential (*Eh*) above +100mV, competitive inhibition by oxygen and nitrate imposes a strict geochemical constraint that suppresses the strongly reducing conditions ($Eh \leq$ -100 mV) required for field-scale CT natural attenuation. These constraints characterize the bulk aquifer geochemistry and define the ambient conditions that limit the field-scale expression of natural attenuation; however, porewater dissolved

oxygen measurements from freshly recovered core materials and the results of batch degradation experiments presented in this report demonstrate that (1) localized anoxic microenvironments persist within the aquifer matrix and (2) within those zones the geochemical prerequisites for both biotic and abiotic CT transformation are met.

Hydrolysis

Batch incubations of CT in site-specific groundwater without sediment contact confirmed that hydrolysis contributes no measurable CT mass removal on experimental timescales. These results are consistent with the 630-year half-life estimated by Amonette et al. (2012)[1] through Arrhenius extrapolation to ambient aquifer temperatures. This finding was consistent across both Phase I and Phase II and across all sampled boreholes. Hydrolysis is not a viable natural attenuation mechanism for CT in the 200-ZP-1 OU and should not be incorporated as a meaningful degradation pathway in fate and transport models. This conclusion applies specifically to CT; chloroform (CF), the primary CT degradation product, has an independently estimated hydrolysis half-life of approximately 3400 years under Hanford groundwater conditions (Amonette et al. 2012) and is similarly not subject to meaningful hydrolytic attenuation on remediation-relevant timescales. Any CT mass reduction observed in the field or in laboratory sediment experiments must therefore originate from biotic or mineral-mediated abiotic transformation processes.

Combined Biotic-Abiotic Degradation

The most significant finding of this investigation is the first site-specific experimental demonstration that native microbial communities in 200-ZP-1 OU sediments are capable of driving rapid and near-complete CT degradation under anoxic conditions without any augmentation of organic carbon or other electron donors. Phase II batch experiments with sediments from boreholes C9993 and D0474 produced quantitative first-order half-lives ranging from approximately 2.5 to 11 days and 7 to 10 days, respectively, achieved in the presence of substantial background nitrate concentrations of 179.0 and 49.8 mg/L. These are the first site-specific experimental measurements of biotic CT degradation rates in the 200-ZP-1 OU and represent a substantial reduction relative to the hydrolysis-only estimate of 630 years.

Critically, although degradation products downstream of CF were not directly monitored, the incomplete recovery of initial CT mass as CF, and the subsequent stabilization and decline of CF concentrations during extended incubation, provide indirect evidence consistent with continued reductive dechlorination beyond the CT-to-CF conversion step. Direct confirmation would require analytical measurement of downstream dechlorination products, which was not performed in this study. This is consistent with, but does not directly confirm, CT transformation beyond the initial CT-to-CF conversion step under native, unaugmented conditions. Complete sequential dichlorination is desirable because it achieves full contaminant mass destruction rather than converting it to another chlorinated compound that may itself be subject to independent cleanup standards. Phase I results, while largely qualitative due to analytical limitations, provided an early positive signal for biotic CT transformation and CF production in C9996 sediments that was consistent with the more definitive Phase II findings.

[1] Amonette, J., P. Jeffers, Q. Qafoku, C. Russell, D. Humphrys, T. Wietsma, and M. Truex. 2012. *Abiotic Degradation Rates for Carbon Tetrachloride and Chloroform: Final Report*. PNNL-22062. Pacific Northwest National Laboratory, Richland, WA.

Abiotic Degradation

Abiotic CT degradation was demonstrated across multiple site-specific sediment intervals under anoxic laboratory conditions, confirming that Hanford sediments possess an inherent mineral-mediated reductive capacity for CT transformation driven by reactive mineral phases. The magnitude of this capacity varied considerably across sampled boreholes and depth intervals, reflecting the spatial heterogeneity of geochemical conditions and reactive mineral phases within the aquifer. Sediment intervals with elevated and accessible Fe(II) mineral fractions exhibited the greatest abiotic reactivity, while intervals dominated by oxidized Fe(III) mineralogy showed limited or negligible CT transformation. Control experiments in which sediments were intentionally oxidized prior to testing resulted in complete conservation of CT mass, confirming that abiotic CT transformation requires reduced, anoxic conditions and is eliminated upon oxidation of reactive mineral surfaces.

The presence of competing electron acceptors, particularly nitrate, and the prevailing redox state of the sediment mineral assemblage were identified as the primary controls on abiotic degradation performance. These findings indicate that abiotic natural attenuation is a real but spatially variable contributor to CT mass reduction in the 200-ZP-1 OU, and its significance at any given location is influenced by sediment mineralogy and local geochemical conditions. It is noted that the biological inhibition treatments employed to isolate abiotic processes were not confirmed to be absolute under all experimental conditions. Residual contribution of microbial activity to observed CT transformation in nominally abiotic treatments cannot be fully excluded. A clear mechanistic differentiation between biotic and abiotic degradation pathways is therefore not possible from the available data alone. Taken together, these findings confirm that 200-ZP-1 OU sediments possess an inherent capacity for CT mass reduction that warrants incorporation into updated site models, and that Fe(II) speciation data obtained during future drilling campaigns could help identify areas of the plume with greater potential for abiotic CT degradation.

Anoxic Microenvironments

A critical finding of this investigation is the evidence of anoxic conditions measured in pore fluids from freshly drilled core materials within the 200-ZP-1 OU aquifer. Preliminary porewater dissolved oxygen measurements from Phase II core materials suggest that reducing conditions persist within at least some sampled intervals, even where the surrounding bulk groundwater is presumed to be oxic based on elevated nitrate concentrations and the absence of redox indicator species in groundwater monitoring data. These localized reducing conditions, which cannot be detected through standard groundwater monitoring, represent the zones most likely to support the biotic and abiotic CT transformation processes demonstrated in this study. Whether these anoxic conditions are confined to specific low-permeability sediment zones or reflect broader redox heterogeneity across the aquifer cannot be determined from the available data. Dissolved oxygen measurements would need to be systematically collected during future drilling operations, and are identified as a priority data gap for improving predictions of long-term CT plume behavior.

The results of this study provide new site-specific experimental evidence consistent with the pre-existing conceptual model that identifies fine-grained silt and clay lenses, the Ringold Lower Mud unit, and deeper aquifer intervals as the sediment types most likely to host anoxic conditions necessary to support CT degradation. Importantly, these findings provide an empirical basis for expanding the current conceptual site model, which represents CT solely as a dissolved aqueous plume, to incorporate biotic and abiotic degradation and transformation pathways that are not currently accounted for in site modeling activities. The total volume of the aquifer conducive to CT degradation is likely currently underestimated in existing site models, and the spatial extent of these anoxic zones is a key uncertainty governing the field-scale contribution of natural attenuation to CT plume remediation.

Implications for Cleanup and Recommendations

The laboratory-derived degradation rates reported in this study were measured under optimal closed-system anoxic conditions and should not be applied directly as input parameters to field-scale transport models. The bulk aquifer is predominantly oxic and subject to continuous advective delivery of nitrate and CT at groundwater velocities of approximately 1 foot per day.[1,2,3] For natural attenuation to translate into a meaningful reduction in plume volume, degradation rates would need to be sustained across a sufficient fraction of the aquifer volume to outpace advective CT transport. Given the carbon-limited, nitrate-rich conditions of the bulk groundwater and the spatially restricted nature of the anoxic microenvironments identified in this study, these conditions are unlikely to be broadly met without active remedial intervention.

Nevertheless, the results presented here provide the first site-specific experimental evidence that combined biotic-abiotic CT half-lives in 200-ZP-1 OU sediments are measurably shorter than the hydrolysis-only estimate, and that the geochemical and microbiological conditions necessary to support sequential dechlorination beyond CF may be present under native conditions, as suggested by indirect mass balance evidence. These findings warrant incorporation into updated groundwater fate and transport simulations and support a more rigorous evaluation of whether natural attenuation, operating in concert with the existing pump-and-treat system, could contribute to achieving the ROD cleanup objective within the designated timeframe.

To improve the accuracy of long-term plume persistence simulations and remediation planning, the following actions are recommended:

1. **Expand Porewater Oxygen Profiling.** Incorporate systematic high-resolution porewater dissolved oxygen measurements during future drilling operations to better define the spatial distribution and volumetric extent of anoxic microenvironments within the aquifer. This information is essential for constraining the fraction of the aquifer where biotic and abiotic CT degradation conditions are met.

2. **Update Fate and Transport Models.** Revise the conceptual site model and associated numerical transport models to incorporate laboratory biotic and abiotic CT degradation rates, informed by the spatial distribution of low-permeability sediment fractions and anoxic zones identified from characterization activities. Effective field-scale half-lives should be derived through calibration against observed CT and CF concentration trends in the groundwater data rather than direct application of laboratory rate constants. However, laboratory calibrations remain valuable for isolating and quantifying the influence of specific controlling factors (e.g., redox conditions, nitrate concentration, microbial community composition, sediment mineralogy) on degradation rates. Controlled laboratory relationships can then be used to inform how field-scale half-lives should be adjusted across zones of varying hydrogeological and geochemical conditions. This provides a mechanistic basis for spatially distributing attenuation parameters within the numerical

[1] DOE/RL. 2006. *Strontium-90 Treatability Test Plan for 100-NR-2 Groundwater Operable Unit*. DOE/RL-2005-96, Rev. 0. U.S. Department of Energy, Richland Operations Office, Richland, WA.
[2] Szecsody, J. E., J. S. Fruchter, J. L. Phillips, M. L. Rockhold, V. R. Vermeul, M. D. Williams, B. J. Devary, and Y. Liu. 2005a. *Effect of Geochemical and Physical Heterogeneity on the Hanford 100 D Area In Situ Redox Manipulation Barrier Longevity*. PNNL-15499. Pacific Northwest National Laboratory, Richland, WA.
[3] Williams, B. A., B. N. Bjornstad, R. Schalla, and W. D. Webber. 2002. *Revised Hydrogeology for the Suprabasalt Aquifer System, 200-West Area and Vicinity, Hanford Site, Washington*. PNNL-13858. Pacific Northwest National Laboratory, Richland, WA.

model, moving away from the oversimplification of a single uniform rate constant applied across the entire aquifer.

3. Evaluate Remedial Enhancement Options

Biotic Degradation: The results of this study demonstrate that indigenous microbial communities can drive CT dechlorination under anoxic conditions, though the extent and completeness of sequential dichlorination (beyond CF) requires further evaluation. While CT degradation was observed even under carbon-limited and elevated nitrate conditions, these factors likely constrain the rate and efficiency of biotic transformation under site-specific conditions. Electron donor supplementation and nitrate management within identified low-permeability anoxic zones therefore merit consideration as strategies to enhance, rather than initiate, natural attenuation processes already occurring within the 200-ZP-1 OU. Such enhancements could accelerate degradation rates beyond what is currently achieved under ambient geochemical conditions

Abiotic Degradation: The results also highlight the contribution of abiotic CT degradation driven by reduced iron minerals present in Hanford sediments. Sediment fractions with higher Fe^{2+} concentrations demonstrated greater abiotic degradation potential, suggesting that the spatial distribution of iron-reducing conditions within the aquifer is an important control on natural attenuation. Remedial strategies that promote and sustain iron-reducing conditions within target zones, potentially through targeted electron donor addition, could serve as a complementary approach to enhance abiotic CT degradation and warrant further field-scale evaluation.

Acknowledgments

We thank Central Plateau Cleanup Company for input and support, Andy Plymale for his technical review, and Matt Wilburn for technical editing.

Acronyms and Abbreviations

bgs	below ground surface
CF	chloroform
CT	carbon tetrachloride
DCM	dichloromethane
DNAPL	dense non-aqueous phase liquid
DO	dissolved oxygen
ECD	electron capture detector
FIO	for information only
FY	fiscal year
GC	gas chromatography
ICP-OES	inductively coupled plasma – optical emission spectroscopy
ID	identification
LOD	level of detection
MS	mass spectrometry
NDIR	non-dispersive infrared
NPOC	non-purgeable organic carbon
PTFE	polytetrafluoroethylene
PNNL	Pacific Northwest National Laboratory
OU	operable unit
RFICS	Reagent-Free Ion Chromatography System
Rlm	Ringold Lower Mud Unit
ROD	Record of Decision
Rwia	Ringold Formation Member of Wooded Island Unit A
Rwie	Ringold Formation Member of Wooded Island Unit E
SPME	solid phase microextraction
TC	total carbon
TIC	total inorganic carbon
TOC	total organic carbon

Contents

Figures

Tables

1.0 Introduction

Carbon tetrachloride (CT) contamination at the Hanford Site represents one of the most persistent and challenging groundwater remediation challenges in the U.S. Department of Energy (DOE) complex. The CT plume within the 200-ZP-1 Operable Unit (OU) originated from large-volume discharges to the subsurface during plutonium production operations in the 200 West Area between 1955 and 1973. Over decades, discharged CT migrated downward through more than 70 meters (230 ft) of unsaturated sediment to reach the underlying unconfined aquifer, where it has since spread as a persistent contaminant plume. Today, the remediation of the 200-ZP-1 OU CT plume relies on an active pump-and-treat system designed to reduce aquifer concentrations of CT, trichloroethylene (TCE), and co-occurring radionuclides. While this system has achieved meaningful reductions in contaminant mass, the long-term trajectory of the plume and the feasibility of meeting regulatory cleanup targets within the required timeframe remain critical and unresolved issues.

The 200-ZP-1 OU Record of Decision (ROD) requires that groundwater cleanup levels for all contaminants of concern, including CT, TCE, chromium, nitrate, iodine-129, technetium-99, and tritium, be achieved within 125 years (DOE 1995). The CT-specific cleanup target is 3.4 µg/L. Current groundwater modeling projections conclude that operating the pump-and-treat system at existing pumping rates for 25 years, followed by 100 years of monitored natural attenuation, will not be sufficient to achieve this target. A central reason for this shortfall is the exceptionally slow rate of CT hydrolysis under Hanford aquifer conditions (e.g., Jeffers et al. 1989). Experimental measurements have established hydrolysis half-lives of 630 years for CT and 3400 years for chloroform (CF), its primary degradation product, making hydrolysis alone an inconsequential contributor to CT mass reduction on any remediation-relevant timescale (Amonette et al. 2012).

These projections highlight a fundamental gap: If the only degradation pathway accounted for in predictive models is hydrolysis, the 125-year cleanup objective cannot be achieved regardless of pumping strategy. Critically, however, biotic and combined biotic-abiotic attenuation mechanisms, which are known to operate at substantially faster rates under appropriate geochemical conditions, had not been measured under site-specific conditions at the time these models were developed. To address this uncertainty, DOE (2020) required that site-specific degradation testing be performed to determine biotic and combined abiotic-biotic half-lives for CT and to evaluate the impact these processes may have on achieving the cleanup levels specified in the ROD. Prior work by Amonette et al. (2008, 2012) examined the potential for CT hydrolysis at the Hanford Site by conducting experiments at elevated temperatures and applying the Arrhenius equation to derive a degradation rate estimate at site-relevant groundwater temperatures. These results provided foundational hydrolysis rate parameters for CT fate and transport modeling, representing an important step in characterizing the abiotic degradation potential at the 200-ZP1-OU.

Building on this earlier work, a preliminary evaluation by Bagwell et al. (2019) reviewed biotic and abiotic mechanisms relevant to CT and CF degradation and analyzed three decades of groundwater chemistry data from the 200 West Area for evidence of natural attenuation. That assessment identified multiple converging lines of evidence for *in situ* CT degradation, including: (1) increasing concentrations of CF, which under site conditions could only have been produced through biological transformation of CT; (2) the detection of dichloromethane (DCM), which is formed exclusively during CT and CF degradation under anoxic and reduced conditions; and (3) the accumulation of nitrite as an indicator of anaerobic nitrate reduction, which is positively correlated with anaerobic CT and CF degradation. A rate assessment based on reductive dechlorination as the primary degradation pathway estimated a bulk aquifer CT half-life of approximately 400 years, with the combined activity of other degradation processes potentially achieving a half-life between 100 and 400 years.

While these estimates represent a substantial improvement over the hydrolysis-only projection, the values in Bagwell et al. (2019) were derived from field-scale indicator chemistry at the bulk plume scale and were not measured under controlled laboratory conditions. The laboratory half-lives reported in the present study were measured under optimized anoxic batch conditions and represent upper-bound intrinsic degradation potential rather than effective field-scale rates. These two categories of estimates are not directly comparable and must each be interpreted within their respective methodological contexts. Site-specific laboratory measurements of degradation rates were identified as a necessary next step to reduce this uncertainty and provide a defensible quantitative basis for updated fate and transport modeling.

This report documents the design, execution, and results of laboratory experiments conducted on Hanford sediment cores to characterize site-specific CT degradation potential within the 200-ZP-1 OU. The experiments were designed to (1) evaluate site-specific sediments for their capacity to support combined biotic-abiotic and purely abiotic degradation of CT and CF, and (2) measure degradation rates for these processes under controlled laboratory conditions using site-specific sediments and groundwater. Sediment cores were collected from both the high-concentration source zone and the lower-concentration perimeter of the 200 West Area CT plume to capture the range of geochemical and mineralogical conditions relevant to natural attenuation across the plume. This spatial sampling strategy was designed to evaluate whether CT degradation capacity differs systematically as a function of contaminant loading history, redox exposure, and mineralogical character between the source zone and plume perimeter, and to identify geochemical indicators that could be used to predict degradation potential at unsampled locations within the aquifer. The conceptual model for CT and CF degradation that guided experimental design holds that these processes primarily occur in anoxic, reduced zones within low-permeability sediments (e.g., silt and clay lenses) and within deeper geological units where reducing conditions are more likely to be sustained.

The investigation was conducted in two sequential phases:

- **Phase I** was a scoping study performed in fiscal year (FY) 2024 using freshly collected core material from the high-concentration zone of the 200-ZP-1 OU plume (C9996, C9739) and stored core material from the low-concentration plume perimeter (D0082, D0083). Batch experiments were spiked with a CT stock solution to achieve site-specific groundwater concentrations, and headspace gases were analyzed for evidence of CT degradation by solid phase microextraction (SPME) with gas chromatography–mass spectrometry (GC/MS). While Phase I successfully established the feasibility of the experimental approach and provided a qualitative indication of CT degradation potential in site-specific sediments, the SPME-GC/MS analytical method proved challenging for measurement precision, particularly at the low CT concentrations characteristic of the plume perimeter boreholes.
- **Phase II** was conducted in FY25 using additional core material obtained from active drilling operations within the high-concentration zone of the 200-ZP-1 OU plume (C9993, D0474). Building directly on the lessons learned in Phase I, Phase II incorporated several critical improvements: Pacific Northwest National Laboratory (PNNL) staff worked onsite with the drill team to preserve core materials and minimize air exposure immediately upon retrieval; laboratory procedures and experimental methodologies were fully standardized; and the gas chromatograph was equipped with an electron capture detector (ECD), providing substantially greater sensitivity and selectivity for chlorinated methane analysis compared to the SPME-GC/MS system used in Phase I.

Together, these two phases provide a refined and increasingly quantitative characterization of site-specific CT degradation potential that forms the empirical foundation for updated natural attenuation assessments within the 200-ZP-1 OU.

2.0 Degradation Pathways and Experimental Design

2.1 CT Degradation Pathways

Three broad categories of processes can degrade CT in the subsurface: hydrolysis (defined as CT reacting with water), abiotic transformation (defined as mineral mediated degradation of CT), and biotic transformation (defined as enzymatic degradation of CT), each of which operates through distinct mechanisms and at characteristically different rates (Figure 1). In practice, these pathways are not mutually exclusive and are more likely to act in concert, collectively contributing to the CT mass reduction in the subsurface. The relative contribution of each pathway to the overall attenuation of CT will vary spatially and temporally depending on local geochemical conditions, minerology, and microbial community composition at any given location in the aquifer (Bagwell et al. 2019). Understanding these relative contributions under site-specific conditions is essential for predicting the long-term fate of CT in the 200-ZP-1 OU aquifer and evaluating whether natural attenuation can meaningfully contribute to achieving the ROD cleanup objective within the designated timeframe.

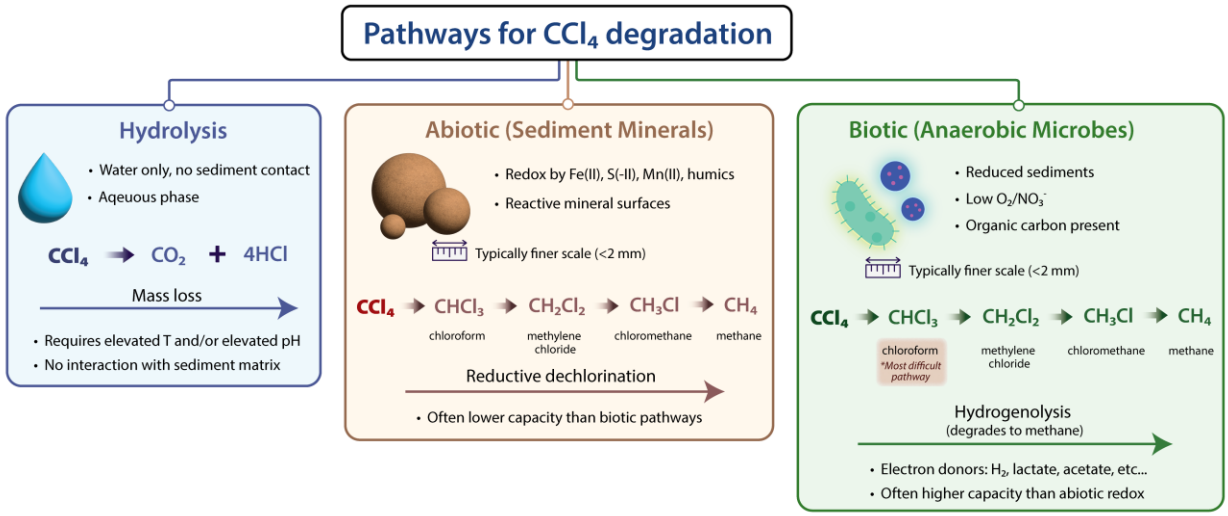

Figure 1. Schematic representing different processes for CT (CCl_4) degradation.

Hydrolysis of CT proceeds abiotically through reaction with water, producing CO_2 as the primary product. This pathway has been experimentally characterized for Hanford groundwater conditions, yielding a half-life of 630 years for CT and 3400 years for CF (Amonette et al. 2012). These rates are too slow to contribute meaningfully to CT mass reduction on remediation-relevant timescales and establish a lower bound on the transformation rates that must be achieved by other pathways if the 125-year cleanup objective is to be met.

Abiotic and biotic degradation pathways of CT are more varied and have been reviewed in detail by Bagwell et al. (2019). The predominant transformation pathway, irrespective of whether the catalyst is biological or mineralogical, occurs under anoxic, reduced conditions and involves the stepwise reductive dechlorination of CT to progressively less chlorinated methane compounds. This sequential pathway proceeds from CT through CF, DCM, and chloromethane, ultimately yielding methane (CH_4) and carbon dioxide (CO_2) as terminal products (Figure 1). Under suitable geochemical conditions, the rate of this process is generally limited by two factors: (1) the availability of organic carbon, which serves as the electron donor to fuel microbial respiratory pathways, and (2) the abundance of reactive mineral surfaces capable of participating in abiotic electron transfer reactions. Carbon stimulated CT degradation has been

previously demonstrated in Hanford sediments (Brouns et al. 1990; Hooker et al. 1994; Koegler et al. 1989; Last et al. 1991; Last and Rohay 1991; Niemet and Semprini 2005; Petersen et al. 1994; Sherwood et al. 1998; Skeen et al. 1992; Truex et al. 1994, 1996, 2001), confirming that the geochemical and biological prerequisites for this pathway exist at the site. However, the relative contributions of native biotic and abiotic pathways to CT natural attenuation, and the rates at which these processes operate under site-specific conditions, had not been directly measured prior to this study.

Biotic CT degradation most commonly occurs through anaerobic co-metabolism during microbial denitrification, in which CT is reductively dechlorinated as a secondary reaction coupled to the oxidation of organic carbon with nitrate serving as the primary terminal electron acceptor. This process typically results in the formation and accumulation of CF as the initial transformation product. CT degradation activity under this pathway is sensitive to, and can be inhibited by, ambient nitrate concentrations. This inhibitory relationship arises because NO_3^- and CT are both highly oxidized compounds that compete as terminal electron acceptors for cellular reducing equivalents. An analogous competition occurs in the abiotic system, where NO_3^- and CT compete for electrons from reduced Fe(II) mineral surfaces and dissolved metal complexes (Bagwell et al. 2019; Kriegman-King and Reinhard 1994; Zhang et al. 2025).

The extent to which this competition suppresses CT reduction depends on the relative concentrations, thermodynamics, and surface-specific reaction kinetics governing each competing reduction pathway. The thermodynamic favorability of nitrate vs. CT as an electron acceptor varies depending on the specific nitrogen reduction product (N_2 vs. NH_4^+) and the redox potential of the specific Fe(II) mineral phase involved. Manganese could participate as a redox shuttle in CT-to-CF reduction only in a mixed-valence, surface-associated, or ligand-stabilized system with an independent electron donor (e.g., O'Loughlin et al. 2022). Dissolved Mn(II) or ordinary Mn(II) mineral surfaces alone are unlikely to mediate the reaction significantly. Previous studies conducted at Hanford (Petersen et al. 1994; Skeen et al. 1994; Franzen et al. 1997; Peyton 1996; Hooker et al. 1998) indicate that maximum sustained CT reduction is achieved when NO_3^- levels are relatively low, on the order of 100 mg/L or less, and periodically depleted to approximately 10 mg/L (Sherwood et al. 1996). These findings have direct relevance to the 200-ZP-1 OU, where groundwater nitrate concentrations are elevated across much of the plume and represent a primary geochemical constraint on both biotic and abiotic CT degradation.

2.2 Experimental Design and Objectives

The objectives of this study were to (1) measure biotic and abiotic rates of CT degradation under anaerobic conditions using site-specific sediments and groundwater and (2) determine whether natural attenuation processes could contribute meaningfully to the remediation of the 200-ZP-1 OU within the designated cleanup timeframe. To support these objectives, a combination of degradation batch experiments and sediment and groundwater characterization activities were designed and executed as summarized in Table 1. Detailed methodology is provided in Appendix A.

Site-specific groundwater and sediment characterization data are a critical component of this study because geochemical and mineralogical properties directly govern the activity and rate of both biotic and abiotic CT degradation pathways. Groundwater anion chemistry, particularly nitrate and nitrite concentrations, provides evidence of the prevailing redox state of the aquifer and informs on the degree to which nitrate competition may inhibit CT transformation. Dissolved and sediment-bound organic carbon measurements constrain the availability of electron donors necessary to sustain microbial activity. Particle size distribution data identify the volume fraction of fine-grained, low-permeability sediment, which is most likely to host anaerobic microenvironments conducive to CT degradation. Mineralogical characterization by powder X-ray diffraction (pXRD) provides a general compositional description of the sediment matrix, while targeted extraction and quantification of Fe and Mn redox species directly constrain the abiotic reduction capacity of site-specific mineral assemblages.

Batch degradation experiments were designed to measure CT transformation rates under two experimental conditions. Combined biotic-abiotic experiments evaluated the CT degradation potential of redox-preserved sediments and native microbial communities attached to site-specific sediments under anoxic conditions, without supplementation of organic carbon or other electron donors (note: headspace did contain 2% H_2). These experiments measure the maximum native biological and mineralogical CT transformation capacity of the sediments as collected. Abiotic experiments employed chemical inhibition of biological activity to isolate the contribution of mineral-mediated electron transfer reactions to CT transformation. Physical and chemical treatments were used as the biological inhibitor in abiotic treatments. Oxidized sediment controls, in which sediments were pre-exposed to air prior to chemical sterilization, were included to evaluate the dependence of CT degradation on reduced, anoxic conditions. Both biotic and abiotic CT transformation pathways require reduced conditions to proceed, and the introduction of oxygen through air exposure is expected to inhibit both classes of reaction. Conservation of CT mass in air-exposed sediment treatments relative to companion anoxic treatments therefore confirms that the observed CT degradation is attributable to reduction processes that are operative only under anoxic conditions, whether biotic, abiotic, or a combination. All batch experiments were initiated by spiking with a prepared CT stock solution to achieve site-specific CT concentrations representative of the groundwater conditions at each borehole location.

There are two key differences between the batch experimental system and field conditions that are particularly important when interpreting and upscaling these results. First, the batch experiments are closed systems in which the primary competing electron acceptor, nitrate, is consumed but not replenished. Under field advective flow conditions, groundwater transport continuously resupplies nitrate and oxygen, which imposes an inhibitory effect on CT reduction. The progressive depletion of nitrate within the closed batch system therefore creates conditions that become increasingly permissive for CT degradation over time, for both biotic and abiotic pathways.

Second, the sediment-to-water ratios in the batch experiments, approximately 1:1 to 1:2 by mass, are substantially higher than those encountered under field aquifer porosity conditions of approximately 10 to 30% (DOE/RL 2019). This means that both the reactive mineral surface area available for abiotic Fe(II)-mediated CT transformation and the sediment-associated microbial biomass available for biotic degradation are proportionally greater per unit volume of pore water in the batch system relative to the field aquifer. The degradation rates measured here therefore represent an upper bound on what would be expected under field conditions at equivalent CT concentrations. Correcting laboratory-derived rate constants for sediment-to-water ratio differences is recommended as part of any future upscaling efforts.

Table 1. Description of experimental and characterization activities performed during the CT degradation evaluation studies.

Experiment Designation	Measurement	Purpose
Combined biotic-abiotic degradation	CT and CF concentration over time	Reduction of CT and formation of CF under anaerobic conditions is evidence of biotic reductive dichlorination.
Abiotic degradation	CT and CF concentration over time	Reduction of CT after sterilization of microbes is evidence of abiotic degradation.
Solid-state characterization • Biogeochemical conditions in the environment could contribute to degradation based on known pathways for biotic and abiotic degradation of CT • Identifying environmental controls on CT degradation and any correlations could inform up-scaling of results	Anions (NO_3^-, NO_2^-, SO_4^{2-})	Microbial nitrate respiration is energetically favorable to CT. Measuring anions allows for a better understanding of site heterogeneity and zones of high relative NO_3^-/ NO_2^- levels
	Particle size distribution	Anaerobic degradation activity is associated with fines and low-K zones and interfaces. This provides for a better understanding of the volume % where degradation is occurring.
	Total carbon (TIC, TOC)	CT biological degraders require electron donors for energy. Understanding the type and quantity will help inform system capacity for sustained CT attenuation.
	Mineralogy	Provides a general mineralogical description of samples by formation and allows for comparison of consistency between other Hanford Site sediments.
	Fe/Mn species	Abiotic transformations with Fe(II) containing minerals may play a significant role in natural attenuation of CT and CF; redox status indicators.
Groundwater characterization	Anions (NO_3^-, NO_2^-, SO_4^{2-})	Groundwater NO_3^-/NO_2^- provides evidence of anaerobic conditions and processes. CT degradation is sensitive to NO_3^- concentration.
	Total carbon (TIC, TOC)	Organic carbon provides carbon and energy for biological processes, i.e., NO^{3-} / CT degradation.

TIC = total inorganic carbon; TOC = total organic carbon

3.0 Site-Specific 200-ZP-1 OU Samples

Site-specific 200-ZP-1 OU samples that were located within the CT plume were used for the degradation experiments summarized in this report. Figure 2 shows the 2023 interpolated CT plume alongside the locations of wells and stratigraphic units where experiments occurred. The overall investigation occurred in two phases designated as a Phase I (performed in FY24) and Phase II (performed in FY25).

In Phase I, core samples from four wells, 299-W11-98 (C9739), 299-W14-24 (C9996), 699-46-70 (D0082), and 699-45-67C (D0083), were evaluated. Drilling of 299-W14-24 was completed in August 2023, and drilling of 299-W11-98 was completed in November 2023. These monitoring wells are located within the high-concentration zone of the CT plume (up to 1000 µg/L). Wells 699-46-70 and 699-45-67C are monitoring wells that were drilled in 2020. These wells are within the low-concentration zone of the CT plume (less than 50 µg/L). These cores were received at PNNL in 2021 and have been stored unopened at -80 °C.

Phase II included core samples from two wells, 299-W11-100 (C9993) and 299-W11-116 (D0474), within the high-concentration zone CT plume (up to 1000 µg/L). Well 299-W11-100 is a monitoring well and 299-W11-116 is an extraction well. These cores were stored at 4 °C.

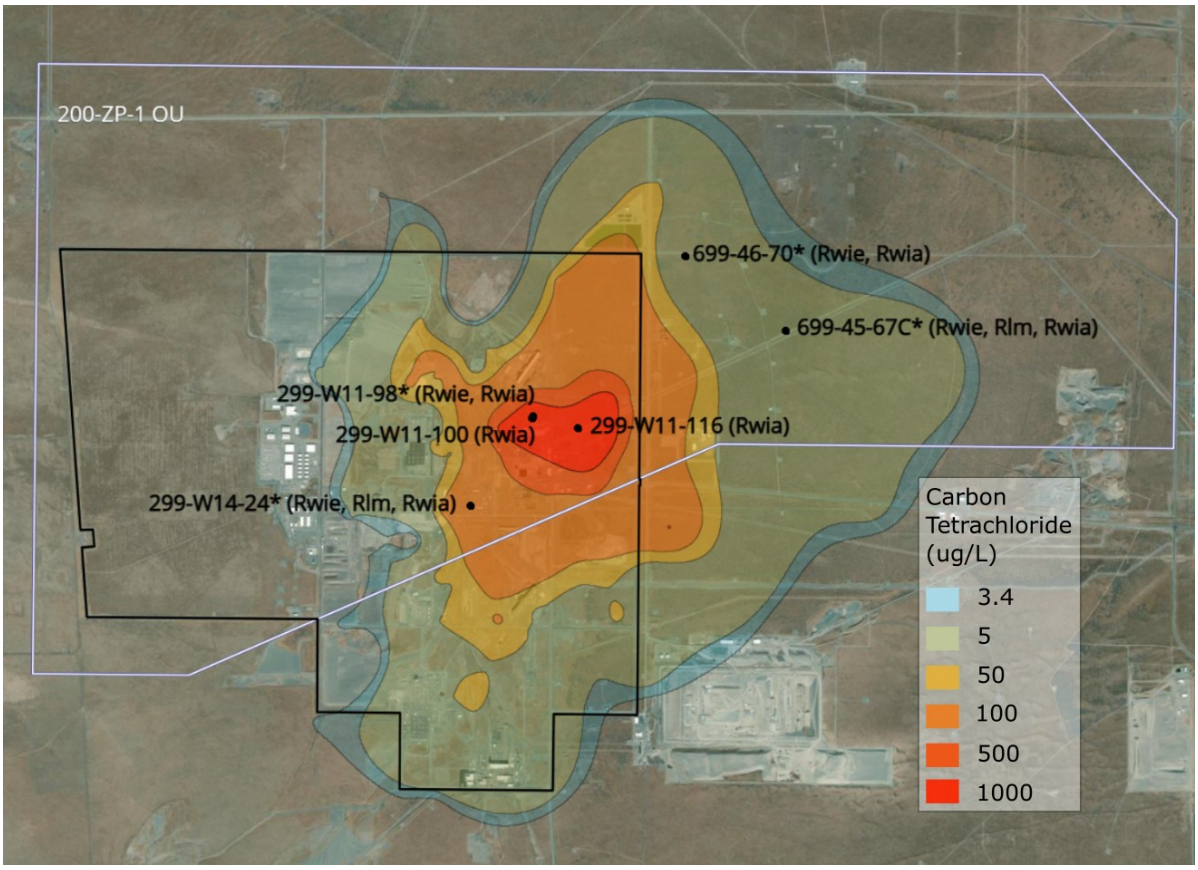

Figure 2. Well locations within the carbon tetrachloride plume (Socrates MARINuS v6.0.0 2023) where core samples were extracted for degradation testing. Stratigraphic units where cores extracted are noted. Well labels with an asterisk (*) indicate samples that were a part of Phase I.

Well drilling at Hanford is typically performed using cable tool or rotary drilling methods. When a target sampling interval is reached, intact sediment samples are usually obtained by driving a split-spoon sampler containing 4-in.-outer-diameter Lexan or stainless-steel liners placed end-to-end into the formation. After the samples have been collected, the sampler is retrieved and opened at the ground surface. The liners, which are either 1 ft or 6 in. long, are removed from the sampler, capped, taped to prevent sediment and moisture loss, and labeled with the sample ID and pertinent information.

It is important to note that CT is a volatile chemical, and losses inevitably occur during drilling, coring, sample preparation, and storage. To preserve the representative nature of CT concentrations, samples were spiked with site-specific concentrations to evaluate degradation.

3.1 Phase I

To determine site-relevant CT concentrations for Phase I sediment testing, we analyzed a decade of groundwater data from the 200-ZP-1 OU. We first established average bulk aquifer concentrations [Ringold Formation Member of Wooded Island Unit E (Rwie)] for wells within both the high-concentration source zone and the low-concentration plume fringe. These base concentrations were then adjusted for specific geologic formations [Ringold Lower Mud Unit (Rlm) and Ringold Formation Member of Wooded Island Unit A (Rwia)]. Because field observations showed that CT levels significantly decrease within the low-permeability Rlm unit and deep within the aquifer (Rwia), we reduced the spiking concentrations by half for samples from these specific units.

Frozen cores (699-46-70 and 699-45-67C) were prepared for testing by cutting the Lexan liner along its vertical axis and transferring the intact core to an anaerobic chamber (98% N_2, 2% H_2) to minimize oxidation during thawing and core preparation. Once the core equilibrated (~24 hours), it was carefully separated along its vertical axis, documented, and examined for heterogeneities and fines. Half of the separated core was used for characterization analyses and the other half was used for degradation batch experiments. Additional split-spoon intervals were available for 299-W14-24 such that characterization analyses and degradation batch experiments could be performed on separate intervals. Intervals B were used for characterization experiments and intervals C were used for characterization experiments. For 299-W11-98, a single core was available at each depth interval. Therefore, the procedure used for frozen cores (699-46-70 and 699-45-67C) was used for 299-W11-98.

The characterization suite of analyses performed on site-specific samples included solid phase characterization (S_c) (quantification of Fe and Mn reactive mineral phases, water extractable anions, particle size distribution, XRD) and groundwater characterization (GW_c) (organic carbon content, and anions). Laboratory testing was performed for biotic degradation (B_d) mechanisms that transform CT to CF and abiotic degradation (A_d) for reduction of CT.

Table 2. Selected core sediments from the 200-ZP-1 OU, Phase I for laboratory testing of CT degradation.

Borehole ID & Well Name	Unit	Sample ID	Interval	Sample Depth (ft bgs)	Analyses	CT Spiking Concentration (µg/L aqueous)
D0082 (699-46-70)	Rwie	B3W6C7	A	313.0 – 313.5	S_c, GW_c, A_d, B_d	50
	Rwia	B3W6F2	B	346.8 – 347.3	S_c, GW_c, A_d, B_d	25
		B3W6H5	B	366.9 – 367.5	S_c, GW_c, A_d, B_d	25
		B3W6J5	B	400.9 – 401.4	S_c, GW_c, A_d, B_d	25
D0083 (699-45-67c)	Rwie	B3WXX5	B	312.83 – 313.33	S_c, GW_c, A_d, B_d	50
	Rlm	B3WXM7	A	330.35 – 331.15	S_c, GW_c, A_d, B_d	25
		B3WXN3	B	350.54 – 351.04	S_c, GW_c, A_d, B_d	25
		B3WXN9	B	367.1 – 367.6	S_c, GW_c, A_d, B_d	25
	Rwia	B3WXP5	B	377.0 – 377.5	S_c, GW_c, A_d, B_d	25
C9996 (299-W14-24)	Rwie	B48BN8	C	400.4 – 400.9	S_c, GW_c	-
			B	400.9 – 401.4	A_d, B_d	700
	Rlm	B48BN9	C	446.1 – 446.6	S_c, GW_c	-
			B	446.6 – 447.1	A_d, B_d	350
	Rwia	B48BP0	C	521.0 – 521.5	S_c, GW_c	-
			B	521.5 – 522.0	A_d, B_d	175
C9739 (299-W11-98)	Rwie	B48BN5	B	417.15 – 419.65	S_c, GW_c, A_d, B_d	950
	Rwie/a	B48BN6	B	457.07 – 459.57	S_c, GW_c, A_d, B_d	800
	Rwia	B48BN7	B	497.17 – 499.67	S_c, GW_c, A_d, B_d	800

There was considerable variation in the measured CT concentrations relative to the intended CT starting concentration, which was pre-determined by trends in groundwater concentrations relative to borehole location in the 200-ZP-1 OU CT plume and the sampled depth. This variation was attributed to multiple factors, including inconsistencies in the preparation of standard solutions, performance longevity of SPME fibers, and precision of the GC/MS particularly at low CT/CF concentrations. As such, the CT degradation results from Phase I are interpreted qualitatively as an initial evaluation of site-specific sediments and groundwater for CT attenuation potential.

Improvements were implemented in Phase II based on the lessons learned in Phase I. As a consequence of these analytical limitations, no quantitative rate constants derived from Phase I combined biotic-abiotic experiments are considered sufficiently reliable to serve as direct inputs to fate and transport models. These results are interpreted as qualitative evidence of CT degradation potential only, and Phase II was designed specifically to provide the quantitative rate estimates required for modeling.

3.2 Phase II

In 2024, two wells were drilled in the high CT plume in 200 West as part of the *Comprehensive Environmental Response, Compensation and Liability Act* Performance Monitoring Plan. As part of these operations, opportunistic core samples were acquired for degradation testing from extraction well 299-W11-116 (D0474) and monitoring well 299-W11-100 (C9993). A full split spoon liner was received from both these wells: in 299-W11-100 (C9993) within Rwie and in 299-W11-116 (D0474) within Rwia.

Except for the shallowest sample depth at 299-W11-100 (C9993), PNNL was on site during drill operations at both wells to (1) measure pore water dissolved oxygen (DO) concentrations since this influences redox conditions and is an indicator of anerobic conditions and (2) preserve core material against unwanted oxidation for follow-on anerobic experiments.

In situ DO was measured using CHEMETS Dissolved Oxygen Kit (R-7512) colorimetric kits. The kit consists of a glass ampule under vacuum filled with a reagent that produces a light-to-dark blue color when DO is present in the pore water. DO is quantified by comparing the color of the sample to the color of prepared standards. At each designated sample depth, Lexan-lined split-spoon samples containing four 6-in. cores were brought to PNNL staff at a safe distance from drilling operations. In the interim between sample retrieval and the DO measurement, air exposure and some drainage occurred. As a result, some samples had an insufficient amount of free pore water to measure, or free pore water contained sediment that impacted the color reading. Additionally, DO measurements may have been impacted by the air rotary drilling method used specifically for 299-W11-116 (D0474). However, because air exposure and partial drainage occurred between core retrieval and DO measurement, and because air rotary drilling was used specifically at 299-W11-116 (D0474), the reported DO values likely represent upper bounds on true *in situ* porewater oxygen concentrations. Actual porewater conditions at the time of core retrieval may have been more reducing than the measurements indicate. These results are therefore interpreted as qualitative indicators of low-oxygen to anoxic conditions rather than precise *in situ* DO measurements. Table 3 presents an inventory of received cores that were used for laboratory experiments and contains pore water DO in cores where this could be measured.

In the field, PNNL preserved cores in metallized bags. Bags were filled with liquid nitrogen, which was allowed to vaporize to nitrogen gas to remove oxygen, sealed, and then stored at 4,°C until laboratory experiments began. Note: DO measurements on the cores that were designated for degradation experiments were not attempted to preserve field conditions.

In addition to the primary combined biotic-abiotic and abiotic degradation experiments described above, two categories of experimental controls were conducted during Phase II. First, oxidized sediment control treatments were prepared by pre-exposing site sediments to laboratory air for a minimum of 48 hours prior to sodium azide addition. These treatments were designed to confirm that CT degradation observed in anoxic abiotic treatments is dependent on the reduced geochemical state of the sediment mineral assemblage and is eliminated upon oxidation of reactive mineral surfaces. Second, replicate abiotic degradation experiments were conducted at an initial CT concentration of 20 µg/L, approximately 40-fold lower than the primary 800 µg/L experiments. This was done to evaluate whether abiotic CT transformation rates are suppressed at CT concentrations approaching the lower end of the plume concentration range where the molar ratio of competing nitrate to CT is substantially higher. Results from both control experiment categories are discussed in Section 5.1.2.

The characterization suite of analyses performed on site-specific samples included solid phase characterization (Sc) (quantification of Fe and Mn reactive mineral phases, water extractable anions, particle size distribution) and groundwater characterization (GWc) (organic carbon content, and anions). Laboratory testing was performed for abiotic degradation (Ad) and biotic degradation (Bd) mechanisms that transform CT to CF. Intervals A and B for sample B4JT78 were combined.

Table 3. Selected core sediments and associated DO pore water measurements from the 200-ZP-1 OU, Phase II laboratory testing of CT degradation. DO is presented for information only (FIO). All batch degradation experiments conducted in Phase II were spiked to an initial starting CT concentration of 800 µg/L, aqueous.

Borehole ID / Well Name	Unit	Sample ID	Interval	Porewater DO (ppm)[(a)]	Sample Depth (ft bgs)	Analyses
C9993 (299-W11-100)	Rwie	B4JT76	B	-	335.6-336.1	A_d, B_d
			A	2-3	336.1-336.6	S_c, GW_c
		B4JT77	C	-	406.7-407.2	A_d, B_d
			B	-	407.2-407.7	S_c, GW_c
		B4JTM3	C	2[(b)]	415.4-415.9	S_c, GW_c
			B	-	415.9-416.4	A_d, B_d
		B4JTM4	C	2	430.7-431.2	S_c, GW_c
			B	-	431.2-431.7	A_d, B_d
D0474 (299-W11-116)	Rwia	B4JT78	A/B	-	457.60-458.60	A_d, B_d, S_c, GW_c
		B4JT79	C	-	478.1-478.6	S_c, GW_c
			B	-	478.6-479.1	A_d, B_d
		B4JTM5	B	-	498.3-498.8	A_d, B_d
			A	3	498.8-499.3	S_c, GW_c

(a) Porewater DO represented by '–' indicates that no measurement was attempted at that interval. Measurements were not attempted at degradation experiment intervals to avoid disturbing core conditions prior to laboratory incubation. DO measurements shown were collected from companion characterization intervals and are FIO for context only. These materials were not used as experimental controls and should be interpreted with caution given the potential for partial air exposure between core retrieval and measurement.

(b) Other DO measurements were collected for Intervals A and D and were 3 ppm. For all samples, the core was muddy, and the soil impacted color interpretation.

4.0 Phase I Results

4.1 Degradation Experiments

4.1.1 Combined Biotic-Abiotic

Measured CT data were evaluated against a first-order degradation kinetic model to assess the rate and extent of combined biotic-abiotic CT transformation in site-specific sediments. Table 4 summarizes the fitted parameters, including the median rate constant (K), 95% confidence intervals, R^2 goodness-of-fit values, and estimated half-lives. CT mass over time for all biotic-abiotic batch experiments is shown in Figure 4. To provide a refined interpretation of these results, the following summary accounts for potential instrument variability by closely examining the relationship between initial CT mass and final measured outcomes across all borehole sediments. Overall, combined biotic-abiotic reduction of CT showed significant variability in performance across the four boreholes, likely reflecting differences in microbial community density, site-specific geochemistry, and the supporting mineralogical matrix.

Table 4. Fitted biotic-abiotic parameters to a first order degradation kinetic model. Standard deviations are shown beside each parameter. The goodness of fit is represented as R^2 and the half-life $t_{1/2}$ is shown.

Borehole (Core ID)	CT (µg/L)	K_{median} (K, 95% CI)	R^2 (fit confidence)	λ (days)	λ 95% CI (days)
D0082 (B3W6C7)	6.25	0.076 (-0.404-0.164)	1.0 (Low)	7.453	-2.172-29.210
D0082 (B3W6F2)	6.25	0.003 (-0.004-0.034)	0.913 (Low)	NA	NA
D0082 (B3W6H5)	6.25	0.006 (-0.003-0.035)	0.903 (Low)	NA	NA
D0082 (B3W6J5)	6.25	0.007 (-0.002-0.037)	0.924 (Low)	NA	NA
D0083 (B3WXM7)	25	-0.009 (-0.041-0.081)	1.0 (Low)	NA	NA
D0083 (B3WXN3)	12.5	-0.008 (-0.031-0.080)	1.0 (Low)	NA	NA
D0083 (B3WXN9)	12.5	-0.007 (-0.021-0.043)	0.830 (Low)	NA	NA
D0083 (B3WXP5)	25	-0.004 (-0.018-0.047)	0.804 (Low)	NA	NA
D0083 (B3WXX5)	25	0.017 (-0.005-0.109)	1.0 (Low)	25.262	-707.361-686.776
C9739 (B48BN5)	700	0.002 (0.00-0.005)	0.286 (Low)	345.454	-1237.997-2838.377
C9739 (B48BN6)	350	0.002 (0.00-0.004)	0.203 (Low)	406.361	-1797.891-2881.674
C9739 (B48BN7)	175	0.002 (0.00-0.029)	0.081 (Low)	NA	NA
C9996 (B48BN8)	800	0.015 (-0.02-0.042)	0.965 (Low)	43.286	-22.507-83.053
C9996 (B48BN9)	800	0.005 (-0.005-0.031)	0.270 (Low)	NA	NA
C9996 (B48BP0)	950	-0.005 (-0.015-0.022)	0.428 (Low)	NA	NA

NA indicates that a half-life estimation could not be calculated due to the poor fit of the data to the first order degradation model. Detailed methodological information is provided in Appendix A.

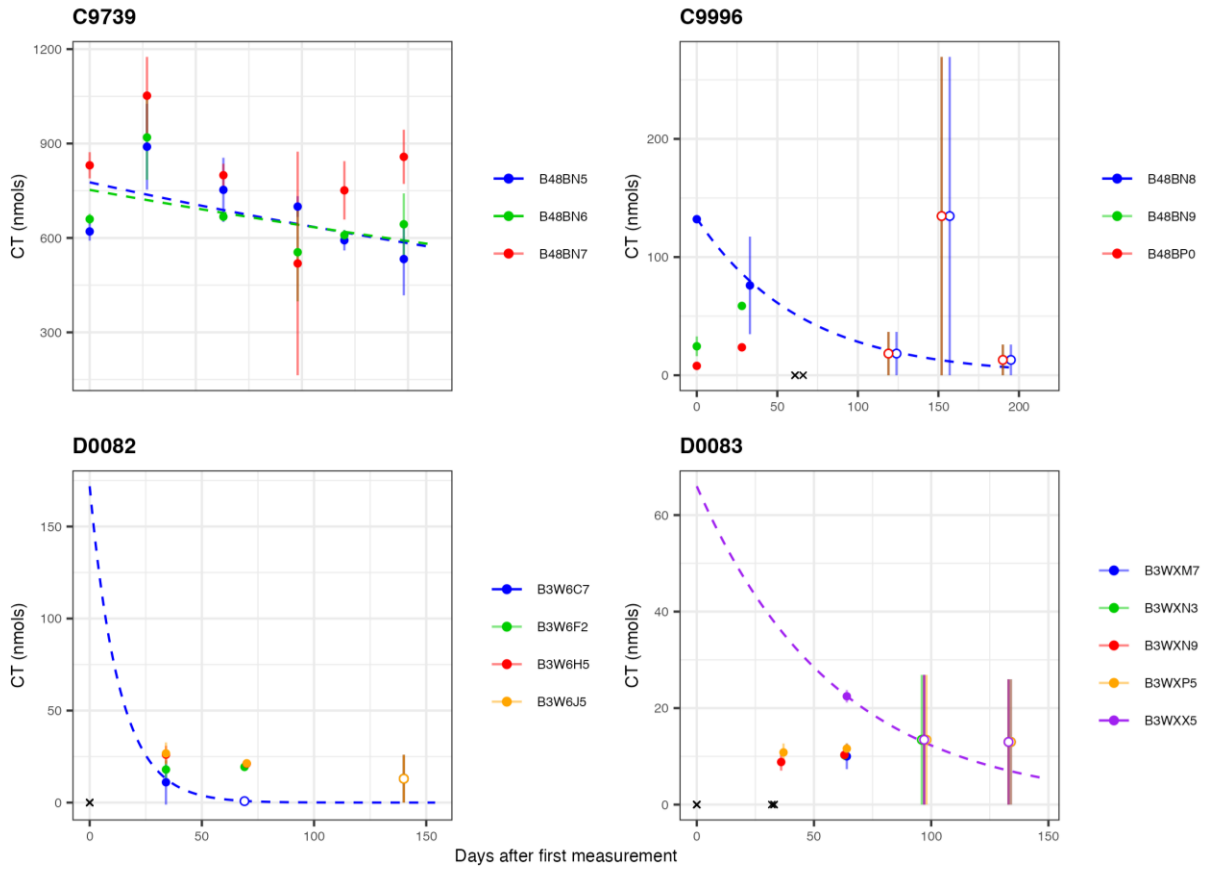

Figure 3. CT degradation profiles from combined biotic-abiotic experiments on Hanford cores with a 1:2 (10 g : 20 mL) sediment-to-groundwater ratio, grouped by well ID. First order degradation rate model fits are plotted where CT degradation was statistically significant: solid line (95% confidence) or dotted line (90% confidence). Filled circles = detections with error bars to capture propagated concentration standard deviation; open circles = values below level of detection (LOD) where error bars span 0 to LOD range with the point plotted at LOD/2; black 'x' at y=0 indicates sample was measured but excluded due to failed calibration quality control. Individual plots of CT and CF are provided for all treatments and boreholes are provided in Appendix B.

Borehole D0082. Despite starting with the lowest initial CT mass of any borehole (~5 to 11 nmol), D0082 sediments exhibited little indication of combined biotic-abiotic degradation. While some scatter is apparent in the early timepoints, the measured responses are near the detection limit of the SPME-GC/MS instrument and do not provide a strong or consistent signal of CT mass removal. Rate constants for all four D0082 intervals are near zero with wide confidence intervals that encompass negative values, and no statistically meaningful half-life could be calculated for any interval (Table 5). These results are interpreted as analytically inconclusive rather than as evidence of an absence of degradation potential, as the low initial CT concentrations used for this borehole (6.25 µg/L) were poorly suited to the detection capabilities of the Phase I analytical method.

Borehole D0083. This borehole displayed the least combined biotic-abiotic activity of all Phase I sediments. Samples B3WXN3 and B3WXN9 showed virtually no change in CT mass over the duration of the experiment, while B3WXX5 showed only a marginal decline. Rate constants for all five D0083 intervals are near zero or slightly negative, with confidence intervals spanning both positive and negative

values (Table 5). The proximity of all data points to the regression line, combined with the low R^2 values and the absence of detectable CF accumulation, suggests that any apparent reduction in CT mass is more likely attributable to instrument variability than to a genuine degradation signal. As with D0082, the low initial CT concentrations (12.5 to 25 µg/L) used for D0083 experiments limited the analytical resolution available to detect small changes in CT mass.

Borehole C9739. Experiments were initiated with the highest initial CT mass across all Phase I samples, ranging from approximately 130 to 160 nmol, which should have provided the most favorable conditions for detecting a combined biotic-abiotic degradation signal. While the regression lines for the three sediment intervals (B48BN5, B48BN6, and B48BN7) suggest a slight downward trend, a direct comparison between CT mass at day 0 and the final measured mass at day 37 reveals a high degree of stability across all three intervals. Final measurements remain near initial starting concentrations, and the estimated rate constants are uniformly low (0.002 day^{-1}) with very low R^2 values, ranging from 0.08 to 0.29, indicating poor model fit. Where half-life values could be calculated, confidence intervals were extremely wide, spanning thousands of days in both directions (Table 5). The observed fluctuations in CT mass are therefore interpreted as analytical noise rather than evidence of sustained microbial CT reduction. The high nitrate concentration of the C9739 groundwater (256 mg/L) is consistent with this outcome, as elevated nitrate is expected to competitively suppress CT reductive dechlorination. However, the available data do not allow the relative contributions of nitrate inhibition and intrinsically low microbial CT-transforming activity to be distinguished. The absence of CT degradation in C9739 sediments may reflect either or both of these factors.

Borehole C9996. Experimental results for C9996 sediments were the most variable of the four Phase I boreholes. Sample B48BN8 exhibited a downward trend in CT mass accompanied by the concurrent accumulation of CF, providing the clearest positive signal for biotic reductive dechlorination observed in Phase I. The appearance of CF as a transformation product is a second and independent line of evidence for CT degradation, consistent with the initial step of sequential reductive dechlorination under anaerobic conditions. A nominal half-life of approximately 43 days was calculated for B48BN8; however, the rate constant confidence interval partially encompassed zero, indicating that the degradation signal cannot be statistically distinguished from zero at the 95% confidence level. This result is therefore treated as qualitative evidence of CT transformation, corroborated by concurrent CF production, rather than a quantitative rate estimate suitable for use in predictive modeling. In contrast, B48BN9 and B48BP0 ended the experiment at nearly the same CT mass as they started, with rate constants near zero and no detectable CF accumulation. The geochemically anomalous character of the C9996 groundwater, with non-detectable nitrate, may partly explain the comparatively stronger biotic signal in B48BN8, as the absence of nitrate would remove a primary inhibitor of CT reductive dechlorination. The variability among C9996 intervals may additionally reflect small-scale heterogeneity in sediment mineralogy and chemistry or microbial community composition across the sampled depth range. While the Phase I results for C9996 are insufficient to support quantitative rate estimates with confidence, the positive qualitative signal from B48BN8 established the basis for the more rigorous Phase II experimental design.

4.1.2 Abiotic

Measured CT data were fit to a first-order degradation kinetic model, where the degradation rate is proportional to the concentration of CT in the system and the effective concentration of the abiotic reactant, principally reduced Fe mineral phases, is assumed to remain constant over the experimental period. The mathematical expressions used to analyze CT degradation over time is represented in Appendix A. Table 5 summarizes the fitted parameters, including the median rate constant (K), 95% confidence intervals, R^2 goodness-of-fit values, and estimated half-lives. CT mass over time for all abiotic batch experiments is shown in Figure 6, and the complete set of individual degradation plots is provided in Appendix B.

Table 5. Fitted abiotic parameters to a first order degradation kinetic model. Standard deviations are shown beside each parameter.

Borehole (Core ID)	CT (µg/L)	K_{median} (K, 95% CI)	R^2 (fit confidence)	λ (days)	λ 95% CI (days)
D0082 (B3W6C7)	6.25	0.146 (0.082-1.132)	0.938 (High)	4.763	0.612-8.456
D0082 (B3W6F2)	6.25	0.068 (0.050-0.089)	0.974 (High)	10.143	7.801-14.00
D0082 (B3W6H5)	6.25	0.225 (0.177-0.293)	0.993 (High)	3.077	2.365-3.921
D0082 (B3W6J5)	6.25	0.014 (0.00-0.05)	0.783 (High)	47.783	1.879-378.571
D0082 (GW)					
D0083 (B3WXM7)	25	0.009 (0.007-0.013)	0.818 (High)	73.784	53.319-104.985
D0083 (B3WXN3)	12.5	0.010 (0.001-0.016)	0.681 (High)	70.754	34.197-210.105
D0083 (B3WXN9)	12.5	0.010 (0.002-0.018)	0.722 (High)	70.394	36.951-235.308
D0083 (B3WXP5)	25	0.007 (0.00-0.028)	0.731 (Low)	88.653	-381.451-814.593
D0083 (B3WXX5)	25	0.007 (0.004-0.010)	0.816 (High)	97.745	71.140-156.424
D0083 (GW)					
C9739 (B48BN5)	700	-0.001 (-0.004-0.003)	0.069 (Low)	NA	NA
C9739 (B48BN6)	350	-0.004 (-0.009-0.002)	0.166 (Low)	NA	NA
C9739 (B48BN7)	175	0.008 (0.003-0.015)	0.628 (High)	85.386	46.133-265.633
C9739 (GW)					
C9996 (B48BN8)	800	0.033 (-0.010-0.097)	0.772 (Low)	NA	NA
C9996 (B48BN9)	800	-0.008 (-0.060-0.072)	0.897 (Low)	NA	NA
C9996 (B48BP0)	950	0.019 (-0.002-0.042)	0.910 (Low)	35.278	-235.544-318.369
C9996 (GW)					

NA indicates that a half-life estimation could not be calculated due to the poor fit of the data to the first order degradation model.
GW = groundwater

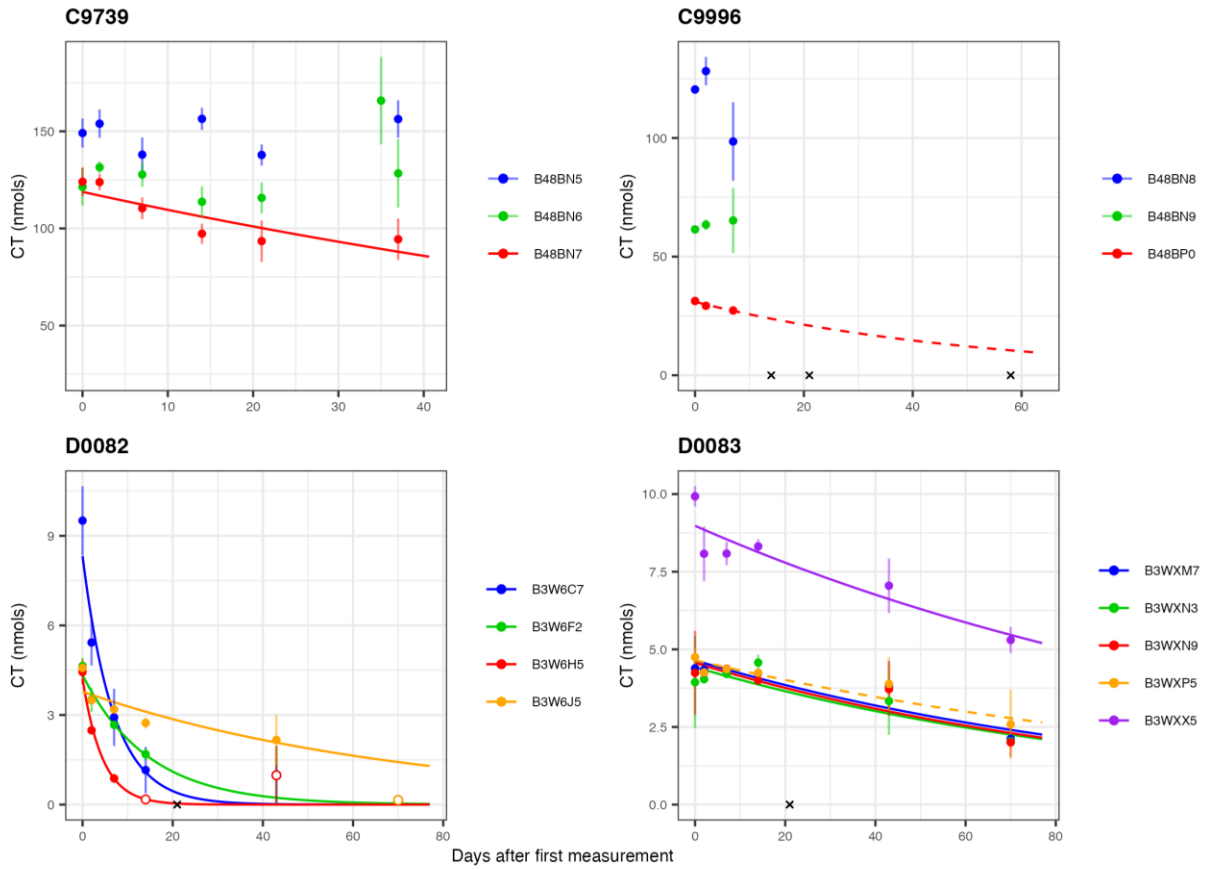

Figure 4. CT degradation profiles from abiotic experiments on cores with a 1:1 (12 g : 12 mL) sediment to groundwater ratio, grouped by well ID. First order degradation rate model fits are plotted where CT degradation was statistically significant: solid line (95% confidence) or dotted line (90% confidence). Filled circles = detections with error bars to capture propagated concentration standard deviation; open circles = values below LOD where error bars span 0 to LOD range with the point plotted at LOD/2; black 'x' at y=0 indicates sample was measured but excluded due to failed calibration quality control. Individual plots of CT and CF for all treatments and boreholes are provided in Appendix B.

Abiotic CT degradation was evaluated across four boreholes, revealing distinct kinetic behaviors and widely varying levels of reductive capacity among the sediment samples. Results are discussed by borehole below.

Borehole D0082. D0082 sediments exhibited the most aggressive abiotic CT reactivity observed in Phase I. Three of the four intervals produced well-constrained first-order rate constants with high R^2 values, indicating a strong and consistent fit to the kinetic model. Samples B3W6C7 (Rwie) and B3W6H5 (Rwia) reached near-complete CT removal within 20 to 30 days, following steep exponential decay curves with estimated half-lives of 4.8 and 3.1 days, respectively. Sample B3W6F2 showed moderately rapid degradation, with a half-life of approximately 10 days. The deepest interval, B3W6J5, was considerably less reactive, with a substantially longer estimated half-life of approximately 48 days and a wider confidence interval, though the R^2 value remained acceptable. The elevated Fe(II) content measured in D0082 acid digests, particularly in the shallower intervals, is consistent with the high abiotic reactivity observed and supports the interpretation that reduced iron mineral phases are the primary drivers of CT transformation in these sediments (Bagwell et al. 2019; Kriegman-King and Reinhard 1994; Pearce et al.

2018; Zhang et al. 2025). The higher average carbonate content of D0082 sediments (0.90 wt%) relative to other boreholes may additionally reflect the presence of Fe(II)-bearing carbonate phases, such as siderite, that could contribute reactive surface sites for electron transfer to CT.

Borehole D0083. In contrast to D0082, D0083 proved to be the least abiotically reactive borehole in Phase I, with nearly horizontal CT degradation curves across all five sampled intervals even after 70 days of reaction time. Estimated half-lives ranged from approximately 70 to 98 days for the four intervals where a half-life could be calculated, and rate constants were uniformly low, ranging from 0.007 to 0.010 day^{-1}. R^2 values were moderate for most intervals, indicating that while a first-order model provides a reasonable description of the slow decreasing trend, the overall extent of CT removal was minimal. The distinctly high mica content of the D0083 Rlm intervals, averaging over 12 wt% by XRD, is notable in this context. Although our mineralogical characterization was limited to total mica weight percentages, we can infer a lack of redox activity from broader Hanford Site characteristics. The site's mica assemblage is heavily associated with low-activity mineral fractions and the rapid surface passivation of any localized, iron-rich phases (Amonette et al. 2008, 2012; Szecsody et al. 2005ab). This systematic lack of available mineralogical Fe(II) electron donors is supported by the low Fe(II) concentrations measured in D0083 acid digests, explaining the limited overall abiotic reactivity observed.

Borehole C9739. Abiotic degradation results for C9739 were mixed across the three sampled depth intervals. Samples B48BN5 (Rwie) and B48BN6 (Rwie/a) showed near-zero or slightly negative rate constants with very low R^2 values of 0.07 and 0.17, respectively, indicating no reliable abiotic CT degradation in these intervals. In contrast, the deepest interval B48BN7 (Rwia) exhibited a more interpretable degradation trend, with an estimated half-life of approximately 85 days, a positive rate constant of 0.008 day^{-1}, and an R^2 of 0.628. This depth-dependent pattern is broadly consistent with the Fe speciation data for C9739, where B48BN7 contained both the highest total Fe (1.10 mg/g) and the most balanced Fe(II)/Fe(III) ratio (0.56/0.55 mg/g) of the three C9739 intervals, suggesting a partially reduced mineral assemblage with greater capacity for electron donation relative to the more Fe(III)-dominated shallower intervals.

Borehole C9996. Abiotic CT degradation results for C9996 were the least well-constrained of the four Phase I boreholes, with low R^2 values and wide confidence intervals for all three sampled intervals. Rate constants for B48BN8 and B48BN9 carried confidence intervals spanning both positive and negative values, precluding reliable half-life estimation for these samples. Sample B48BP0 yielded a nominally positive rate constant of 0.019 day^{-1} and an estimated half-life of approximately 35 days, but the associated confidence interval was extremely wide and partially negative, indicating high uncertainty in this estimate. The high variability and low statistical confidence of the C9996 abiotic results may reflect the geochemical heterogeneity of these sediments. Consistent with the broader conceptual model that deeper aquifer intervals are better protected from surface-derived oxidizing conditions, the deepest C9996 interval (B48BP0, 521 to 522 ft bgs) had the highest Fe(II) content of the three C9996 samples (0.93 mg/g), while the two shallower intervals (B48BN8 and B48BN9) had Fe(II) values of only 0.03 mg/g each. This depth-dependent Fe(II) pattern is consistent with a progressively more oxidized mineral assemblage toward shallower depths and provides mineralogical context for the variable abiotic reactivity observed across C9996 intervals. C9996 contained the highest feldspar and chlorite concentrations of any Phase I borehole, and while these mineral phases are not directly implicated as reductants for CT transformation, the dominance of these phases relative to Fe(II)-bearing minerals is consistent with a lower and more variable abiotic reduction capacity compared to the more reactive D0082 sediments. The low Fe(II) fractions measured in the upper two C9996 intervals (0.03 mg/g each) further support the interpretation that the abiotic redox capacity of these sediments is limited by the availability of reactive reduced mineral phases rather than by total mineral abundance.

Across all Phase I boreholes, the abiotic degradation results provide stronger and more interpretable signals than the corresponding biotic experiments, with several intervals yielding well-constrained first-order rate constants and half-life estimates. The results collectively suggest that abiotic CT degradation potential in Phase I sediments is primarily governed by the availability and speciation of Fe(II) in the reactive mineral fraction, and that differences in bulk mineralogy and chemistry between boreholes are informative as they reflect underlying differences in Fe(II) mineral abundance and accessibility.

4.1.3 Hydrolysis

Hydrolysis experiments were conducted to evaluate the contribution of abiotic aqueous-phase reactions to CT mass removal in the absence of sediment contact. Batch incubations were prepared using site-specific Hanford groundwater spiked with CT at concentrations representative of each borehole location, and CT mass was monitored over time. These experiments serve as a critical control, isolating the contribution of groundwater chemistry alone to CT transformation, providing a reference against which sediment-containing abiotic and biotic treatments can be compared.

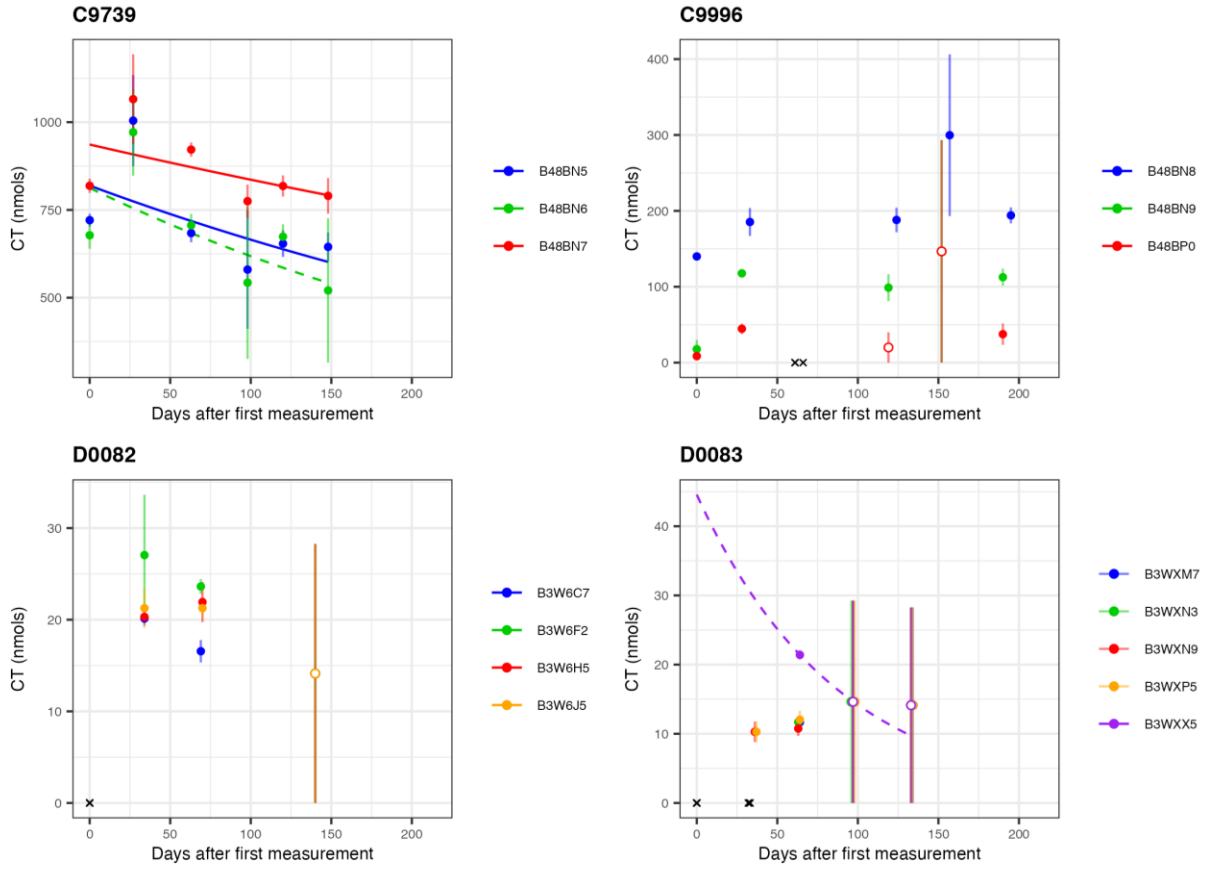

Figure 5. CT degradation profiles hydrolysis experiments in Hanford (12 mL) groundwater (no sediment), grouped by well ID. First order degradation rate model fits are plotted where CT degradation was statistically significant: solid line (95% confidence) or dotted line (90% confidence). Filled circles = detections with error bars to capture propagated concentration standard deviation; open circles = values below LOD where error bars span 0 to LOD range with the point plotted at LOD/2; black ‘x’ at y=0 indicates sample was measured but excluded due to failed calibration quality control. Individual plots of CT and CF for all treatments and boreholes are provided in Appendix B.

Results across all four boreholes show that CT mass at the start and end of the incubation period remained generally stable, despite some variability in individual measurements on certain sampling days. This temporal variability is attributed to analytical scatter rather than systematic CT mass removal, as no consistent declining trend was observed in any of the groundwater-only treatments. The most unambiguous outcomes were obtained for boreholes C9739 and C9996, where experiments were initiated at higher CT masses and incubated for 150 to 180 days. CT mass remained effectively unchanged over this extended period, providing clear evidence that hydrolysis in site-specific Hanford groundwater does not contribute meaningfully to CT mass removal on these timescales. These results are consistent with the previously reported hydrolysis half-life of 630 years estimated for Hanford groundwater conditions by Amonette et al. (2012) and confirm that hydrolysis alone is too slow to contribute to the cleanup objectives of the 200-ZP-1 OU within the designated 125-year timeframe.

For boreholes D0082 and D0083, experiments were initiated at substantially lower initial CT masses relative to C9739 and C9996. As with the biotic experiments conducted at these low concentration levels, the measured responses were near the detection limit of the SPME-GC/MS instrument, and the resulting high variability in replicate measurements prevents any definitive conclusion about CT mass removal in these groundwater-only treatments. However, the absence of any consistent downward trend in these data is broadly consistent with the stable CT mass observed in the higher-concentration C9739 and C9996 hydrolysis controls. These results then provide no basis for inferring a meaningful hydrolysis contribution at these boreholes. Taken together, the Phase I hydrolysis results establish that CT persistence in Hanford groundwater in the absence of reactive sediment is effectively complete on experimental timescales, and that the CT mass removal observed in sediment-containing abiotic and biotic treatments is attributable to mineral-mediated or microbially driven transformation processes rather than aqueous hydrolysis.

4.2 Chemical Characterization

4.2.1 Groundwater

Analysis of the four 200-ZP-1 OU groundwater samples shows a geochemical profile generally consistent with the aerobic, carbon-poor conditions. Nitrate is the primary constituent, reaching a peak concentration of 256 mg/L in well 299-W11-98, a level that is more than double the background concentrations observed in wells 699-46-70 (92.0 mg/L) and 699-45-67c (94.4 mg/L). Notably, well 299-W14-24 stands out as a geochemical outlier, with non-detectable nitrate and significantly lower chloride (4.4 mg/L) and sulfate (19.6 mg/L) concentrations, consistent with its location outside the primary source zone.

Total organic carbon (TOC) was not detected in any of the samples analyzed, suggesting a lack of organic electron donors necessary for biotic CT degradation. The absence of nitrite (NO_2^-) and phosphate (PO_4^{3-}) across all wells implies a stable oxic bulk groundwater environment. Specifically, the lack of nitrite indicates a lack of active microbial dissimilatory nitrate reduction, while the absence of dissolved phosphate suggests it remains bound to solid-phase Fe(III) oxides. Together, these lines of evidence demonstrate that the bulk aquifer's redox sequence has not progressed toward denitrification or more strongly reducing conditions.

Table 6. Groundwater anions and non-purgeable organic carbon (NPOC) in mg/L from the 200-ZP-1 OU, Phase I wells.

Ground Water Anion & Total Organic Carbon Results (mg/L)								
Well Name	Br^-	Cl^-	F^-	NO_3^-	NO_2^-	PO_4^{3-}	SO_4^{2-}	NPOC
699-46-70	ND	26.4	ND	92.0	ND	ND	58.6	ND
699-45-67c	ND	25.8	ND	94.4	ND	ND	59.4	-
299-W14-24	ND	4.4	ND	ND	ND	ND	19.6	ND
299-W11-98	ND	11.8	ND	256	ND	ND	38.7	ND
Detection Limit	0.02	0.01	0.01	0.03	0.04	0.07	0.03	0.05

Values for Br^-, F^-, NO_2^- and PO_4^{3-} were below detection (ND). NPOC represents the dissolved organic carbon fraction remaining after acidification and purging of inorganic carbon species and is used as a proxy for total dissolved organic carbon in groundwater samples. Values reported as ND (not detected) indicate concentrations below the instrument detection limit of 0.05 mg/L

4.2.2 Sediment

4.2.2.1 Anions

Sediments were water-extracted to characterize absorbed anions, or residual anions remaining in interstitial pore fluids (9.0A.2.1). Although a water extraction can fail to extract sorbed ions, Hanford sediments generally exhibit limited anion exchange capacity, which will vary depending on mineralogy, pH, and redox conditions, among others. In general, anion exchange capacity is low for Hanford sediments due to low content of Fe and Al oxides, clays, and NPOC. Most importantly, these results do show that the sediments used in batch degradation testing contributed varying levels of background NO_3^- to these investigations.

The limit of detection varied by processing date as it was calculated separately for each specific data set analyzed (in mg/L). As a result, different limits of detection were applied and reported (Table 7).

Table 7. Water extractable anions from 200-ZP-1 OU, Phase I sediment.

Sediment Anions Results (mg/kg dry sediment)									
Borehole ID	Unit	Sample ID	Br^-	Cl^-	F^-	NO_3^-	NO_2^-	PO_4^{3-}	SO_4^{2-}
D0082	Rwie	B3W6C7**	ND	0.38	0.38	ND	ND	ND	1.83
	Rwia	B3W6F2**	ND	0.38	0.31	0.27	ND	ND	1.66
		B3W6H5**	ND	0.27	0.33	0.67	ND	ND	2.24
		B3W6J5**	ND	0.33	0.29	0.66	ND	ND	1.82
D0083	Rwie	B3WXX5	ND	0.99	0.06	0.48	ND	ND	2.02
	Rlm	B3WXM7	ND	0.16	0.07	0.05	ND	ND	1.05
		B3WXN3	ND	0.20	0.06	0.85	ND	ND	1.17
		B3WXN9	ND	0.29	0.05	0.71	ND	ND	1.08
	Rwia	B3WXP5*	ND	0.51	0.03	3.42	0.15	0.05	0.82
C9996	Rwie	B48BN8**	ND	0.13	0.58	0.67	ND	ND	1.02
	Rlm	B48BN9**	ND	0.43	0.31	0.71	ND	ND	1.37
	Rwia	B48BP0**	ND	0.40	0.31	0.67	ND	ND	2.78
C9739	Rwie	B48BN5	ND	0.57	0.06	2.47	0.44	ND	1.54
	Rwie/a	B48BN6	ND	0.43	0.05	4.77	0.08	ND	1.61
	Rwia	B48BN7	ND	0.47	0.04	0.13	ND	ND	1.96
	Detection Limit		0.17	0.10	0.09	0.24	0.28	0.51	0.19
	Detection Limit*		0.01	0.00	0.00	0.01	0.01	0.03	0.01
	Detection Limit**		0.02	0.01	0.01	0.02	0.03	0.05	0.02

4.2.2.2 Iron / Manganese Quantification

Sediment extractions were performed to quantify the availability of Fe and Mn redox species to participate in geochemical processes for the degradation of CT and as an indicator of sediment redox status. The adsorbed fraction of Fe represents the mineral surface exchangeable fraction could serve as an important interface for electron transfer reactions contributing to CT degradation. Iron redox species, and Mn for nearly half of the sediments examined, were below detection for the methodologies used for Fe(II) (ferrozine colorimetric assay, detection limit approximately 0.01 mg/g) and Fe(III)/Mn [inductively coupled plasma – optical emission spectroscopy (ICP-OES), detection limit approximately 0.02 mg/g] measurements applied to the adsorbed-phase extractions.

The absence of detectable adsorbed Fe-phase indicates that the reducible Fe fraction available for rapid surface-mediated electron transfer to CT is below the analytical detection threshold in these extractions. Therefore, the CT-reducing capacity measured in abiotic batch experiments must be attributed to mineral-phase Fe(II) forms that are released only under acid digestion conditions rather than to readily exchangeable surface-bound Fe(II). Low levels of Mn were detected in adsorbed-phase extractions from approximately half of the Phase I sediment samples, spanning all boreholes except C9996, at concentrations ranging from approximately 10 to 30 µg/g soil. These concentrations were measured by ICP-OES following the adsorbed-phase extraction procedure described in Appendix A. No Mn speciation was determined from these extractions.

Following the adsorbed phase extraction, sediments were acid digested to quantify the total Fe and Mn mineral inventory. Results are summarized in Table 8 and reveal Fe- and Mn-bearing mineral phases that complement the mineralogical results from powder XRD (Table 9). While the bulk mineralogical fraction of Fe and Mn is often considered secondary to redox processes, certain reactive mineral phases such as magnetite, green rust, or surface-bound Fe(II) can significantly contribute to the abiotic degradation of CT via electron transfer to the contaminant (Bagwell et al. 2019; He et al. 2015; Lee and Batchelor 2002a,b).

Across the Phase I dataset, Fe(II) concentrations exceeded 1.0 mg/g in two samples: B3W6C7 from borehole D0082 (1.05 ± 0.15 mg/g) and B3WXN3 from borehole D0083 (1.36 ± 0.28 mg/g). In both cases, Fe(II) accounted for more than 50% of the total extractable Fe, indicating a partially reduced mineral assemblage with meaningful electron donor capacity. Notably, sample B3W6C7, which had the highest Fe(II) concentration among D0082 intervals, also had the highest Mn concentration of any sample in that borehole (0.07 ± 0.01 mg/g), suggesting an occurrence of reduced Fe phases that may contribute to abiotic CT transformation. The remaining samples showed more variable Fe(II) fractions, with several intervals from C9739 and C9996 dominated by Fe(III), indicating a more oxidized mineral assemblage with comparatively limited abiotic reduction capacity. The actual contribution of these mineral phases to CT degradation in this specific system depends on the exact mineral phase identity, the bioavailability and surface accessibility of the metal centers, and the geochemical conditions governing the regeneration of reactive reduced sites.

Table 8. Digested Mineral phase iron and manganese concentrations for 200-ZP-1 OU, Phase I sediment.

Digested Sediment Iron/Manganese Quantification Avg. Analyte (mg/g soil) ± Std. Dev.						
Borehole ID	Unit	Sample ID	Fe (II)	Fe (III)	Total Fe	Mn
D0082	Rwie	B3W6C7	1.05 ± 0.15	0.87 ± 0.05	1.92 ± 0.20	0.07 ± 0.01
	Rwia	B3W6F2	0.49 ± 0.44	0.36 ± 0.02	0.85 ± 0.42	0.08 ± 0.02
		B3W6H5	0.41 ± 0.00	0.48 ± 0.01	0.89 ± 0.01	0.10 ± 0.00
		B3W6J5	0.03 ± 0.00	0.32 ± 0.04	0.35 ± 0.04	0.04 ± 0.01
D0083	Rwie	B3WXX5	0.19 ± 0.04	0.24 ± 0.00	0.43 ± 0.04	0.11 ± 0.00
	Rlm	B3WXM7	0.05 ± 0.00	0.10 ± 0.00	0.15 ± 0.00	0.01 ± 0.00
		B3WXN3	1.36 ± 0.28	0.83 ± 0.37	2.19 ± 0.65	0.13 ± 0.01
		B3WXN9	0.03 ± 0.00	0.20 ± 0.01	0.24 ± 0.01	0.01 ± 0.00
	Rwia	B3WXP5	0.42 ± 0.23	0.08 ± 0.06	0.50 ± 0.17	0.07 ± 0.01
C9996	Rwie	B48BN8	0.03 ± 0.00	0.31 ± 0.03	0.33 ± 0.03	0.04 ± 0.00
	Rlm	B48BN9	0.03 ± 0.01	0.45 ± 0.04	0.48 ± 0.04	0.03 ± 0.00
	Rwia	B48BP0	0.93 ± 0.06	0.04 ± 0.01	0.96 ± 0.07	0.02 ± 0.01
C9739	Rwie	B48BN5	0.04 ± 0.00	0.66 ± 0.00	0.70 ± 0.00	0.02 ± 0.00
	Rwie/a	B48BN6	0.06 ± 0.00	0.82 ± 0.03	0.88 ± 0.03	0.04 ± 0.01
	Rwia	B48BN7	0.56 ± 0.16	0.55 ± 0.02	1.10 ± 0.14	0.07 ± 0.00

4.3 Physical and Mineralogical Characterization

4.3.1 Particle Size Distribution

Particle size distribution was performed by sieving the entire core material to determine coarse (> 2 mm) and fine (<2 mm) fractions. The fine fraction was then analyzed using a laser particle size analyzer to quantify sand (63 µm to 2 mm), silt (63 to 4 µm), and clay (<4 µm) based in three replicate measurements per sample. Additional details are provided in Appendix A, Section A.2.2.

Across the 200-ZP-1 OU Phase I sediments, Rwie and several intervals of Rwia show coarse, sand dominated units (Table 9). A large portion of the bulk material is >2 mm (~56% to 92%). Within the <2-mm fraction, sand is the dominant fraction, with silt making up the next largest fraction, while clay contents are generally low (<3%, commonly <1%). Bulk samples from the Rlm and some Rwia intervals are fine-grained, silt-dominated units (Table 9). Rlm samples contain very little >2-mm material (<1%), indicating that it is a fine-grained unit. One Rwia interval (sample B3WXP5) differs, with a larger coarse fraction (~21%) and the <2-mm fraction dominated by sand, followed by silt, then clay. In contrast, the <2-mm fraction of Rlm material is dominated by silt, with less sand and low clay content.

Overall, Phase I sediments range from very coarse, sand-rich units with minimal fines to finer grained, silt-rich deposits with low clay contents. The Rlm unit is distinctly finer and more silt-rich than the Rwie/Rwia units, which are dominated by sand in the fine fraction and contain substantial coarse (>2-mm) material in bulk.

Table 9. Particle size distribution for 200-ZP-1 OU, Phase I sediment.

Particle Size Distribution (%)							
Borehole ID	Unit	Sample ID	> 2 mm	< 2 mm	Sand (63 µm-2 mm)	Silt (63-4 µm)	Clay (<4 µm)
D0082	Rwie	B3W6C7	81.35	18.65	55.51 ± 4.80	43.12 ± 4.66	1.36 ± 0.15
	Rwia	B3W6F2	79.43	20.57	72.30 ± 12.68	27.28 ± 12.42	0.42 ± 0.27
		B3W6H5	68.02	31.98	79.23 ± 5.22	20.13 ± 5.02	0.64 ± 0.20
		B3W6J5	87.89	12.11	70.85 ± 10.21	28.67 ± 9.95	0.48 ± 0.26
D0083	Rwie	B3WXX5	84.16	15.84	70.64 ± 9.42	29.15 ± 9.34	0.21 ± 0.09
	Rlm	B3WXM7-A[(a)]	0.51	99.49	21.62 ± 6.23	77.55 ± 6.10	0.83 ± 0.14
		B3WXM7-B[(a)]	0.11	99.89	24.40 ± 9.50	74.90 ± 9.27	0.70 ± 0.25
		B3WXN3	0.35	99.65	14.19 ± 2.96	84.88 ± 2.94	0.93 ± 0.07
		B3WXN9	0.23	99.77	13.63 ± 0.50	86.02 ± 0.51	0.35 ± 0.01
	Rwia	B3WXP5	20.60	79.40	54.63 ± 6.60	42.15 ± 6.01	3.22 ± 0.61
C9996	Rwie	B48BN8	75.82	24.18	78.25 ± 3.03	21.60 ± 2.95	0.16 ± 0.08
	Rlm	B48BN9	0.28	99.72	19.28 ± 1.48	78.91 ± 1.45	1.81 ± 0.05
	Rwia	B48BP0	91.73	8.27	83.53 ± 8.66	16.14 ± 8.31	0.34 ± 0.35
C9739	Rwia	B48BN5	78.68	21.32	72.53 ± 2.66	27.28 ± 2.64	0.19 ± 0.02
	Rwie	B48BN6	80.80	19.20	79.15 ± 4.31	20.82 ± 4.28	0.03 ± 0.04
	Rwia/Rwie	B48BN7	53.87	46.13	93.25 ± 0.39	6.75 ± 0.39	0.00 ± 0.00

(a) B3WXM7 had two intervals analyzed, A and B, and are noted as such.

4.3.2 Mineralogy by X-ray Diffraction

The mineralogical analysis of samples from boreholes D0082, D0083, C9996, and C9739 reveals a composition dominated by amorphous material (averaging 46.0 wt%) and quartz (averaging 34.7 wt%). These two components consistently form the bulk of the mineral matrix across all geologic units, though their proportions fluctuate. For instance, amorphous content peaks at nearly 62% in specific samples from borehole D0082, while quartz reaches its highest concentration of 48% in borehole C9996. Feldspar serves as the primary secondary mineral, contributing an average of 12.9 wt%, with notably higher concentrations found in unit Rwie.

The minor mineral constituents – mica, pyroxene, chlorite, and carbonate – show significant variation based on the geologic unit. The Rlm unit is uniquely characterized by a high mica content, averaging over 12 wt%, whereas other units contain less than 2 wt%. Chlorite and pyroxene remain trace components throughout most samples, though borehole C9996 shows a distinct enrichment in these minerals compared to the others. Conversely, borehole C9739 represents the most simplified mineralogical profile, consisting entirely of amorphous material, quartz, and feldspar, with no detectable trace minerals.

Table 10. XRD results for 200-ZP-1 OU, Phase I samples.

			Mineral Group (wt%)						
Borehole ID	Unit	Sample ID	Chlorite	Carbonate	Mica	Pyroxene	Feldspar	Quartz	Amorphous
D0082	Rwie	B3W6C7	-	-	3.49	0.47	13.75	46.36	35.93
	Rwia	B3W6F2	-	-	1.9	1.21	13.92	39.27	43.7
		B3W6H5	-	2.18	1.04	1.18	8.7	30.64	56.27
		B3W6J5	-	1.41	-	2.63	13.89	20.08	61.99
D0083	Rwie	B3WXX5	-	2.49	-	-	12.1	42.14	43.27
	Rlm	B3WXM7-A[(a)]	-	-	12.25	0.64	4.05	21.45	61.61
		B3WXM7-B[(a)]	-	-	13.36	0.78	2.55	24.36	58.96
		B3WXN3	-	-	13.07	0.25	3.2	23.02	60.45
		B3WXN9	-	-	12.85	-	3.63	40.62	42.91
	Rwia	B3WXP5	-	-	6.74	1.22	3.95	35.36	52.73
C9996	Rwie	B48BN8	2.32	-	-	2.49	35.42	39.16	20.61
	Rlm	B48BN9	3.07	-	9	1.69	19.81	46.79	19.64
	Rwia	B48BP0	1.51	-	-	3.35	26.75	48.01	20.38
C9739	Rwie	B48BN5	-	-	-	-	18.27	31.77	49.96
	Rwie/a	B48BN6	-	-	-	-	14.55	33.29	52.16
	Rwia	B48BN7	-	-	-	-	11.76	32.93	55.30

(a) Core B3WMXM7 had two intervals analyzed: A and B.

5.0 Phase II Results

5.1 Degradation Experiments

5.1.1 Combined Abiotic-Biotic

Measured CT data were evaluated against a first-order degradation kinetic model to assess the rate and extent of combined biotic-abiotic CT transformation in Phase II site-specific Hanford sediments. Phase II experiments benefited from improved core preservation protocols, standardized laboratory procedures, and the use of a GC-ECD detector in place of the SPME-GC/MS system employed in Phase I, providing greater sensitivity and selectivity for chlorinated methane analysis. All experiments were initiated at a target aqueous CT concentration of 800 µg/L. Table 11 summarizes the fitted parameters, including the median rate constant (K), 95% confidence intervals, R^2 goodness-of-fit values, and estimated half-lives. CT mass over time for all combined biotic-abiotic batch experiments is shown in Figure 6, and CF production data for representative intervals are provided in Appendix B.

Table 11. Fitted biotic-abiotic parameters to a first order degradation kinetic model. Standard deviations are shown beside each parameter. The goodness of fit is represented as R^2 and the half-life $t_{1/2}$ is shown.

Borehole (Core ID)	K_{median} (K, 95% CI)	R^2 (Fit Confidence)	λ (days)	λ 95% CI (days)
C9993 (B4JT76)	0.273 (0.084-0.717)	1.0 (Low)	2.504	0.899-6.684
C9993 (B4JT77)	0.104 (0.035-0.247)	0.95 (High)	6.616	2.47-14.928
C9993 (B4JTM3)	0.027 (-0.015-0.910)	0.814 (Low)	NA	NA
C9993 (B4JTM4)	0.064 (0.033-0.092)	0.975 (High)	10.877	7.556-21.183
D0474 (B4JT78)	0.094 (0.058-0.216)	0.94 (High)	7.407	3.203-11.958
D0474 (B4JT79)	0.095 (0.048-0.223)	0.918 (High)	7.232	3.014-13.721
D0474 (B4JTM5)	0.069 (-0.136-0.313)	0.704 (Low)	NA	NA

CT degradation responses in both C9993 and D0474 borehole sediments showed well-defined first-order degradation behavior, with the majority of sampled intervals producing positive rate constants and good model fits. Overall, CT degradation rates were higher for C9993 (Rwie) compared to D0474 (Rwia), though sediments from both boreholes were effective at transforming a fixed mass of CT under anoxic conditions. Calculated half-lives ranged from approximately 2.5 to 11 days for C9993 and 7 to 10 days for D0474. Neither borehole displayed a consistent trend in degradation rate as a function of depth, suggesting that factors other than depth alone – such as local variations in microbial community composition, sediment organic carbon quality, or reactive mineral surface availability – govern the spatial distribution of degradation capacity within these units.

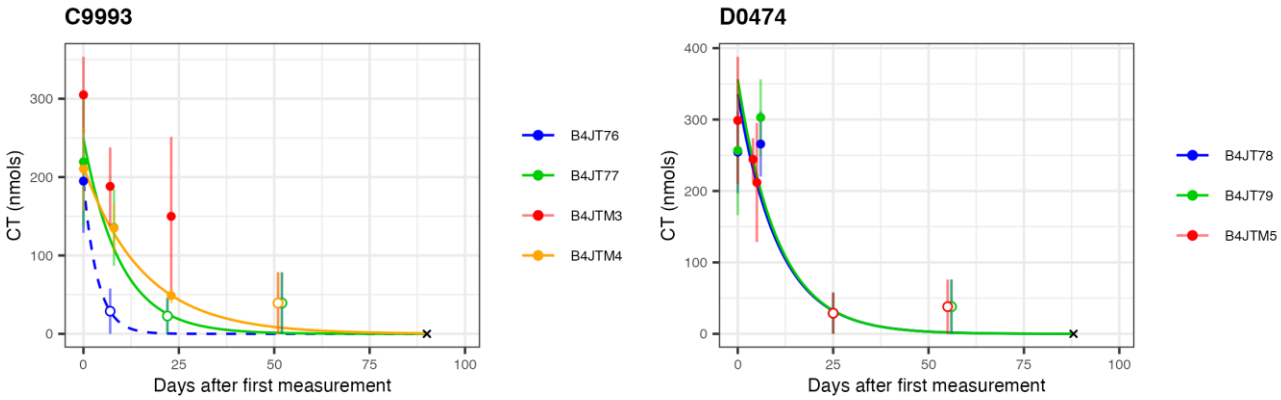

Figure 6. CT degradation profiles from combined biotic-abiotic degradation in well C9993 and D0474 samples. All experiments were initiated at a starting concentration of 800 ppb CT. First order degradation rate model fits are plotted where CT degradation was statistically significant: solid line (95% confidence) or dotted line (90% confidence). Filled circles = detections with error bars to capture propagated concentration standard deviation; open circles = values below LOD where error bars span 0 to LOD range with the point plotted at LOD/2; black 'x' at y=0 indicates sample was measured but excluded due to failed calibration quality control. Individual plots of CT and CF for all treatments and boreholes are provided in Appendix C.

Borehole C9993. All four sampled intervals from C9993 showed measurable CT degradation over the 80-plus day incubation period. The shallowest interval, B4JT76, exhibited the most rapid degradation, with a rate constant of 0.273 day^{-1} and an estimated half-life of approximately 2.5 days, though the R^2 value of 1.0 with a low fit confidence designation reflects the limited number of data points available for this interval and warrants cautious interpretation. Interval B4JT77 produced a well-constrained rate constant of 0.104 day^{-1} with a high-confidence R^2 of 0.95, corresponding to a half-life of approximately 6.6 days. Having a 95% confidence interval of 2.5 to 14.9 days, these results represent one of the most statistically robust degradation estimates obtained in this study. Interval B4JTM3 yielded a rate constant of 0.027 day^{-1} with a confidence interval of (-0.015 to 0.910) that spans zero, paired with an R^2 of 0.814. This combination of a moderately good model fit and a confidence interval that includes zero typically reflects a declining trend but the variance is too large relative to the magnitude of the signal at the 95% confidence level. No statistically meaningful half-life could be calculated for this interval. Interval B4JTM4 produced a well-constrained rate constant of 0.064 day^{-1} with a high-confidence R^2 of 0.975 and an estimated half-life of approximately 11 days. After more than 80 days of incubation, the starting CT mass was effectively eliminated across all C9993 intervals examined, confirming that near-complete CT transformation was achieved under these experimental conditions.

The concurrent production of CF was monitored alongside CT removal in C9993 experiments (Appendix B). CF accumulation patterns varied across the sampled intervals. In the shallowest interval B4JT76, CF began accumulating rapidly as CT declined, reaching a peak before stabilizing, consistent with sequential transformation of CT to CF and onward to further dechlorination products. Interval B4JT77 showed a similar pattern, with CF accumulation tracking the decline in CT mass before plateauing at later timepoints. For the deeper intervals B4JTM3 and B4JTM4, CF accumulation was more modest and gradual, consistent with the slower and less well-constrained CT degradation rates observed for these intervals. Across all C9993 intervals, the stabilization of CF mass at later timepoints, rather than continued accumulation in proportion to CT removal, is consistent with CF consumption and transformation to downstream products concurrently with its production. However, because downstream products were not analytically measured, this interpretation remains inferential.

At the end of the incubation period, approximately 50% of the initial CT mass was accounted for as CF in the shallower intervals. For interval B4JT76, the nominal initial CT mass was approximately 186 nmol (calculated from the 800 µg/L spiking concentration and the aqueous volume used) and the peak measured CF mass was approximately 188 nmol, representing 100% of the initial CT mass. Further incubation results in a mass deficit of 84 nmol, not accounted for as CT or CF, and is inferred to reflect transformation to downstream dechlorination products. Because DCM and other downstream products were not analytically measured in this study, the identity and distribution of these products cannot be directly confirmed.

It is notable that near-complete CT degradation was achieved in C9993 sediments against a background of 179.0 mg/L NO_3^- in the site-specific groundwater used for these experiments. This concentration substantially exceeds the threshold at which nitrate has been reported to competitively inhibit CT reductive dechlorination at Hanford (Hooker et al. 1994, 1998). The observation of rapid and extensive CT transformation under these conditions is noteworthy and may reflect several non-mutually exclusive processes. The indigenous microbial community associated with C9993 sediments may capable of sustaining co-metabolic CT degradation in parallel with active denitrification, or that nitrate may have been progressively depleted within the closed batch system during incubation to permit CT-reducing conditions to develop over time. This interpretation cannot be directly evaluated from the available data because nitrate concentrations were not monitored over time within the microcosms. Future experiments should include time-series measurements of nitrate and nitrite within the batch incubations to test this hypothesis directly. Additionally, abiotic mineral-mediated reduction by Fe(II) phases may have contributed to the observed CT transformation in combination with biotic processes.

Because these experiments measured the combined response of both biotic and abiotic processes operating simultaneously, the relative contribution of each pathway to the observed CT degradation cannot be quantified from the available data. Regardless of the specific mechanisms involved, the results demonstrate that the combined biotic-abiotic system retains a meaningful capacity for CT transformation under site-specific groundwater conditions that would otherwise be considered inhibitory, which is an important and encouraging finding for the assessment of natural attenuation potential in the 200-ZP-1 OU.

Borehole D0474. All three sampled intervals from D0474 showed measurable CT degradation, with rate constants ranging from 0.069 to 0.095 day^{-1} across the intervals where statistically meaningful estimates could be obtained. Intervals B4JT78 and B4JT79 both produced well-constrained rate constants with high-confidence R^2 values of 0.94 and 0.918, respectively, and estimated half-lives of approximately 7 days with relatively narrow confidence intervals. The deepest interval, B4JTM5, yielded a positive rate constant of 0.069 day^{-1} but with a wide confidence interval spanning negative values and a lower R^2 of 0.704, indicating greater uncertainty in the rate estimate for this interval. After more than 80 days of incubation, greater than 80% of the starting CT mass was degraded across all D0474 intervals, confirming that substantial CT transformation was achieved under these experimental conditions.

The CF production profile for D0474 differed notably from that observed in C9993 (Appendix B). For the shallowest interval, B4JT78, CF accumulated to only approximately 50 nmol, accounting for approximately 20% of the initial CT mass despite greater than 80% CT removal by the end of the incubation period. This low CF yield relative to the extent of CT removal suggests that CF transformation to DCM was occurring rapidly and concurrently with CT dichlorination, preventing CF accumulation. This pattern was consistent across all D0474 intervals, with CF remaining at comparatively low levels throughout the incubation relative to the degree of CT mass removal observed.

Together, the CT and CF concentration profiles from D0474 provide indirect evidence consistent with reductive dechlorination proceeding beyond the initial CT-to-CF conversion step under native, unaugmented conditions. Because downstream products were not directly measured, this interpretation is based on the inference that the missing CT mass was transformed to less-chlorinated compounds rather than lost to volatilization or other non-degradative processes. Furthermore, the rate of CF consumption in D0474 is sufficiently rapid relative to its production that CF does not accumulate to the same degree as observed in C9993 sediments. The lower background NO_3^- concentration in D0474 groundwater (49.8 mg/L) relative to C9993 (179.0 mg/L) may contribute to this more complete dechlorination pattern, as reduced competition from nitrate would be expected to favor more sustained and extensive reductive conditions within the batch system.

5.1.2 Abiotic

Measured CT data were evaluated against a first-order degradation kinetic model to assess the rate and extent of abiotic CT transformation in Phase II site-specific Hanford sediments. For abiotic degradation, first-order reaction behavior implies that the degradation rate is proportional to the abundance of adsorbed ferrous iron (Fe^{2+}) and that the effective concentration of these abiotic reactants remain constant over the experimental period. Biological activity was suppressed in all abiotic treatments through the addition of sodium azide (3 mM). The mathematical expression used to analyze CT degradation over time is represented in Appendix A. Table 12 summarizes the fitted parameters, including the median rate constant (K), 95% confidence intervals, R^2 goodness-of-fit values, and estimated half-lives. CT mass over time for all abiotic batch experiments is shown in Figure 10, and the complete set of Phase II abiotic degradation plots is provided in Appendix C.

Table 12. Fitted abiotic parameters to a first order degradation kinetic model. Standard deviations are shown beside each parameter. The goodness of fit is represented as R^2 and the half-life $t_{1/2}$ is shown.

Borehole (Core ID)	K_{median} (K, 95% CI)	R^2 (fit confidence)	λ (days)	λ 95% CI (days)
C9993 (B4JT76)	0.129 (0.042-0.234)	0.943 (High)	5.366	2.941-15.918
C9993 (B4JT77)	0.054 (0.029-0.103)	0.927 (High)	12.868	6.711-23.922
C9993 (B4JTM3)	0.012 (-0.018-0.044)	0.425 (Low)	NA	NA
C9993 (B4JTM4)	0.026 (-0.011-0.077)	0.529 (Low)	NA	NA
C9993 (GW)	0.00 (-0.015-0.011)	0.601 (Low)	NA	NA
D0474 (B4JT78)	0.034 (-0.055-0.264)	0.085 (Low)	NA	NA
D0474 (B4JT79)	0.004 (-0.05-0.053)	0.424 (Low)	NA	NA
D0474 (B4JTM5)	-0.008 (-0.052-0.034)	0.385 (Low)	NA	NA
D0474 (GW)	0.00 (-0.00-0.011)	0.102 (Low)	NA	NA

Abiotic treatments employed 3mM sodium azide to inhibit biological activity. Groundwater-only treatments were conducted to examine hydrolysis of CT in site-specific groundwater. Detailed methodological information is provided in Appendix A.

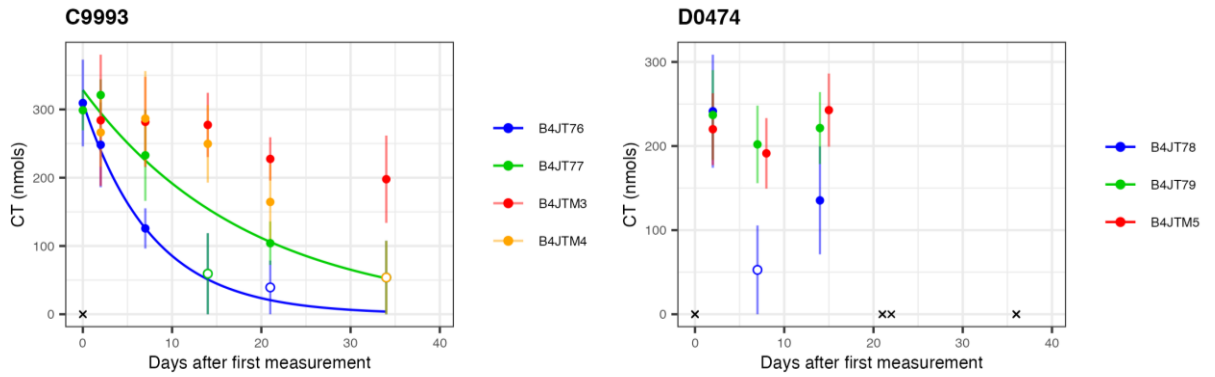

Figure 7. CT degradation profiles from abiotic degradation in wells C9993 and D0474 samples (refer to Table 3 for complete sample information). All experiments were initiated at a starting concentration of 800 ppb CT. Plotted lines show first-order degradation rate models shown in Table 12. First order degradation rate model fits are plotted where CT degradation was statistically significant: solid line (95% confidence) or dotted line (90% confidence). Filled circles = detections with error bars to capture propagated concentration standard deviation; open circles = values below LOD where error bars span 0 to LOD range with the point plotted at LOD/2; black 'x' at y=0 indicates sample was measured but excluded due to failed calibration quality control. Individual plots of CT and CF for all treatments and boreholes are provided in Appendix C.

Borehole C9993. Abiotic CT degradation in C9993 sediments decreased with increasing depth, with the two shallowest intervals producing the most robust and well-constrained rate estimates. Interval B4JT76 yielded a rate constant of 0.129 day^{-1} with a high-confidence R^2 of 0.943 and an estimated half-life of approximately 5.4 days, with a 95% confidence interval of 2.9 to 15.9 days. Interval B4JT77 produced a well-constrained rate constant of 0.054 day^{-1} with a high-confidence R^2 of 0.927 and an estimated half-life of approximately 12.9 days, with a confidence interval of 6.7 to 23.9 days. These two intervals represent the strongest evidence for abiotic CT transformation capacity obtained in Phase II. The deeper intervals, B4JTM3 and B4JTM4, yielded poorly constrained rate constants with confidence intervals spanning negative values and low R^2 values of 0.425 and 0.529, respectively, and no statistically meaningful half-lives could be calculated for these intervals. The decline in abiotic degradation capacity with depth in C9993 is broadly consistent with the Fe speciation data, where the shallowest interval B4JT76 contained the highest Fe(II) content (2.16 mg/g) and highest Fe(II)/Fe(III) ratio of all C9993 samples, while deeper intervals showed progressively more oxidized iron speciation.

CF production was monitored concurrently with CT removal in C9993 abiotic experiments (Appendix BC). As CT mass declined in the reactive shallower intervals, CF accumulated to approximately 50 nmol before stabilizing. This pattern of CF accumulation followed by a plateau, rather than a continued increase, suggests that abiotic dechlorination was proceeding beyond CF to further reduced products, consistent with the sequential dechlorination pathway observed in the combined biotic-abiotic experiments. The relatively modest CF accumulation compared to the extent of CT removal further supports the interpretation that downstream transformation of CF was occurring concurrently with its production under these experimental conditions.

Borehole D0474. Abiotic CT degradation in D0474 sediments was considerably slower and less well-constrained than in C9993 across all three sampled intervals. All three D0474 intervals yielded rate constants near zero with wide confidence intervals spanning negative values and uniformly low R^2 values ranging from 0.085 to 0.424, and no statistically meaningful half-lives could be calculated for any D0474

interval. The two deeper intervals, B4JT79 and B4JTM5, showed very similar and effectively negligible abiotic degradation responses during batch testing. These outcomes are consistent with the Fe speciation data for D0474, where all three intervals were dominated by Fe(III) with low Fe(II) fractions ranging from 0.12 to 0.16 mg/g, indicating a predominantly oxidized mineral assemblage with limited capacity for abiotic electron donation to CT.

The contrasting abiotic degradation behavior between C9993 and D0474 presents an important interpretive consideration with respect to the background groundwater chemistry used in these experiments. Site-specific groundwater from C9993 (299-W11-100) contained considerably higher NO_3^- (179.0 mg/L) than that from D0474 (299-W11-116, 49.8 mg/L NO_3^-). For purely abiotic reduction mechanisms, CT and NO_3^- compete for electrons from reduced Fe/Mn mineral surfaces, and the thermodynamically inverse behavior would be expected; that is, the greatest extent of abiotic CT degradation would be anticipated in the system with the lowest NO_3^- concentration. The observation that C9993 sediments (NO_3^- = 179.0 mg/L, Fe(II) in B4JT76 = 2.16 mg/g) showed substantially greater apparent abiotic CT degradation than D0474 sediments (NO_3^- = 49.8 mg/L, Fe(II) = 0.12–0.16 mg/g across all three intervals) is inconsistent with a system governed purely by nitrate competition, as lower nitrate would be expected to favor greater CT reduction in D0474. The more than order-of-magnitude difference in Fe(II) content between the most reactive C9993 interval (B4JT76, 2.16 mg/g) and all D0474 intervals (0.12–0.16 mg/g) is likely the dominant variable explaining the divergent abiotic reactivity between boreholes, with the incomplete biological inhibition of C9993 sediments as an additional contributing factor that cannot be excluded.

This outcome raises the possibility that the sodium azide treatments at 3 mM concentration were less than fully effective at suppressing biological activity in C9993 sediments. Sodium azide is commonly employed as a biological inhibitor in environmental microbiology studies at concentrations ranging from 1 to 10 mM, and 3 mM is generally considered effective for low-biomass environmental samples. Residual biological contributions to the measured CT transformation in abiotic C9993 treatments cannot be fully excluded, and this uncertainty represents a methodological limitation on the mechanistic interpretation of these abiotic results. Therefore, combined biotic-abiotic mechanisms may have contributed to the measured CT degradation in these abiotic treatments. This interpretation is consistent with the notably rapid degradation rates observed for the two shallowest C9993 intervals relative to the Fe(II) inventories measured for these sediments.

Abiotic batch experiments included an oxidized sediment control treatment, in which site sediments were pre-exposed to air prior to sodium azide addition (as described in Section 3.2) to intentionally oxidize reduced Fe^{2+} mineral phases before biological inhibition was applied. These experiments showed effective conservation of CT mass for both C9993 and D0474 sediments, confirming that CT degradation in the companion anoxic sodium azide treatments is dependent on the reduced geochemical conditions and is inhibited by the introduction of oxygen. These results are not presented graphically but provide an important mechanistic confirmation that the CT transformation observed in abiotic treatments requires reduced, anoxic conditions to be effective, and that oxidation of reactive mineral surfaces through air exposure is sufficient to eliminate the abiotic (or combined biotic-abiotic) degradation capacity of these sediments.

Replicated batch experiments were also conducted at a lower initial CT concentration of 20 µg/L to evaluate concentration-dependent abiotic degradation behavior. These experiments showed no significant change in CT mass across either borehole, and the corresponding plots are not presented. At this low initial CT concentration, NO_3^- in the site-specific groundwater was present at more than three orders of magnitude higher molar concentration than CT. Under these conditions, NO_3^- is expected to substantially outcompete CT as an electron acceptor for the available reduced Fe/Mn mineral surfaces, effectively suppressing abiotic CT transformation. This is driven by concentration-dependent effects, where the

extreme dilution of CT dramatically lowers its effective chemical reduction potential relative to nitrate, as well as a greater thermodynamic energy yield from nitrate reduction. At the low initial CT concentration of 20 µg/L, nitrate was present in site-specific groundwater at more than three orders of magnitude higher molar concentration than CT. Under these conditions, the available reducing equivalents from Fe(II) mineral surfaces are preferentially consumed by nitrate reduction both thermodynamically and kinetically. This outcome highlights an important constraint on the field relevance of abiotic natural attenuation in lower-concentration portions of the CT plume, where the stoichiometric dominance of NO_3^- over CT as a competing electron acceptor would be expected to severely limit the contribution of mineral-mediated CT reduction to overall contaminant mass removal.

5.1.3 Hydrolysis

Batch hydrolysis experiments were conducted to evaluate the contribution of aqueous-phase reactions to CT mass removal in site-specific Hanford groundwater in the absence of sediment contact. Groundwater used in these experiments was not filtered to remove microorganisms prior to incubation. Any biological activity present in the groundwater-only incubations would therefore contribute to any observed CT mass reduction, meaning that these experiments strictly represent an upper bound on CT stability in groundwater rather than a pure measure of chemical hydrolysis. Given the carbon-limited, nitrate-rich character of the site groundwater, significant biological activity in these incubations is considered unlikely.

These experiments serve as a baseline control for the Phase II degradation study, isolating the role of groundwater chemistry alone in CT transformation and providing a direct reference for comparison with the sediment-containing abiotic and biotic treatments. CT mass was monitored over time in groundwater-only incubations prepared from site-specific water collected from wells 299-W11-100 (C9993) and 299-W11-116 (D0474), and results are shown in Figure 8.

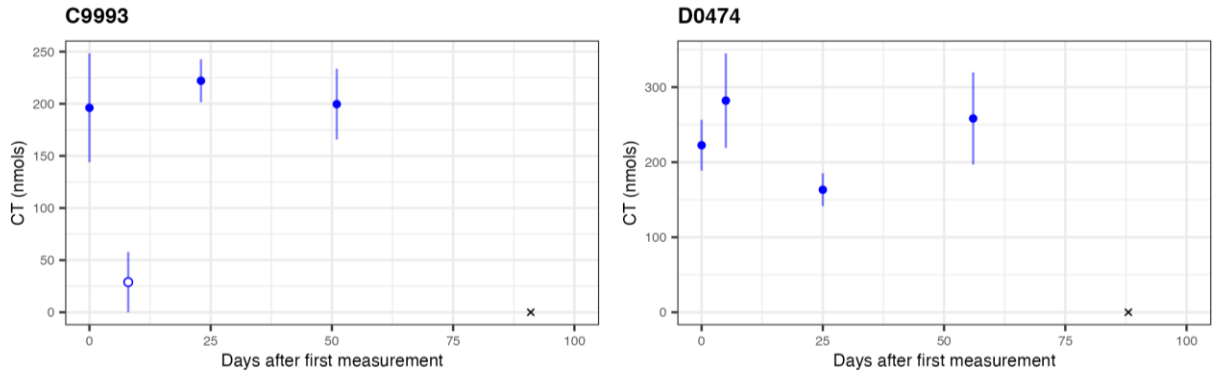

Figure 8. CT degradation profiles from hydrolysis experiments with site groundwater-only incubated at 800 ppb CT. CT concentrations are plotted over time in site-specific groundwater for wells C9993 and D0474. First order degradation rate model fits are plotted where CT degradation was statistically significant: solid line (95% confidence) or dotted line (90% confidence). Filled circles = detections with error bars to capture propagated concentration standard deviation; open circles = values below LOD where error bars span 0 to LOD range with the point plotted at LOD/2; black ‘x’ at y=0 indicates sample was measured but excluded due to failed calibration quality control. Individual plots of CT and CF are provided for all treatments and boreholes are provided in Appendix C.

While the results show some temporal variability in measured CT mass, the concentration of CT at the start and end of the experiment remained effectively unchanged and was consistent between the two

boreholes. No systematic declining trend was observed in either groundwater treatment over the full duration of the incubation period. This outcome is consistent with the Phase I hydrolysis results and agrees with the previously reported hydrolysis half-life of 630 years estimated for Hanford groundwater conditions by Amonette et al. (2012). The groundwater chemistry data for both wells, characterized by elevated nitrate, low to non-detectable organic carbon, and an absence of reduced mineral phases, is not conducive to aqueous-phase CT transformation on experimental timescales.

These results confirm that hydrolysis makes no meaningful contribution to CT mass removal in site-specific 200-ZP-1 OU groundwater and that the CT degradation observed in sediment-containing abiotic and biotic Phase II treatments is attributable entirely to mineral-mediated or microbially driven transformation processes. Hydrolysis is therefore not considered a viable natural attenuation mechanism for CT within the 200-ZP-1 OU on any remediation-relevant timescale.

5.2 Chemical Characterization

5.2.1 Groundwater

Groundwater characterization of the 200-ZP-1 OU reveals a highly aerobic geochemical environment dominated by elevated nitrate (NO_3-) and sulfate (SO_4^2-) concentrations, which significantly influences the potential for both abiotic and biotic degradation of CT. Nitrate levels were particularly high, ranging from 49.8 to 179.0 mg/L, identifying it as a major competing electron acceptor that may inhibit reductive dechlorination of CT. Chloride (Cl-) concentrations varied between 23.9 and 56.0 mg/L, while nitrite (NO_2-) and phosphate (PO_4^3-) remained below detection limits in both samples.

NPOC analysis showed that electron donor availability is extremely limited. While sample 299-W11-100 showed no detectable NPOC, sample 299-W11-116 contained a low concentration of 6.94 mg/L. The chemical composition, bioavailability, and quality of this organic fraction remain uncharacterized and may include a mixture of labile and refractory compounds. Its low concentration suggests that the native groundwater environment is likely carbon-limited for microbial CT degradation under bulk aquifer conditions, though the potential contribution of sediment-bound organic carbon as a supplementary electron donor source is addressed in Section 5.2.2.3. These background parameters established the baseline conditions for subsequent abiotic and biotic batch degradation studies spiked with CT stock solutions.

Table 13. Groundwater anions and NPOC in mg/L from the 200-ZP-1 OU, Phase II.

Groundwater Anion & Total Organic Carbon Results (mg/L)								
Well Name	Br^-	Cl^-	F^-	NO_3^-	NO_2^-	PO_4^{3-}	SO_4^{2-}	NPOC
299-W11-116	0.187	56.0	0.287	49.8	ND	ND	85.6	6.94
299-W11-100	ND	23.9	0.267	179.0	ND	ND	56.0	ND
Detection Limit	0.02	0.01	0.01	0.03	0.04	0.07	0.03	0.05

5.2.2 Sediment

5.2.2.1 Anions

Water-extractable anion analysis of the 200-ZP-1 OU Phase II sediments revealed consistently low concentrations across all measured species, with sulfate (SO_4^{2-}) and chloride (Cl^-) identified as the primary anionic constituents. Sulfate was detected in every sample, ranging from 1.07 to 2.63 mg/kg, and generally represented the highest mass fraction among the anions. Chloride concentrations followed a

similar range of 0.52 to 1.95 mg/kg, with intra-well replicates exhibiting relatively consistent values. Bromide (Br^-) and nitrite (NO_2^-) were not detected in any samples. Fluoride (F^-) concentrations remained low and stable (0.04 to 0.44 mg/kg), though a localized increase in sample B4JT79 (0.44 mg/kg) was measured. Nitrate (NO_3^-) typically was not detected and was only quantified in sample B4JT77 (0.11 mg/kg), with B4JT79 below the reporting threshold (<0.05 mg/kg). Phosphate (PO_4^{3-}) was generally near the reporting threshold, with several samples reported as non-detect or less than values in several samples with quantifiable concentrations observed intermittently (0.15 to 0.18 mg/kg).

Table 14. Water-extractable anions from the 200-ZP-1 OU, Phase II sediment.[(a)]

			Sediment Anions (mg/kg dry sediment)						
Borehole ID	Unit	Sample ID	Br^-	Cl^-	F^-	NO_3^-	NO_2^-	PO_4^{3-}	SO_4^{2-}
C9993	Rwie	B4JT76	ND	1.95 ± 0.11	0.04 ± 0.00	ND	ND	< 0.12 ± 0.04	1.72 ± 0.11
		B4JT77	ND	0.82 ± 0.27	0.12 ± 0.03	0.11 ± 0.04	ND	0.15 ± 0.01	1.54 ± 0.62
		B4JTM3	ND	1.29 ± 0.19	0.05 ± 0.02	ND	ND	< 0.14 ± 0.04	2.04 ± 0.31
		B4JTM4	ND	0.96 ± 0.13	0.04 ± 0.03	ND	ND	0.15 ± 0.01	2.63 ± 0.34
D0474	Rwia	B4JT78	ND	1.50 ± 0.10	0.06 ± 0.01	ND	ND	0.18 ± 0.04	1.15 ± 0.49
		B4JT79	ND	0.52 ± 0.06	0.44 ± 0.05	< 0.05 ± 0.02	ND	< 0.13 ± 0.04	1.26 ± 0.16
		B4JTM5	ND	0.64 ± 0.24	0.05 ± 0.00	ND	ND	ND	1.07 ± 0.42
		Detection Limit	0.02	0.01	0.01	0.03	0.04	0.07	0.03

(a) Samples with a less than sign had replicates that were below detection limits.

5.2.2.2 Iron / Manganese Quantification

Adsorbed-phase extractions from cores collected in boreholes 299-W11-100 and 299-W11-116 showed iron concentrations [Fe(II), Fe(III), and total Fe] below analytical detection limits in all samples. In contrast, low but measurable adsorbed manganese was detected in several cores, ranging from below detection to 0.03 mg/g soil. The highest manganese concentrations (0.03 mg/g) occurred in units classified as Rwie (cores B4JT76 and B4JTM4), while some samples from the Rwie and Rwia units were below detection. Overall, the adsorbed mineral phase appears to contain negligible iron and minor amounts of manganese across the sampled intervals.

Acid digestion of mineral-phases from cores in boreholes 299-W11-100, 299-W11-116, and 299-W11-117 indicated measurable iron and manganese across all samples. Total iron ranged from 1.16 to 2.67 mg/g soil, with Fe(III) species being more prevalent than Fe(II) species in all units. Sample B4JT76 (Rwie) had the highest total iron concentration of all Phase II samples (2.67 ± 0.45 mg/g), with Fe(II) (2.16 ± 0.58 mg/g) substantially exceeding Fe(III) (0.51 ± 0.13 mg/g), indicating a predominantly reduced iron mineral assemblage in this interval. Manganese concentrations were lower than iron but consistently detected, ranging from 0.05 to 0.19 mg/g soil, with the highest value observed in Rwie (B4JT76). Overall, the Rwie and Rwia units contained comparable amounts of mineralogical iron and low but persistent manganese.

Table 15. Mineral phase iron and manganese concentrations for 200-ZP-1 OU, Phase II sediment derived from acid digestion of bulk sediment samples. Fe(II) was quantified by ferrozine colorimetric assay. Fe(III) was calculated as the difference between total Fe measured by ICP-OES and Fe(II). Mn was measured by ICP-OES. Detection limits: Fe(II) ≈ 0.01 mg/g; total Fe and Mn ≈ 0.02 mg/g.

Mineral Phase Iron and Manganese Concentrations (Analyte (mg/g soil) ± Std. Dev.)						
Borehole ID	Unit	Sample ID	Fe (II)	Fe (III)	Total Fe	Manganese
C9993	Rwie	B4JT76	2.16 ± 0.58	0.51 ± 0.13	2.67 ± 0.45	0.19 ± 0.02
		B4JT77	0.17 ± 0.26	0.98 ± 0.14	1.16 ± 0.40	0.08 ± 0.04
		B4JTM3	0.50 ± 0.29	1.35 ± 0.20	1.85 ± 0.25	0.06 ± 0.01
		B4JTM4	0.30 ± 0.17	1.77 ± 0.16	2.08 ± 0.32	0.15 ± 0.01
D0474	Rwia	B4JT78	0.16 ± 0.05	1.09 ± 0.15	1.25 ± 0.19	0.05 ± 0.01
		B4JT79	0.16 ± 0.06	1.33 ± 0.09	1.50 ± 0.04	0.07 ± 0.01
		B4JTM5	0.12 ± 0.03	1.18 ± 0.14	1.29 ± 0.16	0.10 ± 0.01

5.2.2.3 Total Carbon

Carbon analysis was conducted in triplicate on sediment from each core material. Results showed a range of total carbon from 531 to 1990 µg/g, with lower amounts of TIC (203 to 1430 µg/g) compared to the amount of TOC (331.0 to 1383.3 µg/g). Results are presented in Table 16 in µg/g. Analytical variance was calculated for total carbon and TIC where sufficient replicated data were available.

Table 16. Total carbon concentrations for the 200-ZP-1 OU, Phase II sediment.

Borehole ID	Unit	Sample ID	Total Carbon (µg/g)	Total Inorganic Carbon (µg/g)	Total Organic Carbon (µg/g)
C9993	Rwie	B4JT76	1990 ± 26	1430 ± 66	560 ± 71
		B4JT77	618 ± 2	<200	>418 ± 2
		B4JTM3	531 ± 52	<200	>331 ± 52
		B4JTM4	674 ± 95	<200	>474 ± 95
D0474	Rwia	B4JT78	710 ± 42	<200	>510 ± 42
		B4JT79	592 ± 20	203	>389 ± 20
		B4JTM5	1583 ± 647	<200	>1383 ± 647

TIC values that were reported as ND are shown as the LOD of the instrument, 200 µg/g.

Sediment characterization from boreholes C9993 (Rwie) and D0474 (Rwia) reveals low but geochemically significant levels of organic carbon within the sediments. TOC values typically remained below 0.25 wt%, with individual samples ranging from approximately 331 to 1383 µg/g. While the bulk of this sediment-bound organic carbon is expected to be largely refractory in chemical character, consistent with slow turnover rates and limited recent terrestrial carbon inputs at this site (Lin et al. 2012; Stegen et al. 2018), even predominantly refractory organic carbon pools typically contain a small labile fraction capable of supporting limited microbial activity. The batch experiments, which are closed systems with no external carbon replenishment, appear to have consumed this labile fraction to support the CT transformation observed over the incubation period. Under field conditions, where the labile fraction would be subject to ongoing depletion without equivalent replenishment, the electron donor capacity of sediment-bound organic carbon alone is expected to be insufficient to sustain CT degradation

rates comparable to those measured in these batch experiments over the long term. TIC was generally low across both units, frequently falling below the instrument detection limit of 200 µg/g, with the exception of the shallowest sample (B4JT76), which contained 1430 µg/g.

Despite these low absolute concentrations, the indigenous organic carbon appears to be a critical driver for the observed biotic degradation of CT. To illustrate, if we assume acetate (CH_3COO^-) as the electron donor, the stoichiometric reductive dichlorination of 1 mole of CT to 1 mole of CF requires 2 moles of electrons. One mole of acetate provides 8 moles of electrons. At the lowest measured sediment TOC concentration of approximately 331 µg/g, a 10-gram sediment aliquot contains approximately 3.31 mg TOC. If we represent this organic carbon as acetate, this corresponds to approximately 0.055 mmol organic carbon equivalents, providing approximately 0.44 mmol of electrons. The nominal CT mass in a 20 mL aqueous volume spiked to 800 µg/L is approximately 104 nmol aqueous (280 nmol of total CT mass in our closed batch system), requiring 208 nmol of electrons for CT-to-CF conversion (560 nmol of electrons for CT-to-CF conversion).

The sediment TOC therefore has the theoretical electron donor capacity to support CT-to-CF conversion of the experimental CT mass if even a small fraction of the total TOC is bioavailable. This calculation assumes complete electron donor utilization and does not account for competing electron acceptors such as nitrate, which would consume a significant fraction of the available reducing equivalents. The experimental results argue that the quality and capacity of this native organic matter are sufficient to support reductive pathways under these batch experimental conditions.

5.3 Physical and Mineralogical Characterization

5.3.1 Particle Size Distribution

Particle size distribution was performed by sieving the entire core material to determine coarse (> 2 mm) and fine (<2 mm) fractions. The fine fraction was then analyzed using a laser particle size analyzer to quantify sand (63 µm to 2 mm), silt (63 to 4 µm), and clay (<4 µm) based in three replicate measurements per sample. Additional details are provided in Appendix A, Section A.2.2.

Sediments from both wells (Table 17) are dominated by coarse material, with 75% to 89% of the samples in the >2-mm fraction and sand comprising ~50% to 84% of the <2-mm fraction. Silt is the secondary component (approximately 16% to 44%), while clay represents a very small proportion (<6%) of the fine fraction in all samples. Overall, the particle size distributions indicate predominantly sandy, low-clay sediments with some variability in silt content among samples.

Table 17. Particle size distribution for 200-ZP-1 OU, Phase II sediment.

			Particle Size Distribution (%)				
Borehole ID	Unit	Core ID	>2mm	<2mm	Sand (63 µm-2 mm)	Silt (63-4 µm)	Clay (<4 µm)
C9993	Rwie	B4JT76	74.88	25.12	64.58 ± 5.23	34.18 ± 4.99	1.24 ± 0.24
		B4JT77	76.66	23.34	71.19 ± 4.42	28.16 ± 4.28	0.64 ± 0.14
		B4JTM3	76.65	23.35	50.58 ± 7.50	43.82 ± 6.52	5.60 ± 0.99
		B4JTM4	28.89	71.11	81.71 ± 3.46	17.60 ± 3.26	0.68 ± 0.21
D0474	Rwia	B4JT78[(a)]	89.34	10.66	80.07 ± 5.31	19.74 ± 5.19	0.19 ± 0.13
		B4JT79	79.14	20.86	83.50 ± 3.81	16.03 ± 3.60	0.48 ± 0.21
		B4JTM5	87.11	12.89	79.84 ± 3.69	19.97 ± 3.64	0.19 ± 0.05

The particle size distribution for boreholes C9993 and D0474 indicates that the samples are predominantly coarse-grained, with a high percentage of material exceeding 2 mm in diameter. In borehole D0474 (Rwia), this coarse fraction is particularly dominant, averaging approximately 85%, whereas borehole C9993 (Rwie) shows more variability, including one sample (B4JTM4) where the fine-grained fraction (<2 mm) accounts for 71.11%.

Within the fine-grained fraction (<2 mm), sand is the primary constituent across all samples, generally ranging from 50.58% to 83.50%. Sediment samples from borehole D0474 contain at least 79% sand. In contrast, borehole C9993 shows a higher degree of heterogeneity; while some samples are sand-rich, others like B4JTM3 contain significant amounts of silt (43.82%) and a relatively elevated clay content (5.60%).

5.3.2 Mineralogy by X-ray Diffraction

Table 18. XRD results for the 200-ZP-1 OU, Phase II sediment.

			Mineral Group by XRD (wt%)				
Borehole ID	Unit	Core ID	Pyroxene	K-Feldspar	Feldspar	Quartz	Amorphous
C9993	Rwie	B4JT76	2.36	1.00	14.94	33.99	47.71
		B4JT77	1.88	1.50	21.46	37.72	37.45
		B4JTM3	1.95	1.89	18.86	29.37	47.92
		B4JTM4	2.32	1.66	20.26	38.49	37.28
D0474	Rwia	B4JT78	1.68	2.73	13.83	30.33	51.43
		B4JT79	2.49	3.26	18.90	31.29	44.06
		B4JTM5	1.74	2.44	11.72	39.13	44.97

The mineralogical analysis of samples from boreholes C9993 and D0474, as determined by XRD, characterizes these units as being primarily dominated by amorphous material and quartz. Across all samples, amorphous content was the most significant constituent, ranging from 37.28 to 51.43 wt%, while quartz serves as the primary crystalline phase, consistently contributing between 29.37 and 39.13 wt%. These two components together constitute the majority of the mineral matrix, accounting for over 75% of the total weight.

Feldspar is the second dominant mineral group, with total concentrations (including K-feldspar) typically ranging between 14% and 23%. In borehole C9993, Rwie, there is a slightly higher average concentration of total feldspar compared to borehole D0474, Rwia, which tends toward higher amorphous levels. Pyroxene and K-feldspar represent minor constituents, consistently remaining below 3.5 wt% each.

6.0 Discussion

6.1 Phase I

Phase I experiments provided a preliminary assessment of CT degradation potential using site-specific Hanford sediments and groundwater from both the high-concentration source zone (C9739, C9996) and the low-concentration plume perimeter (D0082, D0083). While the analytical limitations of the SPME-GC/MS approach and the statistical rigor applied to data analysis precluded quantitative rate determinations for most samples, the results collectively established that CT degradation potential is heterogeneous across the 200-ZP-1 OU and is strongly governed by the mineralogical and geochemical character of specific geologic units.

6.1.1 Combined Biotic-Abiotic Degradation

Combined biotic-abiotic degradation results from Phase I were largely inconclusive due to the precision limitations of the SPME-GC/MS method, particularly at the low initial CT concentrations used for D0082 and D0083 samples (Table 2). For these boreholes, measured CT responses were frequently near or below the instrument detection limit, and the observed scatter in concentration data could not be reliably distinguished from analytical noise. As a result, rate constants estimated for D0082 and D0083 samples carry wide confidence intervals that encompass zero, precluding meaningful half-life calculations for most intervals (Table 5).

For the high-concentration boreholes C9739 and C9996, experiments were initiated at substantially higher CT masses (130 to 160 nmol), which should have provided a more favorable signal-to-noise environment. However, CT concentrations in C9739 samples (B48BN5, B48BN6, B48BN7) remained near initial values throughout the 37-day incubation period, with regression-derived rate constants close to zero and very low R^2 values (0.08 to 0.29). These outcomes indicate a negligible biotic-abiotic response for C9739 sediments under the experimental conditions tested.

C9996 results were more variable: Sample B48BN8 exhibited a downward trend in CT concentration that was accompanied by the concurrent production and accumulation of CF, providing a second and independent line of evidence for CT transformation. The increase of CF as CT declined is consistent with sequential reductive dichlorination, the stepwise removal of chlorine substituents driven by microbial co-metabolism or Fe(II) reduction under anaerobic conditions, and confirms that the observed CT mass reduction in B48BN8 reflects a chemical transformation rather than volatilization loss or analytical artifact. This constitutes the clearest positive signal for reductive dechlorination observed in Phase I. In contrast, B48BN9 and B48BP0 showed neither a measurable decline in CT nor any detectable CF accumulation, indicating no active reductive dechlorination in these intervals under the conditions tested. The production of CF as a transformation product, while representing only partial dechlorination of the CT parent compound, is nevertheless significant as it demonstrates that the indigenous microbial community and/or minerology associated with C9996 sediments retains the capacity to initiate the reductive dechlorination pathway under the anoxic, unaugmented conditions of these experiments, and establishes a positive qualitative signal that informed the design and interpretation of the more rigorously controlled Phase II experiments.

The limited biotic activity observed in Phase I high-concentration zone sediments is broadly consistent with the groundwater chemistry data. Well 299-W11-98 (C9739) exhibited the highest measured nitrate concentration among Phase I wells at 256 mg/L, a level substantially above the threshold at which nitrate is known to competitively inhibit CT reductive dechlorination (~10 to 100 mg/L). Under these conditions, denitrifying microorganisms would be expected to preferentially reduce NO_3^- rather than CT as the

terminal electron acceptor, suppressing the co-metabolic pathway responsible for CT transformation. Well 299-W14-24 (C9996) was geochemically anomalous, with non-detectable nitrate and substantially lower chloride and sulfate concentrations, suggesting it lies outside the primary contaminant source zone.

The comparatively stronger biotic-abiotic signal observed in B48BN8 relative to other Phase I samples may in part reflect these more favorable redox conditions, as the absence of competing nitrate would remove a principal inhibitor of reductive dechlorination and allow CT to serve more effectively as a terminal electron acceptor for the indigenous microbial community. The complete absence of detectable TOC in all Phase I groundwater samples further constrains the electron donor supply available to sustain indigenous denitrifying populations, consistent with the generally subdued biotic responses observed across Phase I sediments.

Sediment-bound organic carbon was not quantified in Phase I, but the particle size data provided indirect context. The Rlm intervals sampled within D0083 are distinctly fine-grained, with less than 1% coarse material and silt fractions exceeding 75% to 85% of the less than 2-mm fraction. These fine-grained intervals represent the low-permeability zones identified in the conceptual model as most likely to support anaerobic conditions and harbor residual organic carbon capable of sustaining microbial activity. The lack of a measurable combined biotic-abiotic signal from these intervals under Phase I conditions may reflect analytical detection limitations of the SPME-GC/MS approach at low CT concentrations, the absence or suppression of degradation activity under the specific experimental conditions tested, or both. The available data do not allow these explanations to be distinguished. This distinction is consequential. If biotic activity is occurring in fine-grained Rlm sediments but cannot be resolved by the Phase I analytical method, the contribution of these intervals to bulk aquifer CT attenuation would be systematically underestimated. Addressing this uncertainty was a primary motivation for the methodological improvements implemented in Phase II, which were designed to provide the sensitivity and precision necessary to detect and quantify CT degradation signals in sediments where transformation rates or initial contaminant concentrations are low.

6.1.2 Abiotic Degradation

In contrast to the biotic results, the abiotic experiments revealed a stronger and more interpretable signal across several Phase I borehole sediments, with degradation dynamics that correlate meaningfully with mineralogical and geochemical characteristics (Table 4, Figure 6).

D0082 sediments exhibited the most aggressive abiotic CT degradation observed in Phase I. Samples B3W6C7 (Rwie) and B3W6H5 (Rwia) reached near-complete CT removal within 20 to 30 days, following steep exponential decay curves with high R^2 values (0.938 to 0.993) and short half-lives of 3 to 10 days. This reactivity is attributable in part to the elevated total Fe content observed in D0082 acid digests, with B3W6C7 containing the highest total Fe among all Phase I samples (1.92 mg/g), including a substantial Fe(II) fraction (1.05 mg/g). Fe(II)-bearing mineral phases, such as surface-bound ferrous iron and potentially magnetite or green rust, are well-established electron donors for the abiotic reductive dechlorination of CT (Bagwell et al. 2019; Kriegman-King and Reinhard 1994; Zhang et al. 2025). The elevated carbonate content of D0082 sediments (averaging 0.90 wt% by XRD, the highest of the four boreholes) may also play a facilitative role, as carbonate phases can serve as surface sites that promote electron transfer reactions between Fe(II) and chlorinated compounds. The notably low feldspar content in D0082 relative to C9996 is also consistent with a more reactive mineralogical assemblage, as feldspar phases are generally considered inert with respect to reductive transformation reactions.

In contrast, D0083 was the least abiotically reactive borehole, with degradation curves that remained nearly horizontal across all five samples over 70 days and fitted rate constants near zero. The mineralogical profile of D0083 is dominated by high mica content in the Rlm intervals (averaging

>12 wt%), which is substantially higher than in any other borehole. Mica phases do not contribute meaningfully to reductive CT transformation, and the Fe(II) content of D0083 Rlm samples was correspondingly low: B3WXM7 contained only 0.05 mg/g Fe(II) and 0.01 mg/g Mn, well below concentrations measured in reactive D0082 intervals. The one exception within D0083 is sample B3WXN3, which contained a notably higher Fe(II) concentration of 1.36 mg/g, the highest measured in any D0083 sample. While the abiotic half-life estimated for B3WXN3 was still relatively long (~71 days), the elevated Fe(II) content of this interval relative to its co-located D0083 samples is broadly consistent with the positive relationship between Fe(II) availability and abiotic CT degradation capacity observed across the Phase I dataset.

C9739 abiotic results were mixed. B48BN7 (Rwia) showed the most pronounced degradation within this borehole, with an estimated half-life of ~85 days and an R^2 of 0.628. This interval also contained the highest total Fe among C9739 samples (1.10 mg/g), with an approximately equal Fe(II)/Fe(III) ratio (0.56/0.55 mg/g), suggesting a partially reduced mineral assemblage capable of electron donation. Conversely, B48BN5 and B48BN6 showed negligible or slightly negative rate constants with very low R^2 values, indicating no reliable abiotic degradation. These shallower Rwie and Rwie/a intervals had substantially lower total Fe (0.70 and 0.88 mg/g, respectively) and almost exclusively Fe(III) speciation, consistent with more oxidized sediment conditions that are less capable of supporting abiotic reduction.

C9996 abiotic results were the most variable and least well-constrained of all Phase I boreholes, with low R^2 values for all three samples and a rate constant for B48BN8 that carries a confidence interval spanning both positive and negative values. C9996 sediments had the highest concentrations of feldspar (27.3 wt% average) and chlorite (2.3 wt%) of any borehole and notably low Fe(II) fractions in B48BN8 (0.03 mg/g) and B48BN9 (0.03 mg/g), except for B48BP0, which had a relatively elevated Fe(II) content of 0.93 mg/g. The disproportionately high Fe(III)/Fe(II) ratio in the upper two C9996 intervals implies that these sediments are relatively oxidized, consistent with a lower capacity for abiotic CT reduction. The variability of C9996 results, combined with its anomalous groundwater chemistry (non-detectable nitrate), may also reflect spatial heterogeneity in the degree of sediment oxidation encountered at different depth intervals within this borehole.

Taken together, the Phase I abiotic data support a conceptual model in which the rate and extent of abiotic CT degradation in Hanford sediments is primarily controlled by the availability of Fe(II) in the reactive mineral fraction, with higher Fe(II) inventories corresponding to shorter half-lives and more complete CT removal. The failure to observe a similarly clean relationship between total Fe and reactivity across all boreholes, particularly the variability in C9996, underscores the importance of Fe speciation rather than total Fe abundance in governing abiotic transformation potential. Manganese contributed modestly to reductive capacity across Phase I sediments, with low but detectable Mn in samples from all boreholes except C9996, though its quantitative role relative to Fe(II) could not be resolved from the available data.

The hydrolysis control experiments, in which CT was incubated in site-specific groundwater without sediment, showed no statistically significant loss of CT mass over 150 to 180 days for the high-concentration C9739 and C9996 groundwaters. These results are consistent with the previously modeled hydrolysis half-life of 630 years for Hanford groundwater conditions and confirm that hydrolysis makes no meaningful contribution to CT mass reduction on remediation-relevant timescales. Measurements for D0082 and D0083 groundwaters were inconclusive due to instrument detection limit constraints at low initial concentrations.

6.2 Phase II

Phase II addressed the analytical limitations of Phase I through improved core preservation protocols, standardized laboratory procedures, and the adoption of GC-ECD detection, which provided greater sensitivity and selectivity for chlorinated methane analysis. These improvements, combined with the use of sediment cores from the high-concentration zone (C9993, D0474), yielded well-defined first-order degradation curves with higher R^2 values and narrower confidence intervals on rate parameters, enabling quantitative half-life estimates to be made with greater confidence.

6.2.1 Combined Biotic-Abiotic Degradation

Phase II biotic experiments demonstrated substantially more active and measurable CT degradation compared to Phase I. Near-complete CT removal was achieved in multiple sediment intervals and well-constrained first-order rate constants spanning a range of 0.064 to 0.273 day^{-1} for C9993 and 0.069 to 0.095 day^{-1} for D0474 were quantified (Table 11). Corresponding half-lives ranged from approximately 2.5 to 11 days for C9993 and 7 to 10 days for D0474, representing the most rapid site-specific CT degradation rates measured in this study.

For C9993 (Rwie), all four sediment intervals showed measurable CT degradation over the 80+ day incubation, with the shallowest sample B4JT76 exhibiting the fastest degradation ($k = 0.273\ day^{-1}$, $t_{½} \approx$ 2.5 days). Data revealed concurrent accumulation of CF to approximately 100 nmol by day 30, accounting for roughly 50% of the initial CT mass. The stabilization of CF mass beyond day 30 indicates that CF was likely being transformed to lesser chlorinated products, consistent with a sequential reductive dechlorination pathway. This is a significant finding, as it demonstrates not merely CT-to-CF conversion but continued dechlorination beyond CF under native, unaugmented site conditions. The deeper C9993 intervals (B4JTM3, B4JTM4) showed lower rate constants and less well-constrained fits, with B4JTM3 yielding a statistically non-significant rate constant, suggesting that degradation potential may decrease with depth within this borehole.

D0474 (Rwia) exhibited consistently lower biotic degradation rates than C9993 across all three sampled intervals, with comparable rate constants of approximately 0.069 to 0.095 day^{-1}. The CF accumulation profile for D0474 was distinct: Only ~50 nmol CF was recovered by day 80, representing approximately 20% of the initial CT mass. This low CF yield relative to initial CT mass, combined with the rapid overall CT removal (approximately 90% by day 80), implies that CT degradation in D0474 sediments is occurring concurrently with CF transformation to lesser chlorinated products. This pattern is consistent with a more complete dechlorination pathway in D0474 relative to C9993, possibly reflecting differences in microbial community composition or the geochemical conditions within the Rwia that favor more rapid CF consumption.

The occurrence of combined biotic-abiotic degradation in the presence of high background NO_3^- concentrations, 179.0 mg/L in C9993 groundwater and 49.8 mg/L in D0474 groundwater, is a particularly important observation. Previous studies at Hanford have demonstrated that nitrate exerts a competitive inhibitory effect on CT transformation under denitrifying conditions, with concentrations above approximately 8 mg/L shown to inhibit CT transformation by the Hanford denitrifying consortium (Skeen et al. 1995). Sherwood et al. (1996) further demonstrated that CT transformation by the Hanford denitrifying consortium can proceed via two competing pathways. One pathway produces CF as the predominant end product when nitrate and nitrite are depleted, accounting for approximately 50% of transformed CT. The second pathway produces CO_2 as the primary end product when electron donor is limiting, with only approximately 4% of transformed CT appearing as CF. The near-complete CT degradation observed in C9993 sediments against a background of 179.0 mg/L NO_3^- suggests either that (1) the indigenous microbial community retained the capacity for CT transformation despite conditions

that would otherwise be considered inhibitory or (2) nitrate was progressively depleted within the closed batch system during incubation, gradually relieving competitive inhibition and permitting CT-reducing conditions to develop over time. Abiotic mineral-mediated reduction by Fe(II) phases may have additionally contributed to the observed CT transformation in combination with biotic processes, and the relative contribution of each pathway cannot be determined from the available data alone.

The pattern of CF accumulation observed in C9993 experiments, where approximately 50% of the initial CT mass was recovered as CF, is consistent with the nitrate-limiting pathway described by Sherwood et al. (1996). The sediment TOC data provides additional context for this interpretation. TOC values across C9993 intervals ranged from approximately 331 to 560 µg/g, representing the primary source of electron donor in these unaugmented experiments given that groundwater TOC was below detection. The limited and potentially refractory nature of this sediment-bound organic carbon (e.g., Lin et al. 2012; Stegen et al. 2018) suggests that as incubation proceeded, the system likely transitioned through conditions ranging from electron donor limitation toward nitrate limitation as both substrates were progressively consumed, potentially influencing the relative expression of the two competing CT transformation pathways. The comparatively lower NO_3^- background in D0474 groundwater (49.8 mg/L) and the lower CF accumulation observed in those experiments, where sediment TOC ranged from approximately 389 to 1383 µg/g, are broadly consistent with a system in which the relative availability of electron donor and electron acceptor shifted differently over the course of the incubation, though a definitive mechanistic interpretation cannot be made from the available data alone.

Indigenous sediment organic carbon, rather than groundwater-derived dissolved organic carbon, appears to be the primary electron donor sustaining biotic CT degradation under the experimental conditions of this study, given that groundwater TOC was below detection in C9993 and only 6.94 mg/L in D0474. The sediment-bound TOC therefore represents a critical but finite source of reducing capacity. As this native organic carbon pool is progressively consumed, the electron donor available to sustain microbial CT transformation will diminish, potentially shifting the system toward increasingly carbon-limited conditions over time. This depletion of sediment-bound organic carbon, in the absence of external replenishment, is identified as a key limitation on the long-term sustainability of biotic natural attenuation in the 200-ZP-1 OU under current site conditions. This interpretation underscores the potential value of electron donor augmentation as a strategy for enhancing and sustaining CT degradation rates beyond what can be supported by the native sediment carbon reservoir alone.

The particle size distributions of Phase II sediments (Table 18) indicate predominantly coarse-grained, sandy materials in both boreholes, with >2 mm fractions ranging from approximately 75% to 89% in D0474 and showing more variability in C9993. However, sample B4JTM3 from C9993 is a notable exception, containing 43.82% silt and 5.60% clay in the fine fraction – the highest clay content of any Phase II sample. This interval also had the highest amorphous mineral content by XRD (47.92%) and an elevated TOC (>331 µg/g). However, the biotic degradation rate for this interval was among the lower and less well-constrained in C9993, and does not provide clear experimental support for the conceptual model that fine-grained zones preferentially support CT degradation under the conditions tested. The relatively coarse character of the remaining Phase II sediments suggests that even in sandy, higher-permeability units, native microbial populations associated with mineral surfaces retain the capacity for CT degradation, though the volume fraction of the aquifer where these conditions are sustained at steady state may be smaller than in fine-grained units.

6.2.2 Abiotic Degradation

Phase II abiotic experiments demonstrated CT degradation in C9993 sediments with well-defined first-order kinetics for the two shallower intervals, yielding half-lives of approximately 5 and 13 days for B4JT76 and B4JT77, respectively (Table 12). These rates are substantially faster than the hydrolysis half-

life of 630 years and represent a meaningful contribution of abiotic mineral-mediated reduction to overall CT mass removal in Rwie. Abiotic degradation capacity decreased with increasing depth within C9993, with B4JTM3 and B4JTM4 yielding non-significant rate constants and low R^2 values, indicating negligible abiotic activity at these depths under the experimental conditions tested.

The iron and manganese characterization data provide a mechanistic basis for these observations. Sample B4JT76, which exhibited the fastest abiotic degradation ($k = 0.129\ day^{-1}$), contained the highest total Fe concentration of all Phase II samples (2.67 mg/g) and had a substantially higher Fe(II) fraction (2.16 mg/g) relative to Fe(III) (0.51 mg/g), indicating a predominantly reduced iron mineral assemblage. This elevated Fe(II) inventory is consistent with a high capacity for electron donation to CT via surface-catalyzed reductive dechlorination. B4JT76 also had the highest manganese concentration (0.19 mg/g) and the highest TIC content (1430 µg/g), reflecting a carbonate-rich mineral environment. The elevated TIC in this sample may be associated with siderite ($FeCO_3$) or other Fe(II)-bearing carbonate phases that could serve as reactive mineral surfaces for CT reduction (Pearce et al. 2018). This interpretation is consistent with the role of Fe(II)-carbonate phases in promoting abiotic CT degradation observed in D0082 sediments during Phase I and with the generally higher TIC content of Phase I D0082 samples relative to other boreholes.

Deeper within C9993, B4JT77 showed a markedly different Fe speciation profile. Ferric iron, Fe(III) (0.98 mg/g), dominated over Fe(II) (0.17 mg/g), yielding a total Fe of only 1.16 mg/g, the lowest among C9993 samples. Despite this shift toward more oxidized iron speciation, a measurable abiotic half-life of ~13 days was still obtained for B4JT77, suggesting that even relatively small quantities of surface-accessible Fe(II) can catalyze meaningful CT transformation rates under the anoxic batch conditions employed. Sediment samples B4JTM3 and B4JTM4 contained intermediate total Fe values (1.85 and 2.08 mg/g, respectively) with Fe(II) fractions of 0.50 and 0.30 mg/g, but their abiotic degradation rates were statistically indistinguishable from zero. This apparent inconsistency – lower Fe(II) in B4JT77 yet a measurable rate, compared to higher Fe(II) in B4JTM3 yet no measurable CT degradation – may reflect differences in the surface area, mineral phase identity, and accessibility of reactive Fe(II) sites rather than differences in bulk Fe(II) concentration alone. Alternative explanations include the possibility that sodium azide treatment was less effective at fully suppressing biological activity in B4JT76 and B4JT77 relative to the deeper samples, which would inflate apparent abiotic rates for those intervals.

In contrast to C9993, D0474 sediments showed no statistically significant abiotic CT degradation across any of the three sampled intervals, with rate constants near zero and universally low R^2 values (Table 12). The iron characterization data for D0474 (Rwia) support this outcome. All three D0474 samples were dominated by Fe(III) (1.09 to 1.33 mg/g), with correspondingly low Fe(II) fractions (0.12 to 0.16 mg/g), yielding low Fe(II)/Fe(III) ratios that indicate a predominantly oxidized mineral assemblage. Manganese concentrations were also lower in D0474 (0.05 to 0.10 mg/g) compared to C9993 (0.06 to 0.19 mg/g). The oxidized iron speciation in D0474 is consistent with a lower capacity for abiotic reductive dechlorination, and may reflect differences in the depositional environment and degree of post-depositional oxidation between the Rwie (C9993) and the deeper Rwia unit (D0474) site sediments.

Crucially, the air-exposure control experiments, in which sediments were intentionally pre-oxidized before addition of sodium azide, showed conservation of CT mass for both C9993 and D0474. These treatment results confirm that the CT degradation observed in companion anoxic treatments is dependent on reduced geochemical conditions and not an artifact of the sterilization chemistry. This result validates the interpretation that abiotic transformation of CT in these sediments is governed by reduced Fe mineral surfaces whose reactivity is irreversibly lost upon oxidation, and also underscores (1) the critical importance of maintaining anoxic conditions throughout sample collection and experimental preparation and (2) the need to identify anoxic zones in the subsurface.

The replicated batch experiments at 20 µg/L initial CT concentration showed no measurable CT degradation in either C9993 or D0474 sediments. This outcome is attributed to the large stoichiometric excess of NO_3^- relative to CT at this low concentration. Nitrate was present at levels three or more orders of magnitude higher than CT on a molar basis. Electron equivalents from Fe(II) mineral surfaces would therefore be preferentially consumed by nitrate reduction rather than CT reduction, effectively suppressing CT transformation. This concentration-dependent inhibition has important implications for scaling laboratory degradation rates to field conditions, as it suggests that in zones where CT concentrations approach or fall below 20 µg/L while NO_3^- remains in the tens to hundreds of mg/L range, abiotic degradation may contribute minimally to CT mass removal.

6.3 Controls on CT Degradation

Natural attenuation of CT within the 200-ZP-1 OU aquifer is primarily constrained by the oxic nature of the bulk aquifer. However, historical data and current site models suggest that anoxic microenvironments capable of supporting anaerobic CT transformation likely persist in low-permeability zones and hydrogeological transitions (Bagwell et al. 2019). Phase II results offer new, preliminary evidence of these conditions through DO (O_2) porewater measurements from core materials from D0474 and C9993. Although these results are FIO, they suggest that anoxic conditions exist in certain porewaters, indicating that the volume of the aquifer conducive to CT degradation may be underestimated. Quantifying these boundaries is essential for predicting long-term plume persistence, as localized anoxic conditions cannot be inferred from standard groundwater samples.

The potential for biotic degradation is further influenced by the site's specific groundwater chemistry. High concentrations of nitrate, ranging from 49.8 to 256 mg/L, were detected across examined wells and borehole sediments. As a preferred electron acceptor, nitrate likely competes with and inhibits the reductive dechlorination of CT. Furthermore, the pervasive lack of organic carbon in the groundwater suggests that these biotic reactions are carbon-limited. While low levels of indigenous organic carbon were measured in the sediments (typically < 0.25 wt%), and appear sufficient to drive limited biotic degradation, long-term attenuation would likely require external supplementation to overcome these nutrient and electron donor constraints. Expanding oxygen profiling during future drilling operations is recommended to improve the accuracy of plume simulations and remediation strategies.

6.3.1 Biotic Degradation

The groundwater data collected in this investigation consistently indicate a highly aerobic (oxic) environment characterized by high-potential electron acceptors (O_2, NO_3^-) and a scarcity of available energy sources, which together result in low levels of microbial activity. Elevated nitrate concentrations, ranging from 49.8 to 256 mg/L across the examined wells, confirm that the geochemical environment remains in an oxic state, as nitrate is only microbially consumed after DO is exhausted. This interpretation is further supported by the absence of nitrite and phosphate, alongside stable sulfate levels of up to 85.6 mg/L, confirming that the redox sequence has not progressed to the anaerobic stages necessary for robust reductive dechlorination of CT.

Biological activity is further constrained by a lack of available electron donors. NPOC concentrations in the groundwater were frequently below detection limits (0.05 mg/L), indicating a severely carbon-limited system. While the sediments themselves contain low levels of indigenous organic carbon (typically <0.25 wt%), the quality of this carbon is expected to be refractory in nature due to low inputs and slow regional turnover rates (Lin et al. 2012; Stegen et al. 2018). Despite its limited quantity, sediment-bound TOC represents the primary electron donor for the reductive pathways measured in this study and possesses sufficient capacity to stoichiometrically reduce CT to CF if even a small fraction is utilized. In the field, however, this process is hindered by the high nitrate background, which under denitrifying

conditions serves as a competing electron acceptor for CT reduction, though the degree of competitive inhibition is pathway-dependent and varies with the specific terminal nitrogen reduction product and the geochemical conditions of the system (Sherwood et al. 1996).

Denitrification, in which nitrate is reduced to N_2 coupled to the oxidation of organic carbon, is considered the primary microbial process driving CT transformation to CF in the 200-ZP-1 OU aquifer, and the inhibitory effect of elevated nitrate on this process is the principal geochemical constraint on biotic natural attenuation under current site conditions. This competitive inhibition, combined with overall carbon-limited conditions, is consistent with the absence of overwhelming evidence from aerial plume mapping that high rates of natural attenuation are occurring across the bulk aquifer under current geochemical conditions.

It is, however, important to acknowledge that traditional groundwater monitoring, which relies on samples collected over long screened well intervals, may not be capable of resolving depth-discrete signals of CT degradation. Groundwater chemistry averaging across these long screened intervals could obscure localized degradation signatures occurring within thin anoxic zones or fine-grained sediment intervals. Thus, the absence of a clear attenuation signal in monitoring data does not preclude the occurrence of meaningful CT degradation at smaller spatial scales. The batch experimental results reported here should therefore be interpreted as a measure of the inherent degradation potential of site-specific sediments under optimized anoxic conditions, rather than as a direct reflection of the degradation activity occurring across the bulk field aquifer at present.

A critical distinction between the closed batch experimental system employed in this study and open field conditions must be considered when interpreting these results in the context of plume-scale remediation. In the batch experiments, both the mass of CT and the mass of competing electron acceptors, principally nitrate, are fixed at the start of the incubation and are not replenished over the course of the experiment. Under these closed-system conditions, nitrate may be progressively consumed by the indigenous microbial community during the incubation period, gradually relieving competitive inhibition of CT reductive dechlorination and allowing biotic degradation to proceed over experimental timescales.

This dynamic is fundamentally different from the open, advection-dominated system that characterizes the 200-ZP-1 OU aquifer. Groundwater velocities in the 200 West Area are on the order of approximately 1 foot per day (DOE/RL 2006; Szecsody et al. 2005a; Williams et al. 2002), meaning that a volume of groundwater carrying both CT and nitrate at field-representative concentrations is continuously displaced and replaced at any given point in the aquifer. Under these advective conditions, the electron donor demand imposed by the sustained flux of nitrate would continuously suppress the onset of CT-reducing conditions, and the sediment-bound organic carbon available to support microbial activity would be subject to ongoing depletion without equivalent replenishment.

The degradation rates measured in batch experiments, even when statistically robust, should therefore not be interpreted as directly representative of *in situ* transformation rates operating across the plume at field scale. For biotic-abiotic CT degradation to translate into a meaningful reduction in plume volume under advective field conditions, the effective first-order degradation rate would need to be substantially higher than those measured here. The degradation rate must be sufficient to reduce CT concentrations along a given flow path faster than groundwater transport acts to redistribute contaminant mass across the plume.

At the groundwater velocities characteristic of this site, advective transport continuously delivers fresh CT and nitrate to any given point in the aquifer, and degradation must outpace this delivery for a net reduction in plume size to be achieved. Given the carbon-limited, nitrate-rich conditions of the bulk groundwater and the spatially restricted nature of the anoxic microenvironments identified in this study,

these are demanding conditions that are unlikely to be met by natural attenuation alone under current site geochemistry.

A simple plug-flow illustration demonstrates the scale of the gap between laboratory-derived rate constants and the requirements for field-scale plume attenuation. At a groundwater velocity of approximately 1 foot per day and a first-order CT degradation half-life of 7 days (representing the midpoint of the Phase II combined biotic-abiotic range), CT concentrations along a flow path would decrease by 50% over a transport distance of approximately 7 ft if degradation were occurring continuously across the entire aquifer volume. In reality, the anoxic microenvironments where these degradation rates apply likely represent only a small fraction of the total aquifer volume, and CT transported through the oxic bulk aquifer volume would not be subject to these rates. The effective bulk-aquifer half-life governing plume-scale CT attenuation is therefore substantially longer than the laboratory values and must be derived through calibration against field-scale concentration trends rather than from direct application of laboratory rate constants.

While the bulk aquifer is oxic, preliminary porewater measurements from core materials suggest that anoxic microenvironments may persist within low-permeability zones. These localized conditions, which cannot be inferred from standard groundwater samples, may support anaerobic CT transformation in volumes of the aquifer that are currently underestimated in site models. The Phase II biotic experiments demonstrate that, under anoxic conditions, native microbial populations, in combination with reduced iron phases, can drive near-complete CT degradation on timescales of weeks to months, even in the presence of substantial background nitrate concentrations. The half-lives measured in Phase II batch experiments, ranging from 2.5 to 11 days for C9993 and 7 to 10 days for D0474, are orders of magnitude shorter than the 400-year bulk aquifer half-life estimated by Bagwell et al. (2019) for reductive dechlorination under in-situ conditions. This discrepancy is expected, as the batch experiments represent optimal laboratory conditions with sediment-to-water ratios and anoxic environments more conducive to degradation than the bulk oxic aquifer. Nevertheless, these results confirm that the capacity for rapid biotic-abiotic CT transformation exists within the 200-ZP-1 OU sediment column where anoxic conditions and electron donor availability are favorable.

These considerations do not diminish the significance of the degradation capacity demonstrated in this study. Rather, they underscore the importance of carefully bounding the spatial and temporal scales over which laboratory-derived rates can be applied in predictive transport modeling. A clear distinction must be maintained between the intrinsic degradation potential measured in batch experiments and the effective natural attenuation rate that would be expressed under the hydrodynamic and geochemical conditions of the field aquifer. The detection of CF accumulation and its subsequent loss, presumably to DCM, in Phase II experiments provides circumstantial evidence that reductive dechlorination extends beyond the initial CT-to-CF conversion step. This finding is significant because it demonstrates that the indigenous biotic-abiotic processes are likely capable of driving sequential dechlorination under native, unaugmented conditions, and that these more complete dechlorination conditions may be more spatially widespread in the deeper aquifer than current site models assume.

Expanding DO profiling during future drilling operations is therefore recommended as a priority action. More comprehensive oxygen data would improve the accuracy of plume fate and transport simulations and better constrain the volume fraction of the aquifer where biotic degradation may be actively occurring. Together, these improvements would support a more rigorous evaluation of whether natural attenuation, operating in concert with the existing pump-and-treat system, could meaningfully contribute to achieving the 3.4 µg/L CT cleanup objective specified in the 200-ZP-1 OU ROD within the designated 125-year timeframe.

6.3.2 Abiotic Degradation

The abiotic redox capacity of Hanford sediments for CT degradation is primarily driven by the presence and availability of reduced Fe(II) mineral phases, which serve as electron donors for the reductive dechlorination of CT under anoxic conditions. Fe(II)-bearing minerals such as magnetite, green rust, and surface-bound Fe(II) are well-established reductants for CT transformation (Bagwell et al. 2019), and the Fe(II) concentrations measured across Phase I and Phase II sediment intervals are broadly consistent with the observed abiotic degradation responses. An analogous competition occurs in the abiotic system, where NO_3^- and CT compete for electrons from reduced Fe(II) mineral surfaces and dissolved metal complexes (Bagwell et al. 2019; Kriegman-King and Reinhard 1994; Zhang et al. 2025).

The extent to which this competition suppresses CT reduction depends on the relative concentrations, thermodynamics, and surface-specific reaction kinetics governing each competing reduction pathway. It is noted that the thermodynamic favorability of nitrate vs. CT as an electron acceptor varies depending on the specific nitrogen reduction product and the redox potential of the specific Fe(II) mineral phase involved, and therefore the degree to which nitrate suppresses abiotic CT reduction under site-specific conditions cannot be determined from the available data alone.

Reduced manganese phases were detected at low levels across several sediment intervals in this study, ranging from 10 to 30 µg/g. While dissolved Mn(II) or ordinary Mn(II) mineral surfaces alone are unlikely to mediate CT reduction significantly, the distribution of reduced Mn phases serves as a useful indicator of sediment redox status. The presence of reduced Mn is indicative of anoxic, reducing conditions that are prerequisite for both biotic and abiotic CT degradation pathways, and its spatial distribution across sampled intervals provides complementary evidence for the redox zonation inferred from Fe speciation and groundwater chemistry data.

It is further noted that manganese could potentially participate as a redox shuttle in CT-to-CF reduction only under specific conditions involving mixed-valence, surface-associated, or ligand-stabilized systems with an independent electron donor (O'Loughlin et al. 2022), conditions that were not specifically characterized in this study. The quantitative contribution of Mn to abiotic CT transformation in Hanford sediments is therefore considered negligible relative to Fe(II) and is not further evaluated here. It is also noted that sulfide-bearing mineral phases, which were not characterized in this study, represent a potentially important class of abiotic reductants for CT transformation in reduced sediment environments and warrant consideration in future characterization activities.

Despite these constraints, batch experiments using biological inhibitors demonstrate that an inherent abiotic redox capacity persists in the sediments. The observed CT degradation in abiotic treatments (conducted over periods of up to several months) suggests that reactive Fe(II) sites remain accessible and sufficient to reduce site-relevant concentrations of CT provided oxygen is excluded. While bulk acid-digestible Fe(II) was measured at concentrations up to 2.16 mg/g in Phase II sediments, the surface-accessible and dissolved Fe(II) fractions most directly relevant to interfacial electron transfer reactions were not detected in adsorbed-phase extractions. These results suggest that (1) the bioavailable Fe(II) fraction responsible for abiotic CT transformation may represent a small proportion of the total measured Fe(II) inventory and (2) the reactive surface area and accessibility of Fe(II) mineral phases, rather than their bulk abundance, are the primary determinants of abiotic CT degradation capacity in these sediments.

Across both phases of this investigation, the integrated characterization and degradation datasets support the conclusion that the abiotic CT degradation capacity of individual sediment intervals is more strongly correlated with Fe(II) mineral content and speciation than with total Fe, total Mn, or bulk mineralogy alone. Intervals with elevated Fe(II) fractions demonstrated the most rapid and complete abiotic CT removal, while intervals dominated by Fe(III) mineralogy showed negligible reactivity. These

relationships provide a basis for using Fe speciation data obtained from future drilling campaigns as a reliable predictor of abiotic CT degradation potential across the 200-ZP-1 OU, enabling more informed spatial targeting of natural attenuation assessments and potential *in situ* remediation enhancement strategies.

6.4 Implications for Reservoir-Scale Natural Attenuation

The laboratory half-lives measured in Phase I and Phase II batch experiments, ranging from days to months under optimized anoxic conditions, cannot be directly transposed to reservoir-scale predictions without careful consideration of the physical and geochemical heterogeneity of the 200-ZP-1 OU aquifer. Nevertheless, the collective results of this study provide a cautious but scientifically grounded basis for incorporating combined biotic-abiotic natural attenuation into revised conceptual and numerical models of CT plume behavior.

The central premise for upscaling is supported by the convergence of several site-specific observations: (1) the occurrence of measurable DO depletion in sediment porewaters; (2) the association of indigenous organic carbon and reactive Fe(II) mineral phases with finer-grained sediment intervals; and (3) the demonstration that native microbial populations, in combination with native reduced iron phases, can sustain near-complete CT degradation in the presence of site-specific groundwater chemistry.

Taken together, these findings support the interpretation that the fine-grained, low-permeability units within the aquifer represent discrete reactive zones where the geochemical prerequisites for both biotic and abiotic CT degradation are most likely to be simultaneously satisfied. At depth, where the influence of oxygenated recharge and surface-derived nitrate loading diminishes, the probability that these conditions are sustained over meaningful spatial and temporal scales increases, consistent with the conceptual model developed in Bagwell et al. (2019). Upscaling these results to the bulk aquifer therefore requires that future modeling efforts explicitly account for the volumetric fraction of the aquifer occupied by these reactive low-permeability zones, their spatial connectivity, and the mass transfer rates governing CT diffusion from higher-permeability flow paths into adjacent fine-grained materials where degradation preferentially occurs.

Because the batch experiments conducted here represent closed systems with sediment-to-water ratios and contact times that are unlikely to be replicated under advective field conditions, the laboratory-derived half-lives should be treated as upper-bound estimates of degradation potential rather than direct inputs to transport models. A more conservative and defensible approach would be to adopt effective field-scale half-lives that are substantially longer than laboratory values, informed by the spatial distribution of reactive sediment fractions derived from particle size and Fe speciation data and calibrated against observed trends in CT and CF concentration ratios across the groundwater monitoring network.

With these caveats acknowledged, the results presented here provide the first site-specific experimental evidence that the combined biotic-abiotic half-life for CT in 200-ZP-1 OU sediments is measurably shorter than the hydrolysis-only estimate of 630 years. Furthermore, the data demonstrate that CT degradation can proceed beyond CF, potentially to lesser-chlorinated end products.

These more complete dechlorination conditions may be more spatially widespread in the deeper aquifer than current models assume. Together, these findings represent a meaningful advancement in the site-specific understanding of CT natural attenuation within the 200-ZP-1 OU and warrant incorporation into updated groundwater fate and transport simulations to rigorously evaluate whether natural attenuation, in combination with the existing pump-and-treat system, could meaningfully reduce the timeframe required to achieve the 3.4 μg/L cleanup objective specified in the 200-ZP-1 OU ROD.

7.0 Summary and Conclusions

Carbon tetrachloride contamination in the 200-ZP-1 OU represents a long-standing remediation challenge at the Hanford Site, where current pump-and-treat operations are projected to be insufficient on their own to achieve the ROD cleanup target of 3.4 µg/L within the designated 125-year timeframe. A key uncertainty underlying this projection has been the lack of site-specific measurements of biotic and abiotic CT degradation rates. This study was conducted to address that uncertainty directly through controlled laboratory experiments using site-specific sediments and groundwater collected from within the 200-ZP-1 OU CT plume. The principal findings and their implications for cleanup and site-specific modeling activities are summarized below.

7.1 Hydrolysis

Hydrolysis of CT in site-specific Hanford groundwater was confirmed to be negligible on remediation-relevant timescales. Batch incubations of CT in groundwater without sediment contact showed no measurable CT mass removal over experimental periods of up to 180 days. This outcome is expected and is entirely consistent with the physical chemistry underlying the 630-year hydrolysis half-life reported by Amonette et al. (2012). That estimate was not derived from direct observation of CT degradation at ambient temperatures. Rather, it was determined through Arrhenius extrapolation, in which CT hydrolysis rates were measured experimentally at a series of elevated temperatures ranging from 20°C to 93°C. The resulting rate-temperature relationship was mathematically extrapolated back to the site-specific ambient groundwater temperature of 16°C and pH of 7.75. The calculated first-order rate constant at ambient conditions is so small that the corresponding half-life approximates 630 years. The fraction of CT mass lost to hydrolysis over the 180-day incubation of the batch experiments conducted in this study would be well below 0.1%. This is below the measurement uncertainty of the GC-ECD analytical method employed in this study, confirming that no measurable CT loss attributable to hydrolysis would be expected over the experimental timescale. The stability of CT mass observed in the groundwater-only incubations provides confirmation that any CT mass reduction observed in sediment-containing treatments must be attributed to the activity of either microbial communities or reactive mineral phases present in the sediment. These results reaffirm the conclusion of Amonette et al. (2012) that hydrolysis should not be incorporated as a meaningful natural attenuation mechanism in fate and transport models for the 200-ZP-1 OU, and that the physical chemistry of CT hydrolysis under 200-ZP-1 OU aquifer conditions is orders of magnitude too slow to support the ROD cleanup target of 3.4 µg/L within 125 years by this pathway alone. Any CT mass reduction that can realistically contribute to the cleanup objective within the designated timeframe must therefore originate from biotic or abiotic reductive transformation processes operating under the anoxic, reduced conditions that exist in localized zones of the 200-ZP-1 OU aquifer.

7.2 Combined Biotic-Abiotic Degradation

The most significant finding of this study is the first site-specific experimental demonstration that native microbial communities and Fe(II) phases in 200-ZP-1 OU sediments can drive rapid and near-complete CT degradation under anoxic conditions without any addition of organic carbon or electron donors. Phase II experiments produced quantitative first-order half-lives ranging from approximately 2.5 to 11 days for C9993 sediments and 7 to 10 days for D0474 sediments; most notably in the presence of substantial background nitrate concentrations. Equally important, the incomplete recovery of initial CT mass as CF, and the stabilization and subsequent decline of CF concentrations during extended incubation, provide indirect evidence consistent with sequential reductive dechlorination beyond the initial CT-to-CF conversion step. Because DCM and other downstream dechlorination products were not analytically measured in this study, this interpretation remains inferential and is identified as a data gap for future investigation. This is a critical finding, as complete dechlorination rather than accumulation of CF as a

terminal product is a prerequisite for achieving the long-term contaminant mass reduction required by the ROD. Phase I results, while largely qualitative due to analytical limitations, provided an early positive signal for biotic CT transformation and the production of CF as a degradation product in C9996 sediments, establishing the foundation for the more rigorous work performed in Phase II.

7.3 Abiotic Degradation

Site-specific Hanford sediments possess a measurable but spatially variable capacity for abiotic CT transformation driven by reduced Fe^{2+}mineral phases under anoxic conditions. This capacity was most clearly expressed in sediment intervals with elevated and accessible Fe(II) mineral fractions and was effectively absent in intervals dominated by oxidized Fe(III) mineralogy. Critically, air exposure of sediments prior to experiments eliminated abiotic CT degradation entirely, confirming that this pathway requires reduced, anoxic conditions to operate. At low CT concentrations representative of the plume perimeter, abiotic transformation was suppressed by the large stoichiometric excess of nitrate competing for the same reduced mineral surfaces. This finding indicates that this pathway may contribute minimally to natural attenuation in lower-concentration portions of the plume under current groundwater chemistry conditions. Fe(II) speciation data obtained during future drilling campaigns may serve as a useful predictor of abiotic CT degradation potential across the plume and could inform the spatial targeting of natural attenuation assessments.

7.4 Geochemical and Physical Controls on CT Degradation

The bulk 200-ZP-1 OU aquifer groundwater is aerobic, nitrate-rich, and carbon-limited, conditions that are broadly unfavorable for sustained CT natural attenuation. These conditions signify the fundamental geochemical constraints on the field-scale expression of the degradation capacity demonstrated in laboratory experiments. However, preliminary porewater DO measurements from Phase II core materials suggest that anoxic microenvironments persist within certain sediment intervals, particularly in lower-permeability zones that cannot be characterized through standard groundwater sampling. The fine-grained Rlm and silt-enriched lenses within the Rwie and Rwia are identified as the sediment types most likely to host these conditions. Sediment-bound organic carbon, while present at low concentrations and expected to be largely refractory (Lin et al. 2012; Stegen et al. 2018), but appears sufficient to sustain the biotic reductive pathways observed in batch experiments. Expanding DO profiling during future drilling operations is recommended as a priority action to better constrain the spatial distribution and volumetric extent of anoxic zones within the aquifer.

7.5 Implications for Cleanup and Site-Specific Modeling

The laboratory half-lives reported in this study are orders of magnitude shorter than the hydrolysis-only estimate of 630 years and represent a meaningful advancement in the site-specific understanding of CT natural attenuation within the 200-ZP-1 OU. However, these rates were measured under optimal closed-system laboratory conditions and should not be applied directly as input parameters to field-scale transport models. The bulk aquifer is predominantly oxic and subject to continuous advective delivery of nitrate and CT at groundwater velocities of approximately 1 foot per day (DOE/RL 2006; Szecsody et al. 2005a; Williams et al. 2002). The geochemical prerequisites for sustained CT degradation are likely met only within a spatially restricted fraction of the total aquifer volume. Effective field-scale natural attenuation rates are expected to be substantially longer than laboratory values and must be derived through integration of the laboratory rate data with spatial characterization of reactive sediment fractions, DO profiling, and calibration against observed CT and CF concentration trends in groundwater data.

With these considerations acknowledged, the combined evidence from this study supports the conclusion that natural attenuation driven by both biotic and abiotic reduction processes is an active and measurable contributor to CT mass reduction within localized zones of the 200-ZP-1 OU aquifer. These findings provide the empirical foundation necessary to incorporate site-specific natural attenuation rates into revised predictive models and support a more rigorous evaluation of whether natural attenuation, operating in concert with pump-and-treat, can contribute to achieving the cleanup objectives specified in the 200-ZP-1 OU ROD within the designated 125-year timeframe.

8.0 Quality Assurance

This work was performed in accordance with the PNNL Nuclear Quality Assurance Program (NQAP). The NQAP complies with DOE Order 414.1D, *Quality Assurance*. The NQAP uses NQA-1-2012, *Quality Assurance Requirements for Nuclear Facility Application*, as its consensus standard and NQA-1-2012, Subpart 4.2.1, as the basis for its graded approach to quality.

9.0 References

Amonette, J. E., P. M. Jeffers, O. Qafoku, C. K. Russell, T. W. Wietsma, and M. J. Truex. 2008. *Abiotic Degradation Rates for Carbon Tetrachloride and Chloroform: Progress in FY2008*. PNNL-18020. Pacific Northwest National Laboratory, Richland, WA.

Amonette, J., P. Jeffers, O. Qafoku, C. Russell, D. Humphrys, T. Wietsma, and M. Truex. 2012. *Abiotic Degradation Rates for Carbon Tetrachloride and Chloroform: Final Report.* PNNL-22062. Pacific Northwest National Laboratory, Richland, WA.

ASTM D4464-15-2009, *Standard Test Method for Particle Size Distribution of Catalytic Materials by Laser Light Scattering*. ASTM International, West Conshohocken, PA.

Bagwell, C., C. Johnson, G. Wang, I. Demirkanli, and M. Truex. 2019. *Carbon Tetrachloride: Evaluation of Biotic Degradation Mechanisms and Rates.* PNNL-28846. Pacific Northwest National Laboratory, Richland, WA.

Brouns, T. M., S. S. Koegler, W. O. Heath, J. K. Fredrickson, H. D. Stensel, D. L. Johnstone, and T. L. Donaldson. 1990. *Development of a Biological Treatment System for Hanford Groundwater Remediation. FY 1989 Status Report*. PNL-7290. Pacific Northwest Laboratory, Richland, WA.

DOE. 1995. *EPA Superfund Record of Decision: Hanford 200-Area (USDOE) OU 200-ZP-1, Benton County, Washington*. EPA/ROD/R10-95/114. U.S. Department of Energy, Benton County, WA.

DOE. 2020. *200 West Area 200-ZP-1 Pump-and-Treat Remedial Design/Remedial Action Work Plan*. DOE/RL-2008-78, Rev. 1. U.S. Department of Energy, Richland, WA.

DOE/RL. 2006. *Strontium-90 Treatability Test Plan for 100-NR-2 Groundwater Operable Unit*. DOE/RL-2005-96, Rev. 0. U.S. Department of Energy, Richland Operations Office, Richland, WA.

DOE/RL. 2019. H*anford Site Groundwater Monitoring Report for 2019*. DOE/RL-2019-66, Rev. 0. U.S. Department of Energy, Richland Operations Office, Richland, WA.

DOE Order 414.1D, *Quality Assurance*. U.S. Department of Energy, Washington, D.C.

Franzen, M. E. L., J. N. Petersen, T. P. Clement, B. S. Hooker, and R. S. Skeen. 1997. "Pulsing of multiple nutrients as a strategy to achieve biologically active zones during in situ carbon tetrachloride remediation." *Computational Geosciences* 1:271-88.

Gee, G. W., and D. Or. 2002. "Particle-Size Analysis." In J. H. Dane and G. C. Top (eds.), *Methods of Soil Analysis, Part 4, Physical Methods*. Book Series No. 5. Soil Science Society of America, Madison, WI. pp. 201-228.

He T., J. T. Wilson, C. Su, and R. T. Wilkin. 2015. "Review of abiotic degradation of chlorinated solvents by reactive iron minerals in aquifers." *Groundwater Monitoring and Remediation* 35(3):57-75

Hooker B., R. S. Skeen, M. J. Truex, and D. B. Anderson. 1998. "In situ bioremediation of carbon tetrachloride: Field test results." *Bioremediation Journal* 1:181-93.

Hooker, B. S., R. Skeen, and J. Petersen. 1994. "Biological destruction of CCI4: II. Kinetic modeling." Biotechnology and Bioengineering 44:211-218.

Jeffers, P. M., L. M. Ward, L. M. Woytowitch, and N. L. Wolfe. 1989. "Homogeneous hydrolysis rate constants for selected chlorinated methanes, ethanes, ethenes, and propanes." *Environmental Science & Technology* 23:965-969.

Koegler, S. S., T. M. Brouns, W. Heath, and R. J. Hicks. 1989. *Biodenitrification of Hanford Groundwater and Process Effluents: FY 1988 Status Report*. PNL-6917. Pacific Northwest Laboratory, Richland, WA.

Kriegman-King, M., and M. Reinhard. 1994. A*biotic transformation of carbon tetrachloride at mineral surfaces*. EPA/600/R-94/018. U.S. Environmental Protection Agency, Washington, D.C.

Last GV, RJ Lenhard, BN Bjornstad, JC Evans, KR Roberson, FA Spane, JE Amonette, ML Rockhold. 1991. Characteristics of the volatile compounds – Arid Integrated Demonstration Site. PNL-7866.

Last, G. V., and V. J. Rohay. 1991. *Carbon Tetrachloride Contamination, 200 West Area, Hanford Site: arid Site Integrated Demonstration for Remediation of Volatile Organic Compounds*. PNL-SA-19564. Pacific Northwest Laboratory, Richland, WA.

Lee, W., and B. Batchelor. 2002a. "Abiotic reductive dichlorination of chlorinated ethylenes by iron-bearing soil minerals. 1. Pyrite and Magnetite." *Environmental Science & Technology* 36:5147-5154.

Lee, W., and B. Batchelor. 2002b. "Abiotic reductive dichlorination of chlorinated ethylenes by iron-bearing soil minerals. 2. Green Rust." *Environmental Science & Technology* 36: 5348-5354

Lin, X., D. Kennedy, A. Peacock, J. McKinley, C. T. Resch, J. Fredrickson, and A. Konopka. 2012. "Distribution of microbial biomass and potential for anerobic respiration in Hanford Site 300 Area subsurface sediment." *Applied and Environmental Microbiology* 78:759-767.

Niemet, M. R., and L. Semprini. 2005. "Column studies of anaerobic carbon tetrachloride biotransformation with Hanford aquifer material." *Groundwater Monitoring & Remediation* 25:82-82.

NQA-1-2012, *Quality Assurance Requirements for Nuclear Facility Application*. American Society of Mechanical Engineers, New York, NY.

O'Loughlin, E. J., M. I. Boyanov, K. M. Kemner, and D. R. Burris. 2022. "Effects of metal amendments on the reductive dechlorination of carbon tetrachloride by green rust." *Chemrxiv.* https://doi.org/10.26434/chemrxiv-2022-zsx7m

Pearce, C. I., R. J. Serne, S. A. Saslow, W. Um, R. M. Asmussen, M. D. Miller, O. Qafoku, M. M. V. Snyder, C. T. Resch, K. C. Johnson, et al. 2018. "Characterizing technetium in subsurface sediments for contaminant remediation." *ACS Earth Space Chem* 2(11):1145-1160.

Petersen, J. N., R. S. Skeen, K. M. Amos, and B. S. Hooker. 1994. "Biological destruction of CCl4: I. Experimental design and data." *Biotechnology & Bioengineering* 43:521-8.

Peyton, B. 1996. "Improved biomass distribution using pulsed injections of electron donor and acceptor." *Water Research* 30:756-58.

PNNL. 2023. *SOCRATES (Version 6.0) - MARINuS Module* [Software]. Pacific Northwest National Laboratory, Richland, WA. https://socrates.pnnl.gov/

Sherwood, J. L., J. N. Petersen, R. S. Skeen, and N. B. Valentine. 1996. “Effects on nitrate and acetate availability on chloroform production during carbon tetrachloride destruction.” *Biotechnology & Bioengineering* 51:551-7.

Skeen, R. S., K. M. Amos, and J. N. Petersen. 1994. “Influence of nitrate concentration on carbon tetrachloride transformation by a denitrifying microbial consortium.” *Water Resources* 28:2433-38.

Stegen, J. C., T. Johnson, J. K. Fredrickson, M. J. Wilkins, A. E. Konopka, W. C. Nelson, E. V. Arntzen, W. B. Chrisler, R. K. Chu, S. J. Fansler, et al. 2018. “Influences of organic carbon speciation on hyporheic corridor biogeochemistry and microbial ecology.” *Nature Communications* 585.

Szecsody, J. E., J. S. Fruchter, J. L. Phillips, M. L. Rockhold, V. R. Vermeul, M. D. Williams, B. J. Devary, and Y. Liu. 2005a. *Effect of Geochemical and Physical Heterogeneity on the Hanford 100 D Area in Situ Redox Manipulation Barrier Longevity*. PNNL-15499. Pacific Northwest National Laboratory, Richland, WA.

Szecsody, J. E., J. L. Phillips, V. R. Vermeul, J. S. Fruchter, and M. D. Williams. 2005b. *Influence of Nitrate on the Hanford 100D Area In Situ Redox Manipulation Barrier Longevity*. PNNL-15262. Pacific Northwest National Laboratory, Richland, WA.

Truex, M. J., B. S. Hooker, and D. B. Anderson. 1996. *Accelerated In Situ Bioremediation of Groundwater. Innovative Technology Summary Report.* PNNL-11313. Pacific Northwest National Laboratory, Richland, WA.

Truex, M. J., C. D. Johnson, D. R. Newcomer, L. A. Doremus, B. S. Hooker, B. M. Peyton, R. S. Skeen, and A. Chilakapati. 1994. *Deploying In Situ Bioremediation at the Hanford Site*. PNL-SA-24280. Pacific Northwest Laboratory, Richland, WA.

Truex, M. J., C. J. Murray, C. R. Cole, R. J. Cameron, M. D. Johnson, R. S. Skeen, and C. D. Johnson. 2001. Assessment of Carbon Tetrachloride Groundwater Transport in Support of the Hanford Carbon Tetrachloride Innovative Technology Demonstration Program. PNNL-13560. Pacific Northwest National Laboratory, Richland, WA.

Williams, B. A., B. N. Bjornstad, R. Schalla, and W. D. Webber. 2002. *Revised Hydrogeology for the Suprabasalt Aquifer System, 200-West Area and Vicinity, Hanford Site*. PNNL-13858. Pacific Northwest National Laboratory, Richland, WA.

Zhang, X., Z. Ran, G. Yao, H. Guo, R. Zhong, and L.-Z. Huang. 2025. “Halogenated organic pollutant degradation driven by Fe(II) redox chemistry.” *Environmental Science and Technology* 59(45):24151-24176.

Appendix A – Materials and Methods

A.1 Site Groundwater

Site-specific groundwater (40 L/well) was received for 699-46-70, 699-45-67C, 299-W11-98, 299-W14-24, 299-W11-116, and 299-W11-100. Site groundwater was used in two ways: (1) to perform batch experiments with site-specific sediments and (2) to quantify the organic carbon in the 200 West Area carbon tetrachloride (CT) plume. Organic carbon is required to sustain biotic degradation processes.

A.1.1 Anions

Groundwater from 699-46-70, 699-45-67C, 299-W11-98, 299-W14-24, 299-W11-116, and 299-W11-100 was analyzed by ion chromatography to measure anionic species relevant to biotic degradation of CT and chloroform (CF) (e.g., NO_2-, NO_3-, SO_4^2-).

A.1.2 Organic Carbon Analysis

Groundwater from 699-46-70, 699-45-67C, 299-W11-98, 299-W14-24, 299-W11-116, and 299-W11-100 was filtered [0.2-µm polytetrafluoroethylene (PTFE) syringe filter] prior to analysis for total inorganic carbon (TIC) and total organic carbon (TOC) on a carbon analyzer (Shimadzu model TOC-L CSH/CSN E100V).

A.2 Characterization Analyses on Core Sediment

A.2.1 Anions

Deionized water extractions were performed on bulk sediments (699-46-70, 699-45-67C, 299-W11-98, 299-W14-24, 299-W11-116, and 299-W11-100) and analyzed by ion chromatography for anionic species relevant to anoxic respiration and biotic degradation of CT (e.g., NO_2-, NO_3-, SO_4^2-).

Anions were extracted in deionized water (1:1 sediment-to-deionized water ratio) in triplicate. The sediment-water mixture was briefly vortexed and then agitated at 60 rpm for approximately 16 hours (or overnight). Following agitation, the solutions were centrifuged at 3^#000 rpm for 10 minutes and filtered through a 0.2-µm PTFE syringe filter. The resulting supernatant was analyzed quantitatively using a Dionex Reagent-Free Ion Chromatography System (RFICS) 2000 with an AS-1 auto-sampler interface, a Dionex RFICS 5000 with an AS-AP auto-sampler interface, or a Dionex ICS-2000 anion chromatograph with AS40 auto-sampler. The anions analyzed were bromide (Br^-), chloride (Cl^-), fluoride (F^-), nitrite (NO_2^-), nitrate (NO_3^-), phosphate (PO_4^{3-}), and sulfate (SO_4^{2-}). All samples and standards were diluted with twice deionized water with a resistivity no less than 18.0 MΩ·cm. This process was repeated three times on non-consecutive days and averaged to establish a working instrument detection limit in mg/L.

The instruments were calibrated using a multi-element anion standard purchased from Inorganic Ventures to generate calibration curves. The calibration standards ranged from 0.03 to 7.5 mg/L or 25 to 120 mg/L, with a High Calibration Verification standard of 30 mg/L, used to verify the linear calibration range. The calibration was verified with an Initial Calibration Verification standard and during sample analysis with a Continuing Calibration Verification standard run every 10 samples, at a minimum. Calibration blanks were analyzed following each calibration verification solution to flush the instrument and to confirm that potential carryover effects were not a factor. The calibration was independently verified using anion standards purchased from SPEX CertiPrep.

A.2.2 Particle Size Distribution

Mechanical sieving (Gee and Or 2002) and laser light scattering (ASTM D4464-15) were used to determine particle size distributions. Sieving was performed on the dried, bulk sediment that was removed from Lexan core liners using standard sieve sizes of 3 in., 2 in., 1.5 in., 1 in., 3/4 in., #8, and #4, corresponding to particle sizes of 75 mm, 50 mm, 37.5 mm, 25 mm, 19 mm, 8 mm, and 4 mm, respectively. The laser light scattering method was used on subsamples of the <2-mm size fraction that were collected from the catch pan at the bottom of the sieve stack. The <2-mm size fraction contains particles that are sand-sized and smaller. The data generated by the sieve and laser light scattering methods were combined to determine the complete particle size distributions for the bulk sediments.

A.2.3 Elemental Characterization for Reactive Mineral Species

Sequential extractions were conducted to quantify adsorbed and total Fe and Mn species and assess redox species availability for contribution to CT degradation reactions. These measurements provide information about the potential capacity of sediments to perform and sustain abiotic degradation of CT and CF. Extractions were performed in an anoxic chamber (~98% N_2, ~2% H_2, O_2 < 20 ppm). For the first extraction, sediment samples (2.0 ± 0.5 g) were mixed with 10.0 mL of a deoxygenated ion exchange solution (1.0 M $CaCl_2$) for 50 minutes at 6 rpm, centrifuged (3000 rpm, 10 minutes) to pellet solids, and the aqueous phase was filtered (0.45-µm) and acidified for analysis of the adsorbed fraction of Fe(II) and Mn(II) extracted from the mineral surfaces. For the second extraction, sediment samples (2.0 ± 0.5 g) were mixed with 10.0 mL of 0.5M HCl for 24 hours at 6 rpm, centrifuged (3000 rpm, 10 minutes), and the aqueous phase filtered (0.45-µm) for total elemental analysis by inductively coupled plasma – optical emission spectroscopy (ICP-OES). This recovered fraction corresponds to the amorphous Fe(III), Fe and Mn carbonate and sulfide species extracted that are indicative of sediment redox status. Fe(II) concentration in the extracted solution was determined using Hach 8147 method by reaction with ferrozine.

A.2.4 Mineralogy Powder X-Ray Diffraction

Bulk mineralogy of each sample was characterized using a Rigaku Miniflex II X-ray diffraction (XRD) unit equipped with a Cu Kα radiation (λ = 1.5418 Å with 30 kV and 15 mA) source. To the sample powder, ~ 10 wt% ZnO chemical standard was added for pattern quantification and the sample/standard mixture was homogenized using a mortar and pestle. When ZnO was not available, TiO_2 was added at ~10 wt% as the internal standard instead. Samples were then loaded into zero-background quartz sample holders for analysis and patterns were collected over the course of ~3 hours in fixed time mode from 3 to 90° 2θ. The scan step size was 0.04°, and the step count time was 5 seconds. Mineral identification was performed using EVA software (v7, Bruker AXS, Germany). Then, phase quantification by the whole pattern fitting (Rietveld refinement) method was performed using Topas software (v7, Bruker AXS, Germany), with the pattern for each phase calculated from published crystal structures (Inorganic Crystal Structure Database, Fachinformationszentrum Karlsruhe, Germany).

A.2.5 Organic Carbon Analysis

A subsample (~5 g) of each core was air-dried until a constant weight was achieved. The dried samples were then processed using a ball mill to produce a fine sand-like consistency, ensuring sample homogeneity. For total carbon (TC) and TIC analysis, 1.5 g of the ball-milled material was weighed in triplicate for each sample.

TC and TIC of sediments were measured using a carbon analyzer (Shimadzu model TOC-L CSH/CSN E100V). For TC analysis of solid samples, the combustion temperature in the SSM-5000A solid sample module was set to 900 °C. The evolved CO_2 gas was measured by a non-dispersive infrared (NDIR) gas analyzer. For TIC analysis of solid samples using the SSM-5000A solid sample module, 25% phosphoric acid was added to the ceramic sample boat at 200 °C to dissolve carbonates. The evolved inorganic CO_2 was measured by the NDIR detector, as described above. TOC was calculated by subtracting TIC from TC.

A.3 Experimental Design for Batch Degradation Testing

A.3.1 Phase I

Experimental Objectives and Approach. Phase I testing was designed as an exploratory evaluation to (1) assess the natural attenuation capacity of site-specific sediments for CT degradation, and (2) determine the corresponding degradation rates and underlying mechanisms (biotic vs. abiotic). Due to the non-standardized and highly adaptive nature of the Phase I experimental design, methodologies varied across geologic units and borehole locations. These foundational outcomes and lessons learned directly informed the standardized protocols later deployed in Phase II.

Sediment and Groundwater Collection. Evaluations encompassed sediment core materials collected from four distinct boreholes across three geologic units: Ringold Formation Member of Wooded Island Unit E (Rwie), Ringold Formation Member of Wooded Island Unit A (Rwia), and the Ringold Lower Mud Unit (Rlm). To capture spatial variability across the site, samples were collected from two distinct zones:

- **High-Concentration Zone (Boreholes C9996 and C9739):** Cores were packaged by the onsite drilling team immediately upon recovery, maintained at 4 °C, and delivered to the laboratory within 3 days of collection.
- **Low-Concentration Plume Perimeter (Boreholes D0082 and D0083):** Legacy core materials were retrieved from storage at –80 °C, where they had been archived for approximately 4 years prior to experimental setup.

Site-specific groundwater was used for all batch experiments to simulate ambient geochemical conditions.

Experimental Design and Batch Treatments. Batch experiments were constructed using varying solid-to-liquid ratios and reaction vessel scales depending on the mechanism(s) being isolated. Due to high analytical sampling demands and instrumentation constraints, all treatments were prepared in experimental duplicates.

Treatment Type	Solid-to-Liquid Ratio	Vessel Scale	Purpose & Design
Combined biotic-abiotic	1:2	125-mL glass bottles	Evaluated total degradation potential under low initial biomass or slow kinetics using 10- and 30-g sediment masses. Headspace samples were measured monthly.
Abiotic only	1:1	12-mL glass vials	Isolated purely chemical pathways at a compressed scale. Headspace samples were measured daily-weekly for up to 60 days.
Groundwater controls	Groundwater only	Both	Replicated prior hydrolysis treatments and quantified background volatile/hydrolysis mass loss over time. Headspace samples were measured monthly.

Spiking and Analytical Initiation. To initiate the experiments, reactors were spiked with concentrated target stocks. Initial CT concentrations were varied strategically based on the borehole location and specific geologic unit of the sediment matrix (see Table 2 in the main report). To evaluate potential preparation artifacts, CT and CF stocks were prepared using two distinct methodologies:

- **Aqueous-Based Stock (DNAPL in Groundwater):** Formulated as a dense non-aqueous phase liquid (DNAPL) dissolved directly in site groundwater. This method was initially selected to maintain ambient site-specific chemistry and minimize the introduction of co-solvents that could interfere with degradation pathways or reactions. However, this approach proved problematic, as reliable dissolution and equilibrium between the CT and groundwater could not be achieved in a timely fashion. Consequently, target concentrations in several instances could not be achieved, and those specific experimental systems were initiated at lower-than-intended initial CT concentrations.
- **Methanol-Based Stock:** CT was dissolved in a methanol carrier solvent stock. This alternative approach was subsequently adopted to ensure rapid, precise, and reproducible delivery of CT mass into the experimental systems. The introduction of methanol was assumed to be of minimal biogeochemical concern, as the volume of concentrated stock required to achieve target CT concentrations represented less than 1% of the total aqueous volume.

The introduction of these stock solutions marked the initiation of the experimental timeline (T=0). Headspace samples were collected at predetermined intervals over the course of the incubation period to monitor the consumption of CT and the production of transformation byproducts (CF). To ensure data quality despite high sampling demands, duplicate reactors were analyzed at each time point, with the variance between duplicates was used to assess experimental reproducibility.

Microbial Inhibition and Control Efficacy

Distinct biological control treatments were applied across the experiments to isolate abiotic mechanisms, yielding varying degrees of long-term efficacy:

- **Chemical Inhibition (Abiotic Set):** Sodium azide was added as a potent chemical inhibitor. This treatment inhibited biological activity for the short duration of the abiotic-only experiments.
- **Thermal/Antimicrobial Inhibition (Biotic Set):** A combined regimen of heat inactivation and antibiotic amendment was applied. This approach proved ineffective for long-term biological inhibition, as evidenced by a progressive decrease in CT mass over extended incubation times, indicating rebounding microbial activity.

A.3.2 Phase II

Experimental Objectives and Approach

Phase II testing sought to build upon the findings of Phase I by (1) collecting additional high-resolution data for CT degradation in site-specific sediments, and (2) identifying relationships among key physical, chemical, and biological variables to reduce uncertainty when scaling interpretations to the field.

In contrast to the exploratory nature of Phase I, the Phase II experimental design was simplified, fully integrated, and standardized across both biotic and abiotic testing regimes. Procedural variables were streamlined to establish a uniform, robust platform for comparing degradation kinetics and mechanisms.

Sediment Collection and Preservation of Anaerobic Integrity

Evaluations focused on freshly drilled core materials collected from two boreholes located within the high CT concentration zone (C9993 and D0474), targeting two distinct geologic units (Rwie and Rwia). Team members were present on site during drilling operations to ensure immediate sample handling.

Upon recovery of the core materials, porewater analysis was immediately performed to measure dissolved oxygen (DO). These data are presented in this report as for information only. To preserve native chemical conditions and prevent the oxidation of redox-sensitive minerals, core materials were instantly sealed in metalized bags under a nitrogen (N_2) atmosphere for transport and storage in the lab at 4 °C.

Standardized Experimental Design and Batch Setup

All batch degradation experiments were conducted in uniform 50-mL glass bottles using a single solid-to-liquid ratio of 1:1 across all setups. To minimize experimental variance, all treatments and controls were prepared in experimental triplicates.

The experimental matrix consisted of the following treatments and controls:

- **Active Biotic-Abiotic Treatments:** Live sediment and groundwater mixtures designed to capture total degradation potential under native conditions.
- **Abiotic Only Treatments:** Sediment and groundwater mixtures treated with sodium azide to a final concentration of 3 mM to provide robust, long-term biological inhibition.
- **Groundwater-Only Controls:** Reactors containing groundwater alone (no sediment) to maintain consistency with prior hydrolysis work and to account for potential CT mass loss over time.
- **Oxic Controls (Oxygen Exposure):** Active sediment and groundwater mixtures were deliberately exposed to atmospheric air. This control was designed to demonstrate that the observed degradation mechanisms are oxygen-sensitive and require anoxic, reduced chemical conditions to proceed.

Spiking, Calibration, and Analytical Quality Assurance

To eliminate the equilibration and delivery issues encountered during Phase I, all experimental spikes and analytical calibration standards were prepared identically using a methanol carrier solvent. The stock solution was spiked into the reactors to achieve a uniform initial aqueous starting concentration of 800 ppb CT. The volume of methanol introduced was kept below 1% of the total aqueous volume to prevent co-solvent effects.

Quantification was performed using a gas chromatography (GC) instrument equipped with an electron capture detector (ECD). This specific detector modification provided an exceptionally low background signal and significantly enhanced precision, allowing for confident compound detection and quantification well below ppb levels.

To ensure rigorous analytical quality control across the expanded sample load, each analytical batch run included a full suite of calibration standards. Furthermore, continuous calibration verification (check standards) was measured at regular intervals throughout each analytical run to guarantee consistent instrument performance and baseline stability over time.

Sampling Intervals and Analytical Monitoring

To accurately capture degradation kinetics, headspace gas sampling intervals were tailored based on the expected rates of mass loss for each experiment type:

- **Abiotic Experiments:** Headspace gases were sampled frequently on a daily to weekly time scale to monitor rapid, short-term abiotic transformation pathways.
- **Biotic-Abiotic Experiments:** Headspace measurements were initially conducted weekly, then transitioned to every other week, and ultimately moved to a monthly schedule. This dynamic sampling strategy was specifically designed to capture high-resolution data during the early, rapid degradation phase observed in prior experiments, while still tracking long-term trends.

The objectives of Phase II were to (1) collect additional data for CT degradation from site-specific sediments and (2) identify the relationships among key variables (physical, chemical, biological) that reduce uncertainty of interpretation to field scale. In Phase II, the experimental design was simplified, integrated, and consistent across biotic and abiotic degradation testing. Phase II included freshly drilled sediments from two boreholes in the high CT concentration zone (C9993, D0474) and two units were evaluated (Rwie, Rwia). Team members were onsite during drilling. Upon receiving core materials porewater analysis for DO was performed and core materials were immediately sealed in metalized bags under N_2 to maintain native conditions.

Methodology was standardized for all core characterization activities and batch degradation testing in Phase II. Biotic and abiotic experiments were designed to include redundancy in experimental treatments and controls. Batch experiments were conducted using a single, field-relevant sediment-to-liquid ratio, and all CT stocks and calibration standards were prepared identically to achieve an initial CT starting concentration (800 ppb aqueous). Replication was performed as experimental triplicates. Sampling-date-specific calibration curves were evaluated against strict quality standards ($R^2 > 0.99$) and applied for data analysis. Each sampling event of batch samples included calibration standards as well as check standards measured throughout the run to ensure consistent instrument performance.

A significant improvement in Phase II was equipping the GC instrument with an ECD for low background and improved precision. This modification improved confidence in compound detection and quantification well below ppb levels.

GC/MS and GC/MS-ECD Headspace Measurements: Gas sampling of the batch experiments was performed using a solid phase microextraction (SPME) fiber to measure the concentration chloro-organics in the headspace GC mass spectrometry (MS) (Phase I) or GC/MS-ECD (Phase II) system. SPME sampling has emerged as the preferred gas sampling approach for high-throughput, consistent recoveries and avoids aqueous sampling and contaminant mass removal. CT and CF were analyzed with an Agilent GC/MS system (7890 B GC, 5977A MS). Separation of the analytes will be achieved on a DB-624 capillary column (30 m × 0.25 mm inside diameter, 1.4 µm film thickness) with a temperature program of 11 minutes at 540 °C then to 17,500 °C with 10 °C/min, then to 250 °C with 30 °C/min and 52 minutes at 25100 °C.

Calibration: CT and CF were quantified using compound- and date-specific external calibration curves generated from four to six pure-standard levels prepared in site-specific groundwater. Additionally, check standards were analyzed over sequential days of GC operation to account for instrument drift. The percent variance in peak area of prepared calibration standards over sequential sampling days was <2. Calibrations were flagged as unacceptabled when model fit was poor ($R^2 < 0.9$). To additionally control for anomalous response factors, calibration slopes from otherwise passing fits were evaluated across dates; any date with a slope deviating by more than two standard deviations from the mean slope (within

compound) was flagged and excluded. Sample data collected on dates with rejected calibrations was not used in downstream analyses.

Calculation of Detection Limits: Limits of detection (LOD) were estimated as three times the calibration residual standard deviation using the following equation:

$$\text{LOD} = \frac{\mathbf{3}\,\boldsymbol{\sigma}}{|\,\boldsymbol{m}\,|} \tag{A.1}$$

where σ is the calibration residual standard deviation (in area units) and m is the calibration slope.

Calculation of Uncertainty in Measured Concentration: Standard deviations in sample concentrations associated with calibration uncertainty $\sigma(\hat{C})$ were propagated from calibration residual error using first-order error propagation with slope and intercept treated as fixed using the following equation:

$$\sigma(\hat{C})_{calibration} = \frac{\sigma}{|\,m\,|}\sqrt{\frac{1}{k}+\frac{1}{n}+\frac{(A-\bar{A})^2}{m^2\Sigma(x_i-\bar{x})^2}} \tag{A.2}$$

with k as the number of injections of each sample (always 1 for this work), n is the number of calibration points retained, $\bar{A}$ is the mean calibration area, x_i is each individual concentration in the calibration curve, $\bar{x}$ is the mean concentration of the calibration curve, and m and σ the same as in Eq. (A.1).

Replicate measurements were averaged for each experimental time point, and replicate-level uncertainty was calculated by calculating the standard deviation of the calculated concentrations in each compound- experiment- and time point- group ($\sigma(\hat{C})_{replicates}$). Finally, both the calibration-associated and replicate-associated errors were combined to get a total uncertainty on each concentration ($\sigma(\hat{C})_{total} =$) in each compound- experiment- and time point- group by combining both replication-based uncertainty with calibration-associated uncertainty in the following equation:

$$\sigma(\hat{C})_{total} = \sqrt{\sigma(\hat{C})_{calibration}{}^2 + \sigma(\hat{C})_{replicates}{}^2} \tag{A.3}$$

Computation of total CT and CF: Both CT and CF are volatile compounds and therefore partition readily between aqueous phase and gas phase. All calibrations were performed and applied to obtain aqueous concentration of the analytes and the total amount of each analyte in a sealed vial was computed as the sum of the aqueous and gas-phase amounts:

$$n_{total} = n_{aq} + n_{gas} \tag{A.4}$$

Using Henry's law to relate gas- and aqueous-phase concentrations, the amounts were calculated as:

$$n_{\text{aq}} = \frac{\hat{C}\,V_{\text{aq}}}{M} \tag{A.5}$$

$$n_{\text{gas}} = \frac{\hat{C}\,k_H\,V_{\text{air}}}{M} \tag{A.6}$$

where $\hat{C}$is the estimated aqueous concentration of the analyte (ng/mL), V_{aq} and V_{air} are the aqueous and headspace volumes (mL), respectively, M is the molar mass (g/mol) of the analytes (153.82 g/mol for CT,

119.37 g/mol for CF), k_H is an experimentally determined dimensionless Henry's constant (CT=1.12, CF=0.13).

All subsequent analyses were performed on n_{total}(nmol) derived from $\hat{C}$ and the measured vial volumes. Uncertainty was propagated by scaling the concentration uncertainty by the same factor, as in:

$$\sigma(n)_{total} = \sigma(\hat{C})_{total}\left(\frac{V_{\text{aq}} + k_H V_{\text{air}}}{M}\right) \tag{A.7}$$

Calculations of CT degradation rates: To estimate CT degradation rates, time series were analyzed using a first-order decay model as shown in Eqs. (A.8) and (A.9).

$$(n)_{total} = (n)_{total_0} e^{-kt} \tag{A.8}$$

$$\ln[(n)_{total}] = -kt + \ln[(n)_{total_0}] \tag{A.9}$$

where $(n)_{total_0}$is the initial total moles of CT, t is time in days, and k is the first order rate constant. The model parameters k and $(n)_{total_0}$ values were deterimined by fitting a linear regression expressed as in Eq. (A.9).

Uncertainty was propagated via Monte Carlo simulation (5000 iterations). For each iteration, concentrations above the LOD were sampled from a normal distribution truncated at 0 using the n_{total} as the mean and $\sigma(n)_{total}$ as the standard deviation; points below the LOD were sampled from a uniform distribution between 0 and LOD to represent censoring. To reduce bias from complex censoring patterns, time series with three or greater time points with concentrations above the LOD used only those points (excluded all time points below the LOD). In scenarios with less than three time points with concentrations above the LOD, we also included the first below-LOD value after a detected value to represent the decay tail. Model outputs were summarized from the Monte Carlo distributions using medians, and confidence intervals. For interpretable kinetic metrics, half life ($t_{1/2}$) was calculated for each Monte Carlo draw as in Eq. (A.10) and reported as median with confidence intervals as well:

$$t_{1/2} = \ln[2]\,/k \tag{A.10}$$

Degradation rates were classified as (1) high-confidence when the 95% lower confidence bound of k exceeded 0 and (2) low-confidence when the 90% lower bound exceeded 0 but the 95% lower bound did not. Fits with only two points where the second was below LOD were conservatively downgraded to low-confidence.

Appendix B – Phase I Degradation Plots

B.1 699-46-70 / D0082

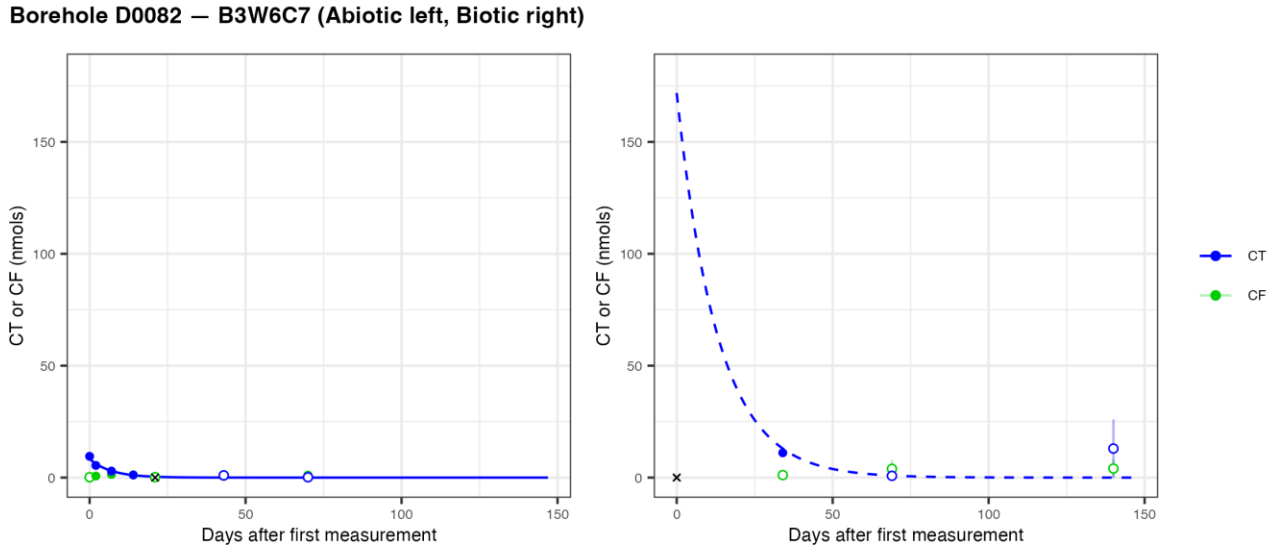

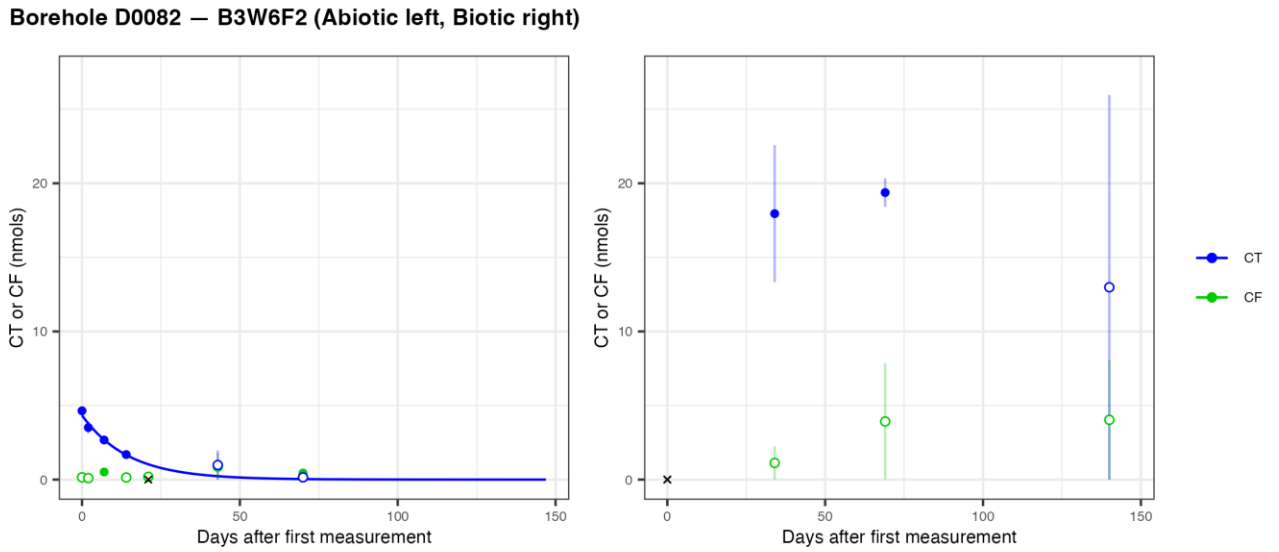

Borehole D0082 — B3W6H5 (Abiotic left, Biotic right)

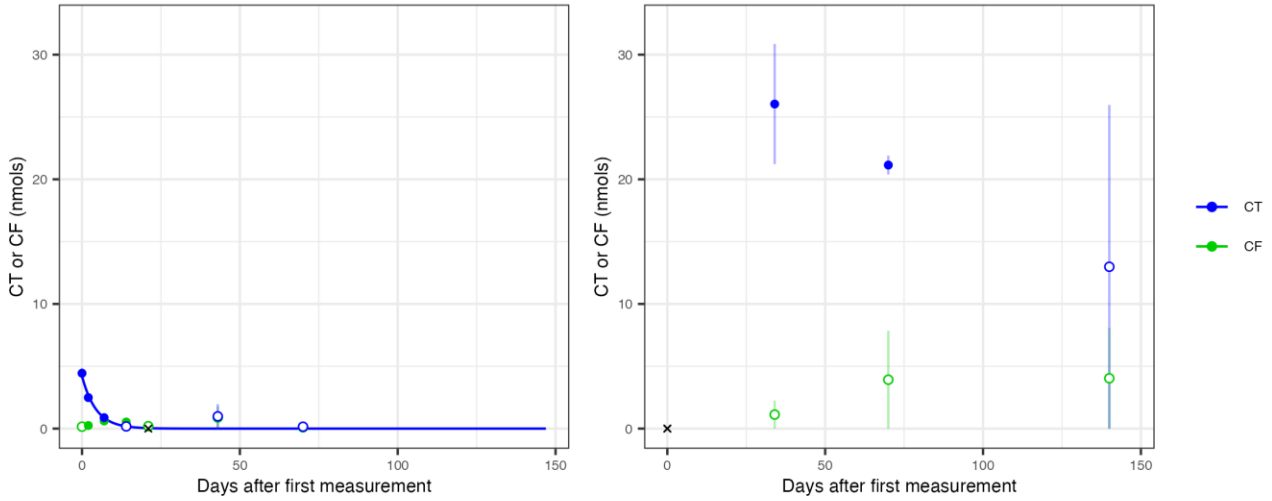

Borehole D0082 — B3W6J5 (Abiotic left, Biotic right)

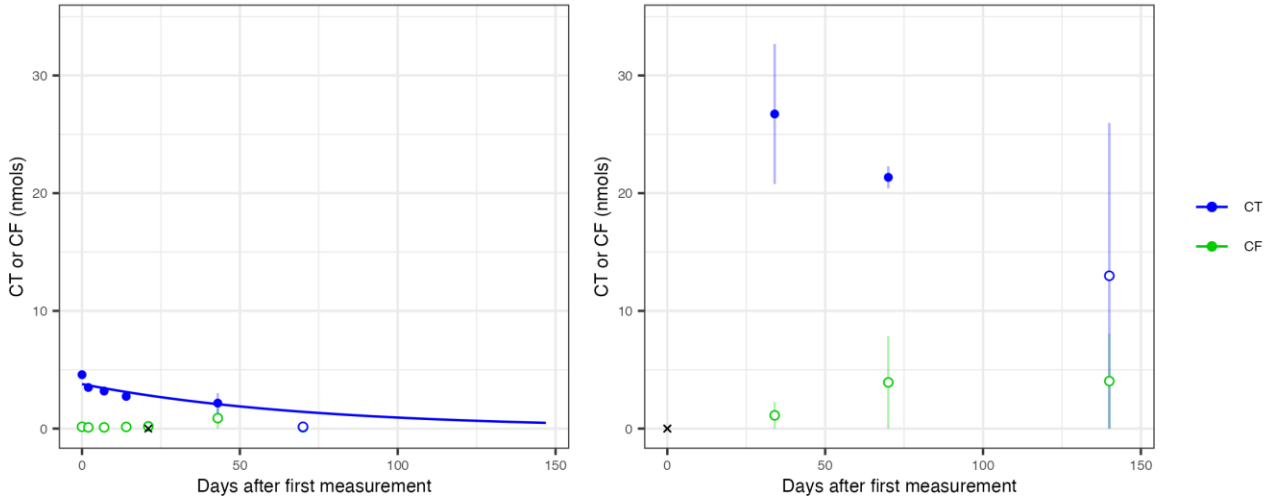

B.2 699-45-67C / D0083

Borehole D0083 — B3WXM7 (Abiotic left, Biotic right)

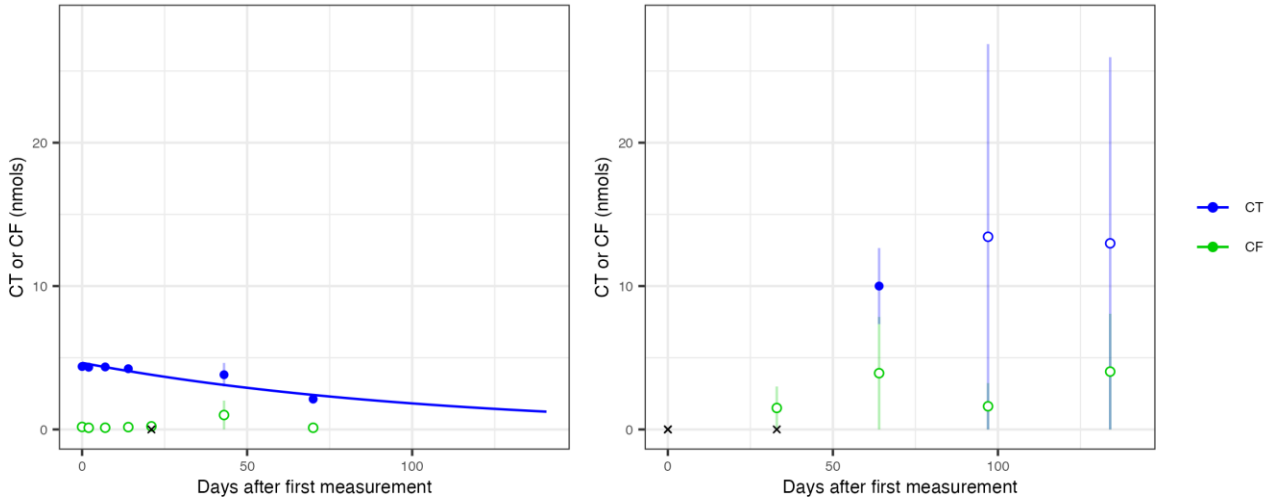

Borehole D0083 — B3WXN3 (Abiotic left, Biotic right)

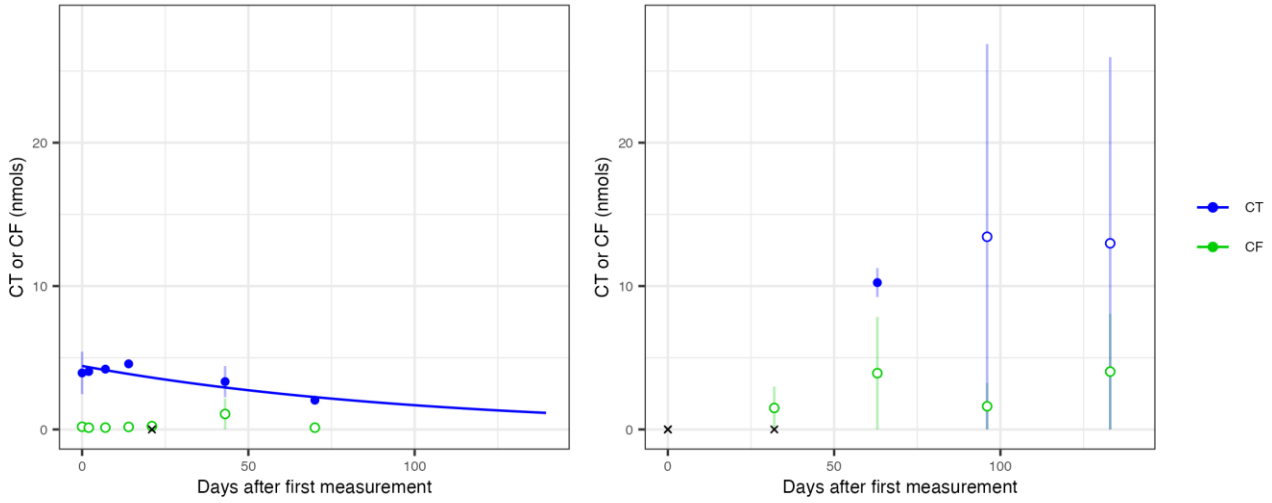

Borehole D0083 — B3WXN9 (Abiotic left, Biotic right)

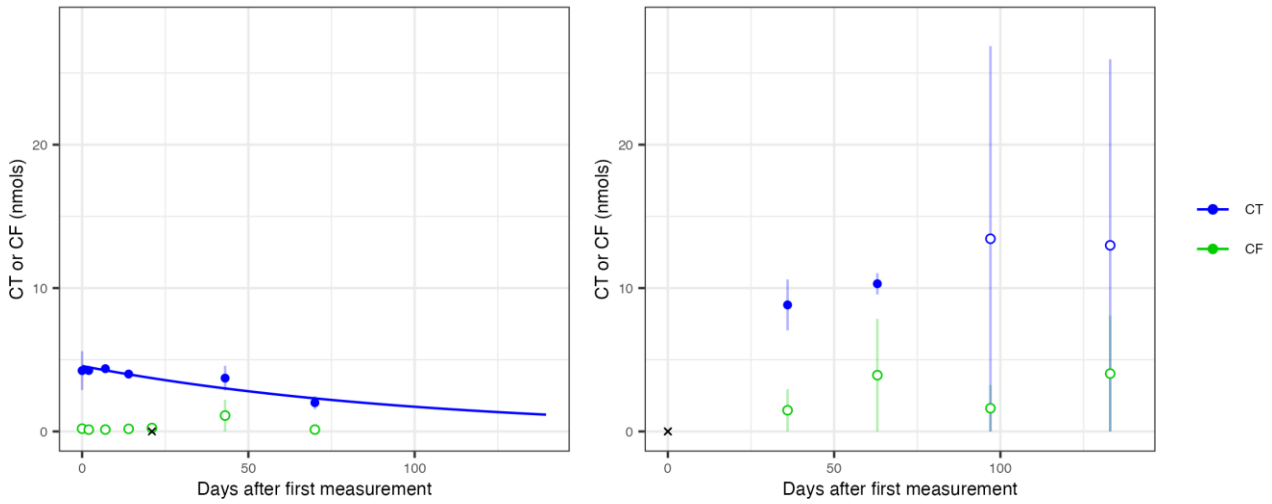

Borehole D0083 — B3WXP5 (Abiotic left, Biotic right)

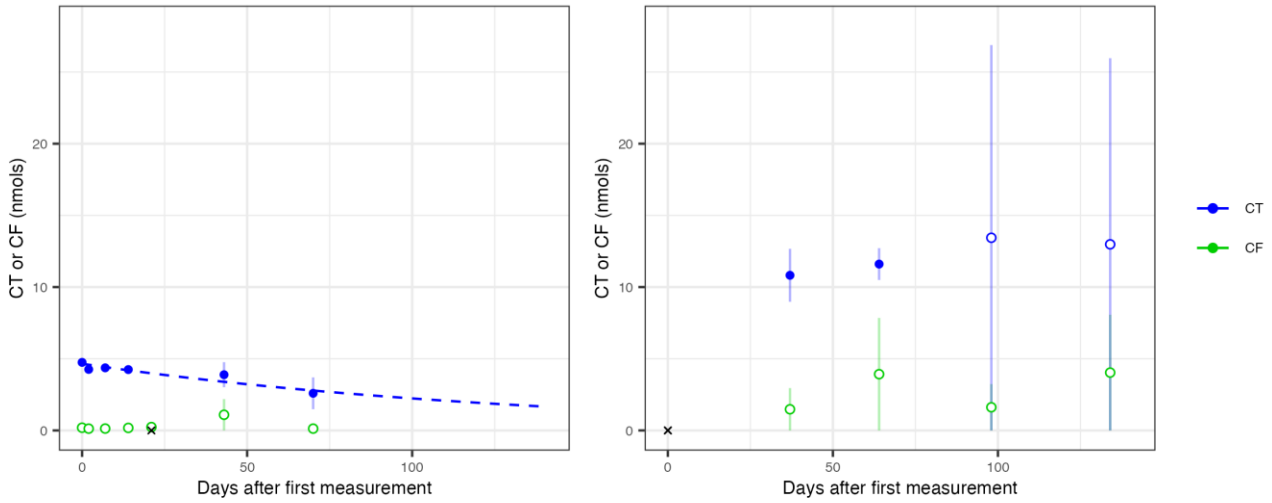

Borehole D0083 — B3WXX5 (Abiotic left, Biotic right)

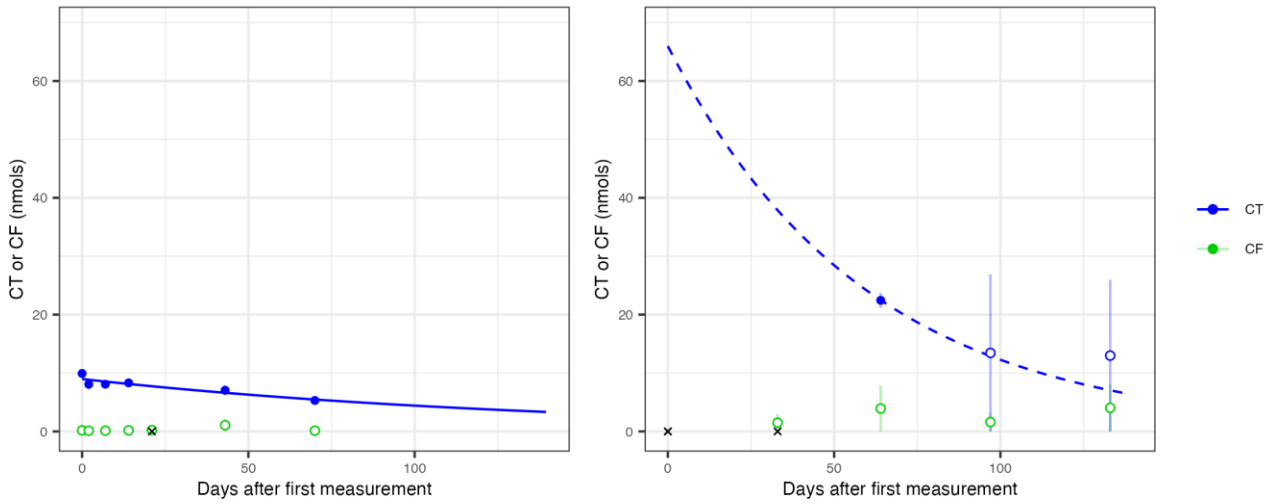

B.3 299-W14-24 / C9996

Borehole C9996 — B48BP0 (Abiotic left, Biotic right)

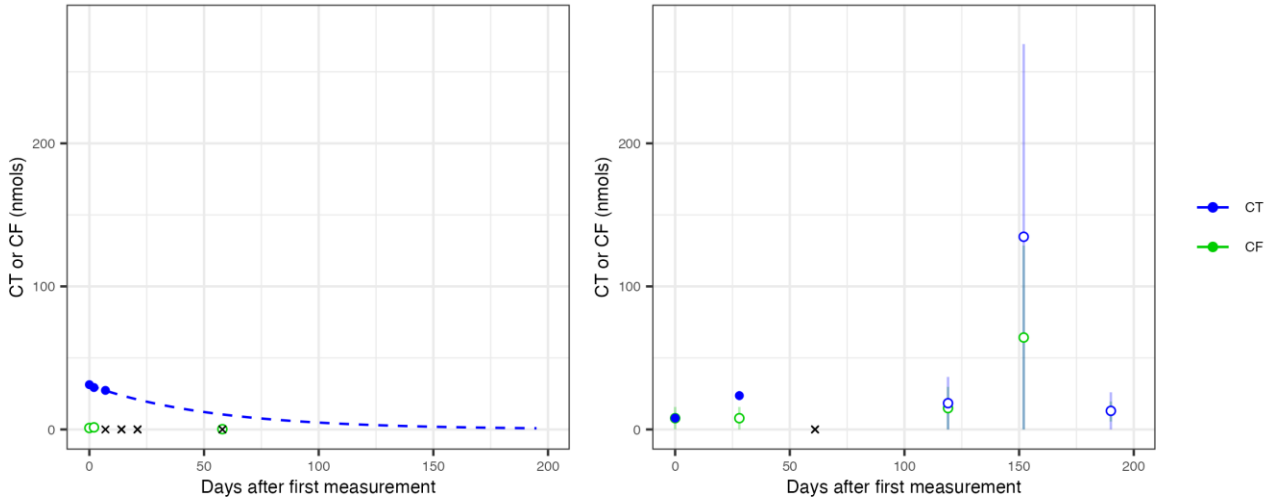

Borehole C9996 — B48BN8 (Abiotic left, Biotic right)

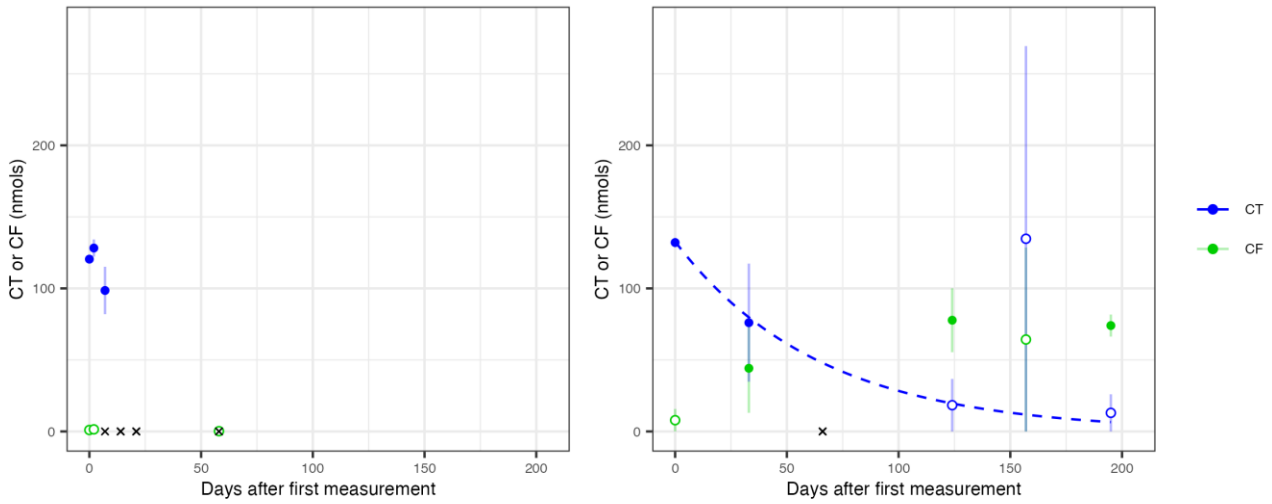

Borehole C9996 — B48BN9 (Abiotic left, Biotic right)

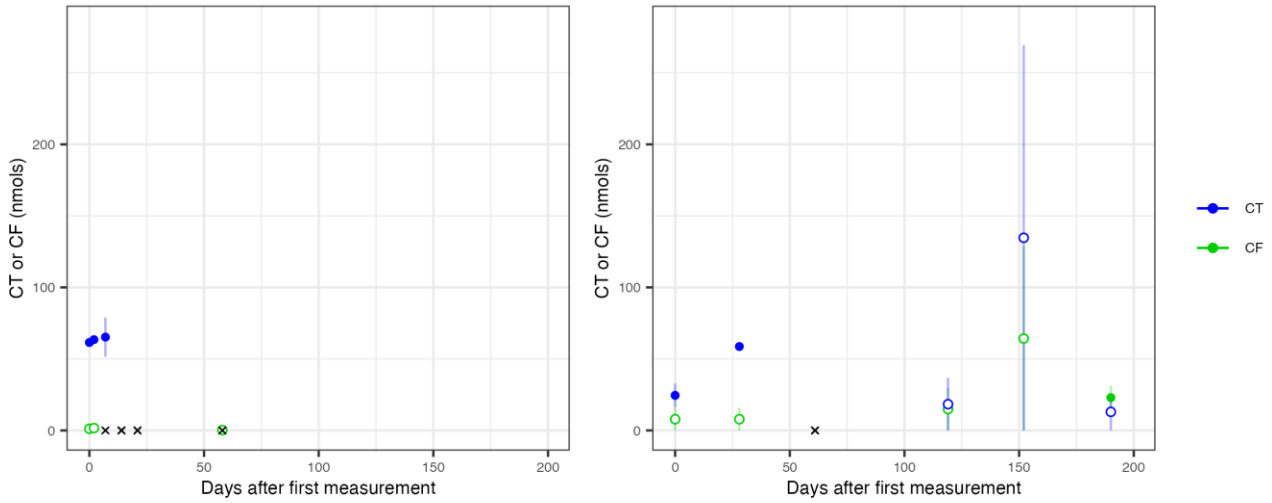

B.4 299-W11-98 / C9739

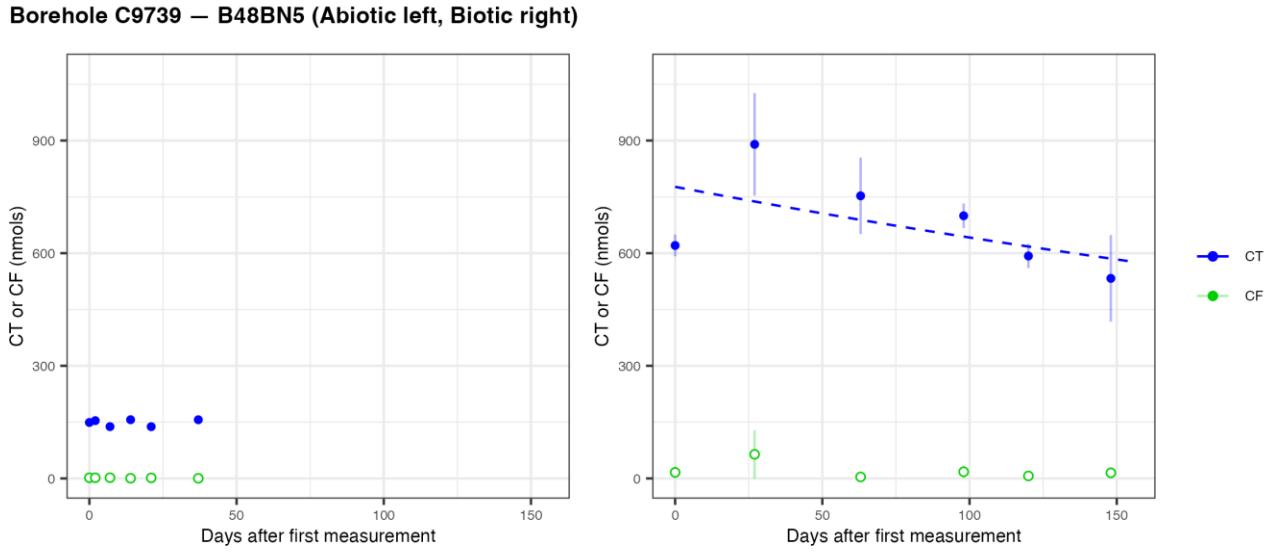

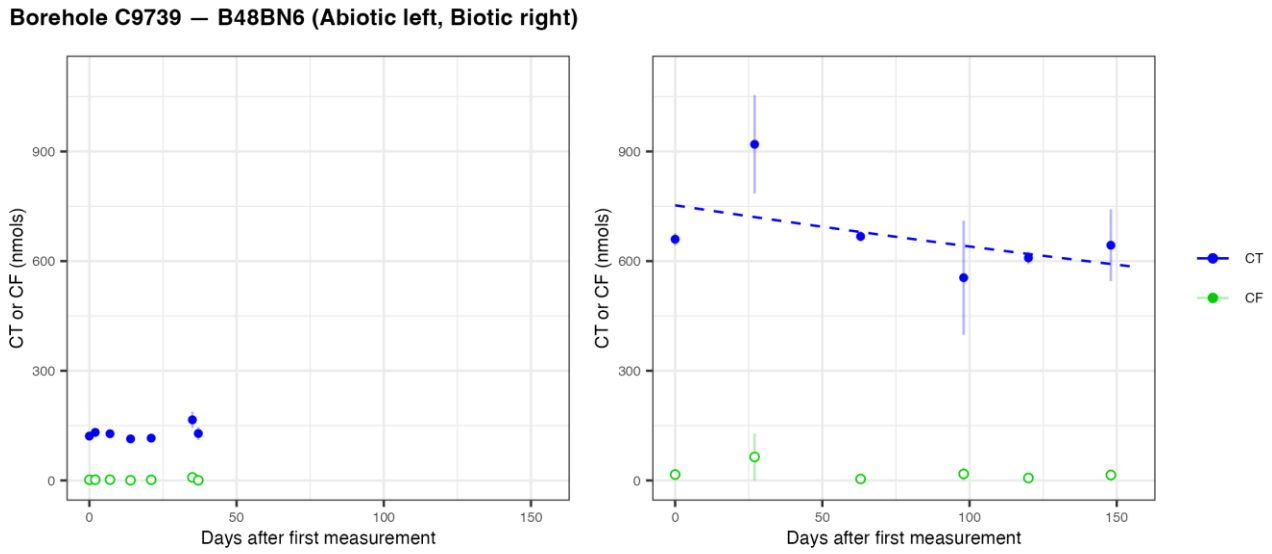

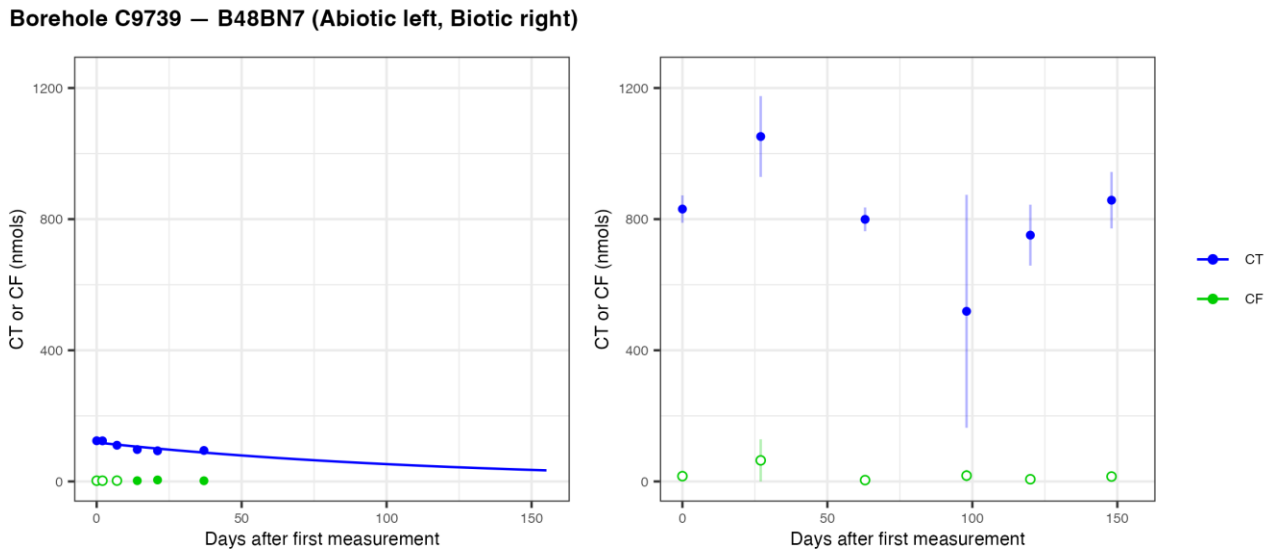
Borehole C9739 — B48BN7 (Abiotic left, Biotic right)
CT or CF (nmols)
1200
800
400
0
0
50
100
150
Days after first measurement
CT
CF

Appendix C – Phase II Degradation Plots

C.1 299-W11-100 / C9993

Borehole C9993 — B4JT76 (Abiotic left, Biotic right)

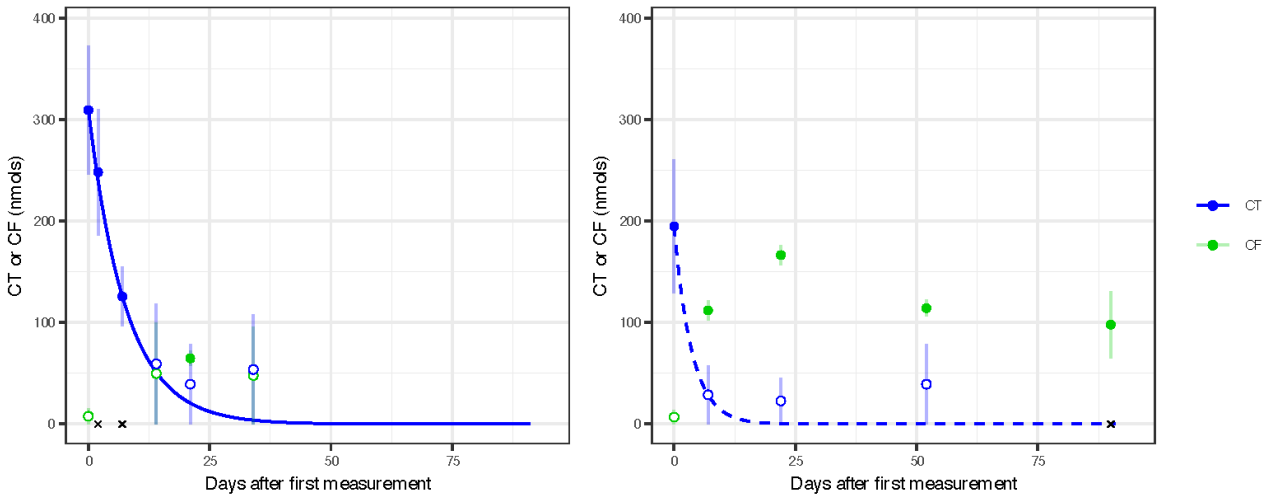

Borehole C9993 — B4JT77 (Abiotic left, Biotic right)

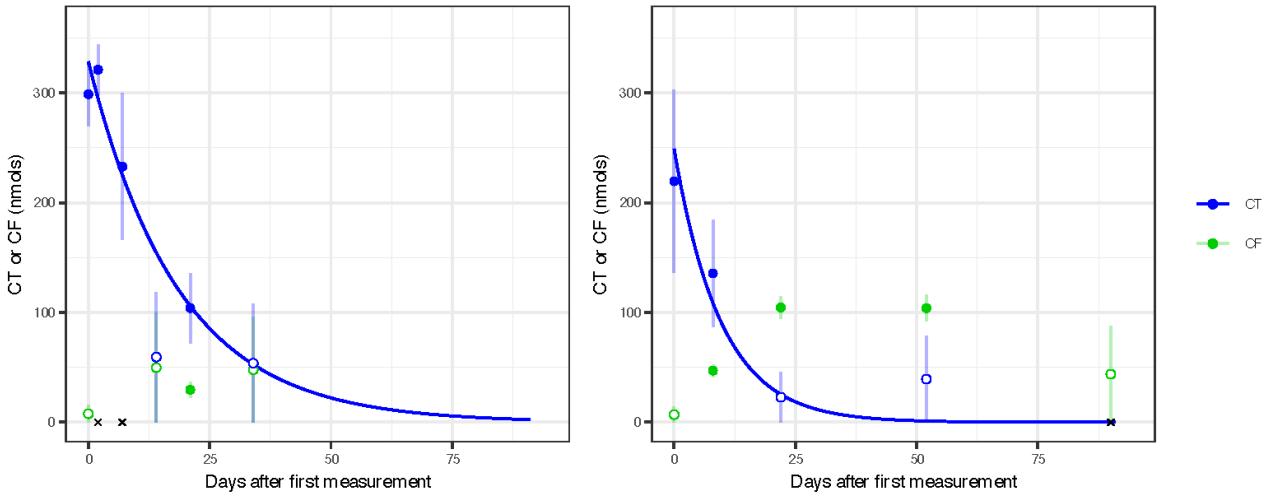

Borehole C9993 — B4JTM3 (Abiotic left, Biotic right)

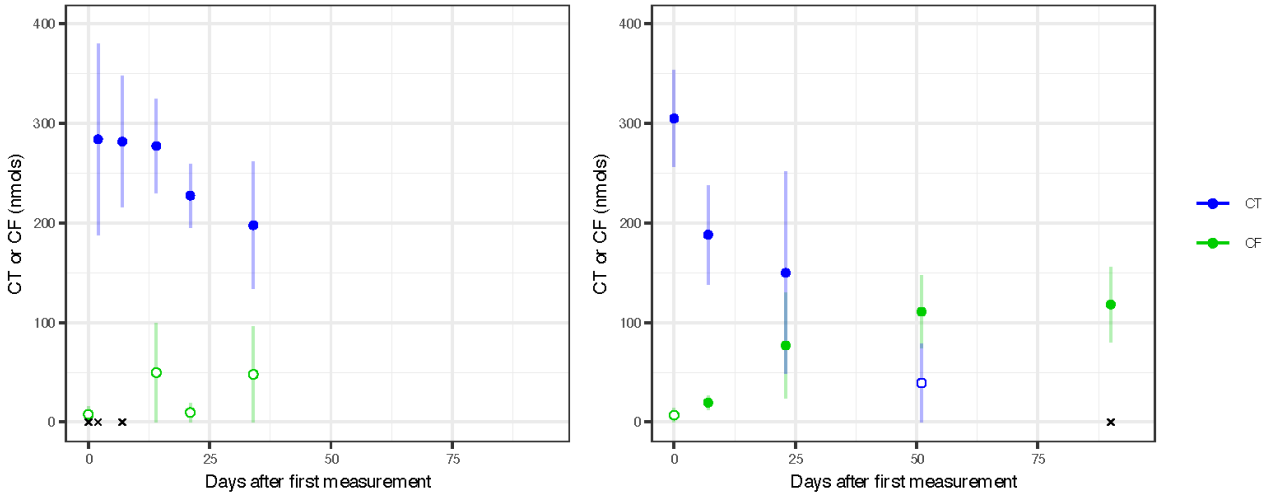

Borehole C9993 — B4JTM4 (Abiotic left, Biotic right)

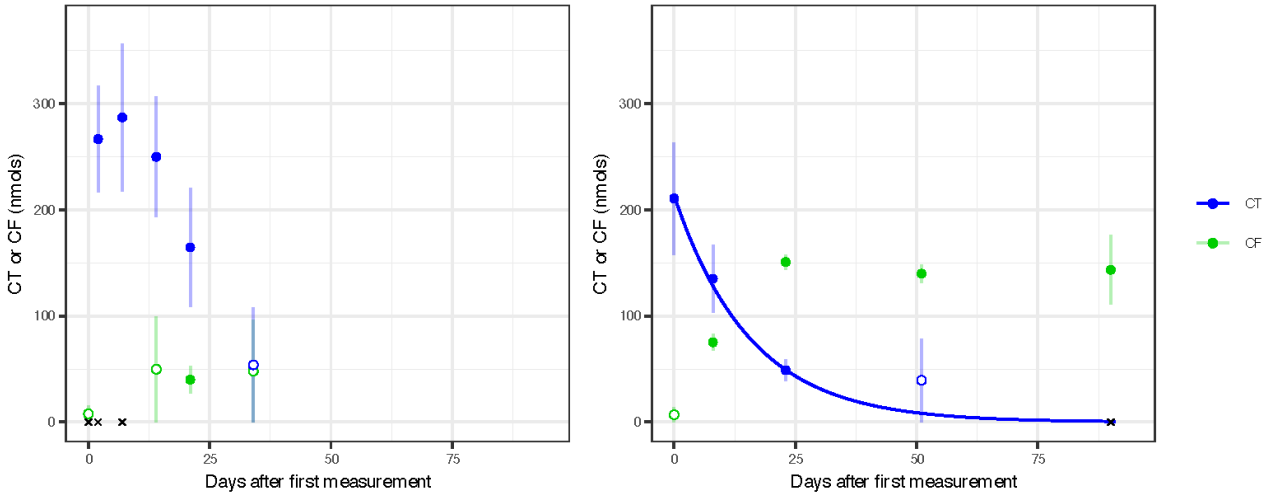

C.2 299-W11-116 / D0474

Borehole D0474 — B4JT78 (Abiotic left, Biotic right)

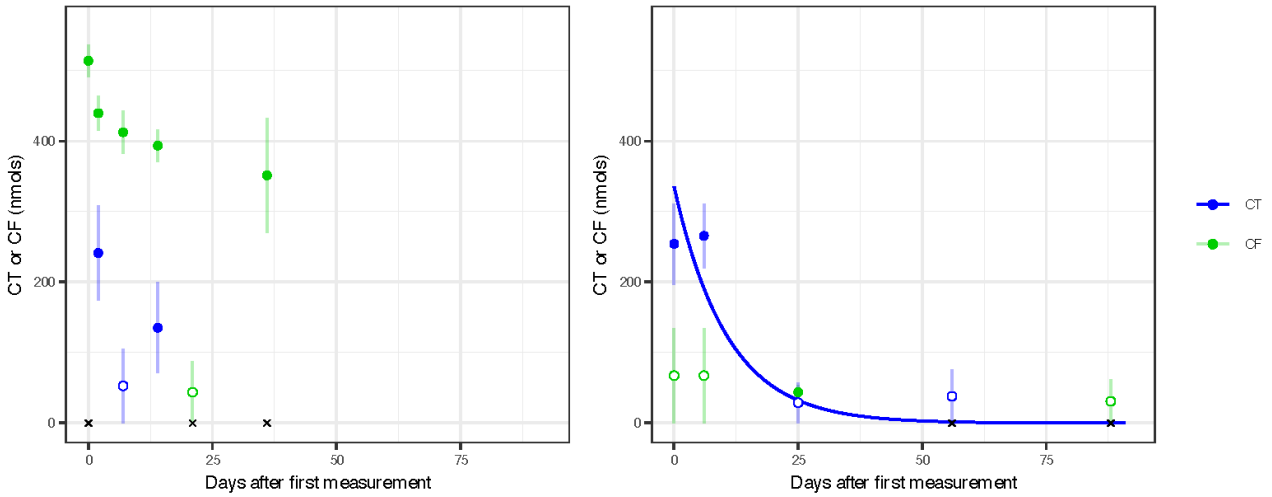

Borehole D0474 — B4JT79 (Abiotic left, Biotic right)

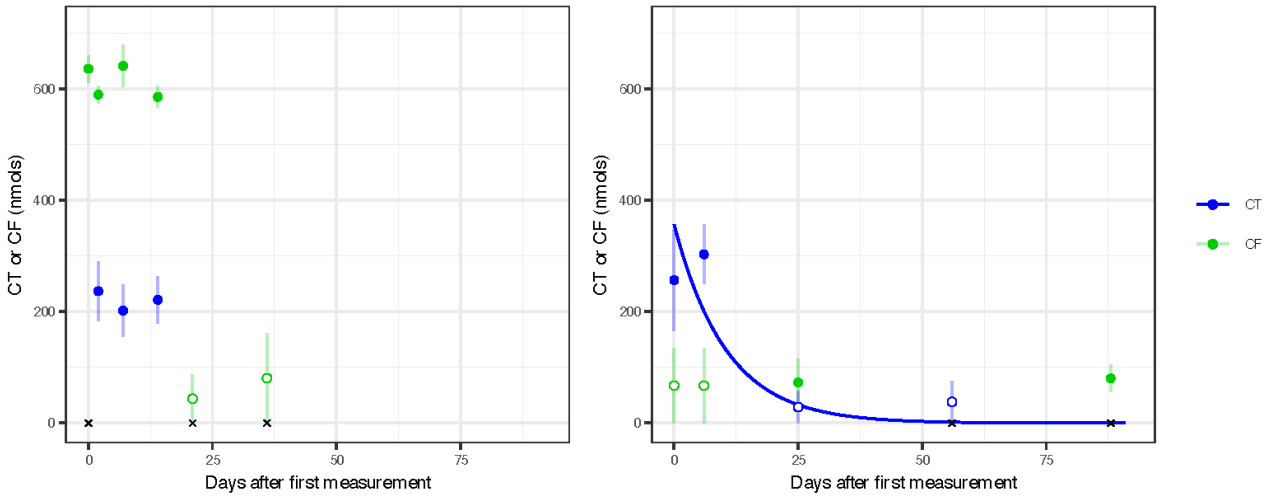

Borehole D0474 — B4JTM5 (Abiotic left, Biotic right)

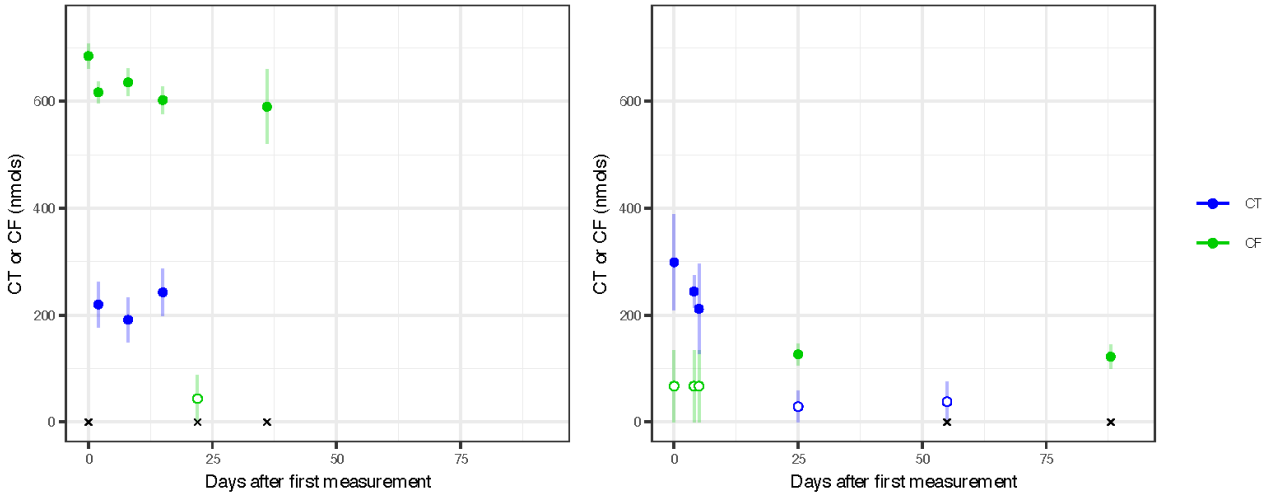

Pacific Northwest National Laboratory

902 Battelle Boulevard
P.O. Box 999
Richland, WA 99354

1-888-375-PNNL (7665)

www.pnnl.gov